2017

Poly(ethylenimine)-Functionalized Pyroxene Nanoparticles Embedded on Diatomite for Removal of Total Organic Carbon from Industrial Wastewater: Batch and Fixed-bed studies

Hethnawi, Afif

UNIVERSITY OF CALGARY

Poly(ethylenimine)-Functionalized Pyroxene Nanoparticles Embedded on Diatomite for Removal of Total Organic Carbon from Industrial Wastewater: Batch and Fixed-bed studies

by

Afif Jawad Hethnawi

A THESIS

SUBMITTED TO THE FACULTY OF GRADUATE STUDIES
IN PARTIAL FULFILMENT OF THE REQUIRMENTS FOR THE
DEGREE OF MASTER OF SCIENCE

GRADUATE PROGRAM IN CHEMICAL ENGINEERING

CALGARY, ALBERTA

March 2017

Abstract

Providing clean and affordable water to meet the human needs is a big challenge in this century. Globally, the water supply for many industries struggles to keep up with the strong demand. This demand issue is exacerbated by industrialization, which led to water quality deterioration, forming polluted wastewater. Existence of treatment processes to overcome wastewater problems are not efficient and appropriate to maintaining the industrial effluent composition within the standard limits. Specifically, presence of dissolved organic compounds not properly eliminated during the wastewater treatment has a negative impact on human health and the environment. As a novel solution, nanotechnology holds great potential in water and wastewater treatment to improve water quality efficiently. Here, we introduce an innovative technique using environmentally friendly, multifunctional, and effective poly(ethylenimine)-functionalized pyroxene nanoparticles to provide an efficient removal of the dissolved total organic carbon from industrial wastewater in batch and contenuious fixed-bed column studies under various conditions. Our study includes arrays of characterization techniques for the prepared nanoparticles and for Diatomite (commonly used filter aid) before and after embedding it with the nanoparticles at a very low mass ratio (<5 wt%). Diatomite, on its own, has a very low adsorption capacity for the dissolved organic contaminants in field applications. Among these applications is the employment of Diatomite with a rotary drum filter (RDF). Therefore, we embedded the nanoparticles to improve the performance of the Diatomite employed with a rotary drum filter used for the removal of dissolved organic pollutants. This followed our bench scale adsorption experiment using a continuous fixed-bed column that is considered to be the best lab scale model for the rotary drum filter.

The experimental results showed that, compared to using activated carbon and magnetic nanoparticles, the prepared nanoparticles were very effective in the removal of dissolved organic contaminants in batch and continuous fixed-bed column experiments. In continuous fixed-bed column experiments, the breakthrough behavior was described using a convection-axial dispersion model that had a good fit with the obtained experimental data. Interestingly, this innovative technique was successfully applied at Executive Mat Ltd, here in Calgary in their rotary drum filter after optimizing some operational conditions.

Acknowledgments

First and foremost, I would like to thank Almighty God for establishing me to complete this thesis. God, who is the only one who gives me the power in my passion and pursue my dream.

I would like to express my grateful to my supervisor, Dr. Nashaat N. Nassar at the University of Calgary, for his support, guidance, valuable contribution, feedbacks, advices, and for providing the opportunity to work in the Catalysis for Bitumen Upgrading Group CBUG with many professional people. My special thanks go to Dr. Gerardo Vitale, a true description of "actual scientist", for all his practical advices and his helpful discussions. I wish to extend my gratitude to Prof. Pedro Pereira-Almao, Dr. Azfar Hassan, Dr. Josefina Scott, Dr. Carlos Scott, Dr. Lante Carbognani, Dr. Monica Bartolini, Argenis Aguero, Mitra Roustapisheh, Marianna Trujillo, and Josune Carbognani for their valuable assistance through my research. Sincere thanks to my examiners: Dr. Hossein Hejazi and Dr. Qingye Gemma Lu for their contribution and valuable time.

I am thankful and grateful to Amjad El-Qanni for his advices and support in my experimental work. I am grateful to Abdallah D. Manasrah for his help and contribution. I am also thankful to Nedal Marei, Ghada Nafie, Suraj Gurung, Jose Humberto, Maysam Alnajjar and all members of Dr. Nassar Group for Nanotechnology Research. Many thanks for Executive Mat Ltd. presented by Dr. Marwan Shamel for their financial support and in providing time, space, and chemicals to conduct the field test experiments.

More importantly, I wish to express my deepest appreciation to my family: My parents and sisters, who supported me to achieve my goal. I would gratefully acknowledge the friends, Hatem Hammad, Ralf Pollock, and Linda Sunderland for their help in language editing. My thanks also to the friends, Kotaybah Hashlamoun, Njood El-Qalash, Hothifa Rajoub, Yaser Saffar, Yahya

Shubbak, Alaa Dabboor, Norm Geitzler, Ahmad Awwad, Yousef Qassrawi, Annas Dawood, and Mohamed Harb.

Dedication

To the spirit of my childhood friend, who deliberately killed by the Zionists without guilt when we were together at school, El-Shaheed "Ibraheem Qmail".

CONTENTS

LIST OF TABLES

LIST OF FIGURES

CHAPTER ONE

Introduction

1.1 Background

Although water has a vital role for the operation of various industrial processes, wastewater treatment has previously been neglected as an important element of industrial practice and the end-users primarily focused on the quality of their output without having an in-house expertise in wastewater treatment. Besides, end-users concerned with treating wastewater effluents only if it is essential for reducing the risk in production processes [1] However, treatment and management of water in industry has become more seriously recognised in the last decades as a prominent issue due to increased pressure on water recourses and low quality feed water since fresh water is becoming progressively difficult to obtained [2–6]. Consequently, industrial end users are increasingly exploring ways in which to reduce their impact on fresh water resources through approach such as wastewater treatment or water reuse.

Canada in 2011, as reported by industrial wastewater survey that was re-instituted by statistics Canada in 2014, had total water intake by three industries surveyed (thermal-electric power producers, manufacturing industries, and mining industries) around 27.6 billion cubic meters. Total wastewater discharge for the three industries group, on the other hand, was 26.9 billion cubic meters. The thermal-electric power producers accounted for 85.8% of this total, manufacturing industries discharged 12% of the total and the mining industries the remaining 2.2% [7]. By manufacturing industries, for instance, most of the wastewater was discharged (76.6 %) to surface fresh water bodies and to tidewater (13%). The balance was discharged to public/municipal sewers, groundwater or other points [7]. Of the water discharged by the manufactures, 34% was not treated

before being release [7]. The most advance level of treatment for 17.9% of the total discharge was primary treatment while 36.2% of the total discharge secondary or biological treatment as a highest level of treatment before being discharged [7]. Only 12 % underwent tertiary or advance treatment [7,8].

1.2 Research motivation

With high consumption of freshwater by many industries and increased the discharge wastewater amount, pure water progressively becomes a rare source and day by day access to clean drinking water is being an enormous problem faced by many people all over the word [9–12]. Accordingly, many intensive contributions have been made to preserve water recourses. Furthermore, the industrial wastewater may contain a plenty of high toxicity ions of heavy metals and various types of organic pollutants. Recently, treatment of total organic carbon from industrial effluents has been recognized because many industries, including: petroleum refining, petrochemical, pulp and paper, food, and textile involve processes, which produces types of effluents typically has high levels of colloidal suspended and dissolved organic pollutants [3,13,14]. These pollutants, which can be characterized by having a great difference in chemical composition, often need to be treated appropriately. Otherwise, they cause negative impacts for human health and environment. Despite of developing various physiochemical techniques for adequate treatment of these pollutants, still there is a dire need for efficient, costly effective, and environmentally friendly methods to treat them, especially the ones that are dissolved or difficult to degrade and cannot be detected in wastewater effluents [3,15,16]. Adsorption using various types of adsorbents like the activated carbon (AC) has been widely used to remove these dissolved organic pollutants [3,12,17–20]. AC shown very satisfactory results in the dissolved organic removal especially when it was integrated with biological treatment as tertiary or advance treatment [21,22]. Also, AC had an outstanding

performance in total dissolved solids when it followed coagulation/flocculation method [9,23]. Nevertheless, it has a low efficiency due to its slow mass transfer kinetics in adsorbing the heavy molecules, which lengthens the adsorption equilibrium time [24–26]. Furthermore, production and regeneration of the AC are not environmentally safe nor cost-effective in industrial applications [15,27–29]. Thus, many studies focus their efforts on developing an adsorbent with unique properties that can provide better performance than AC [30–33]. Alternatively, nanoadsorbents offer good sorption efficiency, large surface area, and easily accessible sorption sites with organic contaminants [13,27,28,30,32,34]. Hence, using nanoparticles may allow for better and more affordable wastewater process development. Nanoparticles in a synergistic combination with other conventional techniques provides a greater possibility for large-scale applications of wastewater treatment. For multifunctionality and stability purposes, various types of nanoparticles have been anchored during or after the synthesis with a wide range of functionalizing agents like polymers, surfactants, and inorganic materials [15,35–37]. Nevertheless, nanoparticles need an initiator that primarily attaches to the surface of the nanoparticles under a well monitored and high specificity conditions [15,37,38]. This initiator binds the nanoparticle surface before the final functionalization, which can be considered as one significant drawback of using the functionalized nanoparticles in the wastewater treatment fields.

At high industrial level, Executive Mat Ltd, in Calgary, is using a conventional treatment method by a rotary drum filter (RDF) to remove the suspended solids and colloids from their industrial wastewater. RDF is pre-coated with a filter aid, typically Diatomite. Although RDF is effective in some types of wastewater, it is inefficient, especially when the wastewater contains a high level of dissolved total organic carbon. This is because the employed Diatomite has a very weak adsorption capacity[39,40]. It is therefore ineffective in the adsorption of the dissolved solids, especially the

dissolved solid including dyes. Thus, there is a dire need for an improvement in the filtration efficiency of the Diatomite.

The motivation of this effort is to explore a possible pathway for efficient, costly effective, and environmentally friendly treatment of dissolved total organic carbon from an industrial wastewater, which ultimately can be introduced as a good alternative method for the conventional treatment methods and outstandingly can provide a better performance than AC individually or as an integrated technique with the others. Furthermore, studying the ability of using such technique to improve the removal efficiency of the TOC on the RDF at Executive Mat Ltd after optimizing some operational conditions.

1.3 Research objectives

The following items are considered as the main objective of this research:

- Synthesizing an environmentally-friendly, costly effective, and multifunctional type of nanoadsorbents that is a good alternative and has a better performance than AC and other widely used nanoadsorbents in the removal of dissolved total organic carbons.
- Functionalizing the nanoadsorbent by using a multifunctional stabilizer without using an initiator before the end-grafting at optimal conditions by using suitable characterization techniques.
- Investigating the ability to improve the adsorption surface area and the performance of the Diatomite by integrating it with such effective functionalized-nanoadsorbents.
- Testing the adsorption capacity in batch and continuous fixed-bed modes of the nanoadsorbent embedded on Diatomite toward a dissolved commercial red dye (CRD) from the textile wastewater.

- Studding the kinetic of the continuous fixed-bed column adsorption under the effect of controlled operational parameters of bed depth, inlet concentration, flow rate, and the concentration of the embedded nanoparticles on the Diatomite.
- Investigate the possibility of utilizing our adsorptive technique in batch and continuous fixed-bed in cleaning-up a real and locally provided industrial effluent.
- Utilizing the novel nanoparticle adsorbent in a continuous mode using a RDF at Executive Mat Ltd.

1.4 Thesis organization

This thesis is divided into six chapters and one appendix of a collection of three journal papers. The first author, Afif Hethnawi, performed all of the experimental work and data analysis, and participated in interpreting the results and core part of writing. Nashaat Nassar is the principal investigator (PI), supervisor and the corresponding author. Gerardo Vitale helped in preparing and characterizing the nanoparticles as well as computational modeling performing. Abdallah D. Manasrah contributed with modeling the breakthrough curves in the packed-bed adsorption experiments.

Chapter 1 provides a brief background, objectives and organization of thesis.

Chapter 2 provides a brief description on preparation of the pyroxene nanoparticles and then, their functionalization with poly(ethylenimine) followed by detailed characterization of the synthesized nanoparticles. This chapter also includes testing the adsorption capacity of the prepared nanoparticles for removal of commercial red dye (CRD) from the textile wastewater in batch adsorption processes. This chapter was submitted to the "Colloids and Surfaces A: Physicochemical and Engineering Aspects" journal with the title, "Preparation and

Characterization of Poly(ethylenimine)-Functionalized Pyroxene Nanoparticles and its Application in Wastewater Treatment."

In **Chapter 3**, the possibility of improving the Diatomite by embedding it at very low mass fraction of the functionalized nanoparticles is discussed in addition to a brief detail of the removal efficiency of the CRD via batch and continuous fixed-bed modes of adsorption. Then, the adsorption performance of fixed-bed column was tested for Diatomite before and after embedding it with version and functionalized nanoparticles that are compared with that of activated carbon (AC) and magnetic nanoparticles. This chapter also includes fixed-bed column experiments to determine the breakthrough curves under different operational conditions (e.g., inlet concentration of CRD, inlet flow rate, bed height, and nanoparticle concentration in Diatomite). Furthermore, in this Chapter a convection-axial dispersion model was presented that is used to describe the obtained experimental results under effect of various dynamic conditions. This chapter was submitted to "Chemical Engineering Journal" with the title "Poly(ethylenimine)-Functionalized Pyroxene Nanoparticles Embedded on Diatomite for Adsorptive Removal of Dye from Textile Wastewater: Batch and Fixed-bed Studies."

In **Chapter 4**, the adsorption of total organic carbon (TOC) from an industrial effluent using the functionalized nanoparticles embedded into Diatomite at <5 wt% is described in a batch and continuous fixed-bed column. This Chapter contains the breakthrough behavior of the column experiment under different operational conditions (e.g., influent TOC concentration, inlet flow rate, bed height, and nanoparticle concentration in Diatomite). This chapter also includes a description of breakthrough behaviour in the concept of mass transfer phenomena by using suitable correlations. This chapter is to be submitted to "Journal of Hazardous Materials" with the title

"Poly(ethylenimine)-Functionalized Pyroxene Nanoparticles Embedded on Diatomite for Removal of Total Organic Carbon from Industrial Wastewater."

Through **Chapter 5**, a scalable application in a continuous mode using a RDF at Executive Mat Ltd. The INPs is described in details at various mass ratios. Then the removal efficiency and the effect of nanoparticle concentration, as one of the dynamic parameters, is explained in details.

In **Chapter 6**, summery and conclusions of the study are presented as well as several recommendations for future studies in this field are suggested. Finally, **Appendix A** containing supplementary information is provided.

CHAPTER TWO

Preparation and Characterization of Poly(ethylenimine)-Functionalized Pyroxene Nanoparticles and Its Application in Wastewater Treatment

This chapter is adapted from the following publication

A. Hethnawi, N. N. Nassar, G. Vitale, Preparation and Characterization of Poly(ethylenimine)-Functionalized Pyroxene Nanoparticles and its Application in Wastewater Treatment, Colloids and Surfaces A: Physicochemical and Engineering Aspects (Submitted), (2017)

2.1 Abstract

In this study, poly(ethylenimine)-functionalized pyroxene nanoparticles were successfully prepared in-house for removal of commercial red dye (CRD) from the textile wastewater by a two-step preparation method. A conventional hydrothermal synthesis at mild conditions was carried out to prepare the pyroxene nanoparticles (PNPs), and then, their functionalization was accomplished by anchoring poly(ethylenimine) (PEI) onto the surface without surface modifications or preliminary coating. Characterization was followed out by textural properties, X-ray diffraction (XRD), high-resolution transmission electron microscopy (HRTEM), infrared (IR) spectroscopy, and thermogravimetric analysis (TGA). The characterization results showed that the prepared nanoparticles were successfully functionalized by the PEI. Also, they had granulated-like morphologies with average crystaline domain sizes around 10 nm, low BET surface area (~18 m^2/g) that increased reasonably to ~119 m^2/g by drying using lyophilizing method instead of conventional drying of the synthesized materials. The prepared PEI-PNPs showed an excellent adsorption removal efficiency (~ 340 mg/g) and fast adsorption kinetics (< 15 min) of the CRD from a textile wastewater in batch mode of adsorption compared with that of magnetite nanoparticles and a commercial activated carbon that had lower adsorption capacity of the dye (<50 mg/g). The adsorption kinetics and isotherm of the dye on PEI-PNPs were described by the external mass transfer diffusion and the Sips models, respectively.

2.2 Introduction

All industrial wastewater effluents create significant and hazardous environmental footprints, which substantially vary from process to process. It is important that every effort be made to minimize the amount of generated wastewater and to provide optimum water quality that meets human and environmental needs [41,42]. The textile industry, which consumes a high quantity of

fresh water, usually produces wastewater that is characterized by having a high level of total organic carbon [43]. Moreover, textile wastewater generally contains various compounds, most of which are synthetic in origin [14]. For example, it contains dissolved dyes that are commonly used to impart color to cellulose fibers [44]. These dyes are difficult to remediate since they do not degrade easily and quickly become chemically stable [45]. Furthermore, they may end up producing toxic materials or mutagenic compounds as in case of azo dyes [46]. Many widely used technologies, including chemical and biological treatments [47], advanced oxidation processes [48], photocatalytic degradation [49–51], Fenton oxidation [52], and coagulation and flocculation [53] have been adapted to provide high efficiency removal of organic and inorganic pollutants. However, these typical technological treatments have no robust effect in textile wastewater treatment. Several factors hinder the efficiency of these processes, such as cost and process workability [14].

Adsorption is a more effective alternative to these inefficient and costly technologies [54–60]. Adsorption is a promising technology that is more capable of removing pollutants from textile wastewater, as it is superior in terms of flexibility and simplicity. Because it is flexible, it can be applied on its own or as an integrated technology; like the case of combining magnetic field and adsorption for treatment of the biologically treated palm mill effluent [61]. In column experiments, activated carbon (AC) is a widely used adsorbent which performs well when used for the removal of different types of heavy metals and organic pollutants from the wastewater [12,62,63]. Further, AC and ozonisation process interact effectively to remediate some of the toxic aromatics found in textile wastewater (e.g., diclofenac and nitro phenol) [64]. However, AC has serious challenges that are represented by its high costs and non-environmentally friendly manufacturing and

regeneration processes [27] in addition to its low adsorption capacity for large molecules and slow mass transfer kinetics that typically results in very long adsorption equilibration time [24–26,65].

Nanomaterials are today's novel adsorbents, characterized by their small size (i.e., < 100 nm in one dimension) which allows for a high surface areas crating more corresponding sorption sites and small interparticular diffusional distances [2,66]. Nanomaterials have wide ranges of applications [66,67], of which wastewater treatment is a very important one [13,15,30,31,36,68–72]. For instance, iron oxide nanomaterials have been extensively used to remove different types of pollutants from wastewater such as heavy metals and polycyclic aromatic [27,33,73–76]. To be effective, this type of nanoparticles should be thermodynamically stable to stay in a solution without aggregating and to maximize dispersity. Specifically, the stability of nanoparticles related to the energy of their surface molecules is reduced by their electrostatic interaction with the surrounding molecules (Van der Waal's interactions) [57,60]. Therefore, much work is needed to overcome this drawback, which limits the nanoparticle potential range of application. Thus, functionalization, a practical and an innovative technique, has been proposed and experimentally used which can be described as anchoring the desired functional group, like polymer, dendrimer or highly specific ligand that maintains the surface stability of the nanoparticles [60]. Further, it provides multi-functionality through the decoration of the surface of nanoparticles with specific molecules which are able to attract complex compounds [12,61–63]. For example, Fe_3O_4 magnetic nanoparticles were grafted by poly-(methyl methacrylate) [77] and γ-Fe_2O_3 magnetic nanoparticles were grafted by poly-(hydroxyl ethyl methacrylate) or poly-(methacrylic acid) [78]. These polymer-grafted nanoparticles could efficiently and specifically remove total organic carbon and heavy metals like lead, nickel and cadmium from wastewater [2,27,64]. However, grafting a polymer on a nanoparticle surface requires surface modifications such as introducing initiators

under well-monitored conditions or supplying the surface of the nanoparticle with a bridge (binding agent) so that the functionalizing agent is attached to the nanoparticle surface [15].

Branched poly-(ethylenimine) (PEI), a cationic and multifunctional polymer since it has a wide range of buffering capacities (i.e., working at broad range of pH) in an aqueous solution under normal conditions, has been shown to coat the magnetic nanoparticles in order to efficiently remove the TOC from sewage wastewater in addition to trapping several types of heavy metals (e.g., uranium, cadmium, lead, zinc, copper, and nickel) [27,57,66]. Typically, the PEI is added after primarily coating the nanoparticles with tri-sodium citrate (TSC) [15], which imparted free carboxylic group (COO-) (negative charge) resulting in binding the free PEI to the surface of the magnetic nanoparticles [79].

To maximize the sustainability of the adsorption processes, it is important that the developed nanoadsorbents be earth abundant, naturally occurring, economic and environmental friendly. In addition, on an industrial scale, there is a dire need for environmentally safe types of nanoparticles that are multifunctional, cost effective, and efficient in wastewater treatment. Accordingly, in addition to understanding the adsorption behavior of PEI-functionalized silicate-based nanoparticles, another major purpose of this study is to develop new nanoadsorbent based on iron-silicate minerals (pyroxene aegirine) [80,81], which are widespread in nature and innocuous materials, for adsorptive removal of total organic carbon (TOC) from wastewater. These iron-silicate minerals also possess superficial ionic exchange properties that permit surface modification to introduce Brønsted acid sites [80,81], which could positively impact its adsorptive and catalytic properties. The iron-silicate nanoparticles ($NaFeSi_2O_6$) is successfully prepared in-house in nano-crystalline sizes with a novel and easy synthesis method under mild conditions like that for commercial zeolites [80], and tested for the first time for adsorptive removal of TOC from

wastewater. This field of study is highly novel, and is of strategic importance to the industrial wastewater treatment processes.

Herein, the purposes of this study include: (1) synthesizing pyroxene nanoparticles (PNPs) using a hydrothermal method under mild conditions and functionalizing them with PEI at optimal conditions, without using any binding agent like tri-sodium citrate as typically used for surface modification of other types of nanoparticles reported in literature [15]; (2) comparing the adsorptive performances (i.e., kinetics and isotherm) of the as prepared PEI-functionalized pyroxene with conventional adsorbents (like magnetite nanoparticles and commercial AC and silica) for adsorptive removal of real dye from textile wastewater at an adjustable pH. The adsorption kinetics and isotherm of the dye on PEI-PNPs were described by the external mass transfer diffusion model and the Sips model, respectively.

2.3 Experimental section

2.3.1 Materials

The following chemicals were purchased from Sigma Aldrich, Ontario, Canada: sulfuric acid (95-98%), iron tri-chloride (97%), sodium silicate solution (10.6% Na_2O, and 26.5% SiO_2), iron sulfate hexa-hydrate (≥99%), ammonium hydroxide (28-30% NH_3), hydrogen peroxide (30-35%), methanol (97%), and polyethylenimine (PEI) (99%). The sodium hydroxide beads (99.99%) were purchased from VWR International, Edmonton, Canada. The GAC (90%) was acquired from the CABOT Company, Estevan, Saskatchewan, Canada. A commercially used red dye sample in the textile industry (CRD) was kindly supplied by Executive Mat Ltd, Calgary, Canada and used as adsorbate in this study. Acid red dye 27 (AR27) obtained from Sigma–Aldrich (90%, Sigma–Aldrich, Toronto, ON) was used for comparison purposes. All chemicals were used as received without any further purifications.

2.3.2 Synthesis of PEI-functionalized pyroxene nanoparticles

The pyroxene nanoparticles were prepared hydrothermally from a typical synthesis treated gel at low temperature and pressure, as published previously [80,81]. The gel was prepared via a reaction between an acidic solution of iron and a basic solution of silicate. The acidic solution was produced by dissolving 18.067 g of sulfuric acid in 90 g of deionized water and 20.793 g of iron tri-chloride was gradually added to the solution while continuously stirring the solution at 300 rpm. The basic solution was formed by adding 21.413 g of sodium hydroxide to 60.0 g deionized water followed by gradually adding 30.707 g of sodium silicate while the solution was being stirred. Then, the acidic solution was added slowly to the basic solution while stirring for 15 min to produce a homogeneous orange-yellowish gel. After that, a hydrothermal crystallization was carried out by transferring the prepared gel to a 300-ml reactor vessel (A2230HCEB, Parr Instrument Company, Moline, Il, USA). The reactor vessel was equipped with a heating mantle connected to a temperature control loop, a gauge pressure and a mechanical stirrer with speed controller. After performing leak test and confirming no leak detection, the reactor was heated to 433 K at 300 rpm for 72 h [81]. Then, at the end of experiment, the reactor was cooled down to room temperature and the resulting gel was carefully discharged from the reactor vessel, filtered and washed with deionized water. Finally, the gel was left overnight to dry at room temperature. These pyroxene nanoparticles were then functionalized with PEI by adding 50 ml of a solution of the polymer having different concentrations (ca. 0.2, 0.4, 0.8, 1.2, and 1.6 wt%) to 1.0 g of nanoparticles suspended in 100 ml of water. Each mixture was stirred for 3 h at room temperature to allow the anchoring of the polymer onto the surface of the nanoparticles. Finally, the suspension was filtered, washed, and dried by vacuum overnight at room temperature. According to the added concentrations of the PEI, the PEI-functionalized pyroxene nanoparticles were identified as PEI-

PNPs preceded by the nominal concentration of PEI. Thus, PEI-PNPs with 0.2 wt% PEI nominal concentration was denoted as 0.2-PEI-PNPs. A selected sample (e.g., 0.8-PEI-PNPs) was lyophilized (freeze-dried) to sublimate the frozen water after the preparation. This sample finally was denoted as 0.8-PEI-PNPs-FD to distinguish it from the non-freeze-dried one.

2.3.3 Synthesis of PEI-functionalized magnetite nanoparticles

The magnetite nanoparticles were prepared using an in-house chemical co-precipitation method. In brief, 6 g of ferrous sulfate hexa-hydrate was dissolved in 100 g of deionized water followed by adding 5 ml of ammonium hydroxide to the solution. Then, approximately 15 drops of hydrogen peroxide were added gradually using a dropper to achieve a specific blackish color indicating the formation of magnetite. Finally, the solution was filtered, washed, and dried by vacuum overnight to recover the produced iron oxide nanoparticles (INPs). The PEI-functionalization of the prepared INPs followed a modified version of the protocol reported in literature [15]. A 0.8 wt% of PEI solution was gradually added to the solution that contains dispersed INPs at 293 K. This solution was then continuously stirred for 2 h. Thereafter, the PEI-functionalized INPs, which was denoted as 0.8-PEI-INP, were washed to remove the unbounded PEI, and the pH of the solution was adjusted to approximately 7. Finally, the solution was filtered and the product vacuum dried and recovered. These 0.8-PEI-INP nanoparticles were prepared for comparison purposes to test the efficiency of the developed PEI-pyroxene nanoparticles.

2.3.4 Characterization of the synthesized nanoparticles

2.3.4.1 Textural properties

To determine the effect of adding different concentrations of PEI on the surface area and porosity of the previously prepared nanoparticles, the Bruneur-Emmett-Teller (BET) tests of surface area

and porosity were carried out using a surface area and porosity analyzer (TriStar II 3020, Micromeritics Instrument Corporation, Norcross, GA). Before the analysis, the dried samples were pre-treated, inside sample holder cells, with a flow of nitrogen gas and simultaneously heated to 423 K overnight. Then, the pre-treated samples were submitted to the adsorption-desorption of nitrogen at 77 K produce the adsorption-desorption isotherms. Finally, the surface area was estimated using BET equation. This analysis was also conducted for the virgin PNPs, INP, 0.8-PEI-INP, 0.8-PEI-PNPs-FD and the commercial AC sample.

2.3.4.2 X-ray diffraction (XRD)

The structural identity and the average crystalline domain sizes of the dried powders of the PNPs and the PEI-functionalized PNPs were obtained using an Ultima III Multipurpose Diffraction system (Rigarku corporation, The woodlands, TX, the USA) with Cu Kα radiation as the X-ray source at 40 kV and 44 mA with a θ-2θ goniometer. For the analysis, each sample was placed in a glass top-loaded sample holder, having a 0.5 mm depth cavity. The sample was distributed evenly on the cavity of the sample holder with the help of a microscope slide. Scans were performed in the range of 3-90° 2-θ degrees using a 0.02° step and a counting time of 1.0° per min. The crystalline domain sizes were obtained by the Scherrer equation that is expressed in eq 2.1 as follows [82]

$$L(2\theta) = \frac{K\lambda}{B\cos\theta} \tag{2.1}$$

where λ is the X-ray wavelength in nanometer (nm), β is the peak width of the diffraction peak profile at half maximum height resulting from small crystallite size in radians and K is a constant related to crystallite shape, normally taken as 0.9. The value of β in 2θ axis of diffraction profile must be in radians. The θ can be in degrees or radians, since the cos θ corresponds to the same

number. Eq. (1) was implemented in the commercial software JADE [83]. This software allowed the fitting of the experimental profile to a pseudo-Voigt profile function, and then, the calculation of the full width at half maximum (FWHM) of the peaks to compute the crystalline domain sizes.

2.3.4.3 High-resolution transmission electron microscopy (HRTEM)

High-resolution transmission electron microscopy (HRTEM) analysis was carried out on selected PNPs and INP nanoparticles before and after PEI-functionalizing to study their size, morphology, and structural topology. Each sample was prepared for the analysis by suspending ~0.5 mg of the nanoparticles in 4 ml of ethanol and sonicating it. Some drops of the sonicated suspension of nanoparticles were deposited into a Formvar/carbon copper grid sample holder and allowed to dry. The images were collected using a FEI Tecnai F20 FEG TEM with an accelerating voltage of 200 kV.

2.3.4.4 Infrared spectroscopy (FTIR)

The molecular bonds and the functional groups were identified for the PNPs nanoparticles before and after anchoring different concentrations (e.g., 0.2, 0.4, 0.8 wt%) of PEI using a Nicolet 6700 FTIR instrument that was produced by the Thermo Electron Corporation. The instrument had a smart diffused reflectance attachment to carry out DRIFT (Diffuse Reflectance Infrared Fourier Transform Spectroscopy) analysis. Generally, the FTIR spectra for each sample was measured in the range of 400-4000 cm^{-1}, with a resolution of 2 cm^{-1} and the spectrum was the average of 128 scans. The sample for analysis was prepared by mixing small amounts of the nanoparticle sample (~5 mg) with KBr (~500 mg), and then, mounted in the DRIFTS sample holder for analysis using the conditions described above.

2.3.4.5 Thermo-gravimetric analysis (TGA)

The dried PNPs and all the PEI-functionalized PNPs were analyzed using thermo-gravimetric analysis (TGA) to estimate the organic content in each prepared sample (i.e., the loaded amount of PEI at the surface of the nanoparticles). A small amount of each sample (~5 mg) was used for this analysis, avoiding in this way diffusional limitation [84,85]. The samples were heated up to 1173 K under an air flow rate of 100 cm^3/min and a heating rate of 10 K/min using a simultaneous thermo-gravimetric analysis/differential scanning calorimetry (TGA/DSC) analyzer (SDT Q600, TA Instruments, Inc., New Castle, DE). The instrument was calibrated for mass and heat changes by using sapphire and zinc as references, respectively.

2.3.5 Model dye sample of textile wastewater

A commercially used red dye sample in the textile industry (CRD) was kindly supplied by Executive Mat Ltd, Calgary, Canada. This dye should represent the source of pollutant in textile wastewater that might provide a better understanding of the adsorptive behavior of the real textile wastewater. The chemical composition of the CRD was not readily available as the raw data sheet does not disclose the raw components of the dye. Therefore, before any adsorption experiment, the dye was analyzed by the XRD and the TGA to get an indication about their inorganic and organic mass percentages, respectively. Then for more details about the structure, the presence of carbon (C), hydrogen (H), and nitrogen (N) in the CRD was detected by using a Perkin Elmer instrument (serious II, C H N S/O analyzer, 2400). The metallic composition of the dye was estimated by inductively coupled plasma-atomic emission spectroscopy, ICP-AES (IRIS Intrepid II XDL, Thermo-Instruments Canada, Inc., Mississauga, ON, Canada). Additionally, the presence of Sulfur (S) and Nitrogen (N) in the sample was tested using Sulfur-Nitrogen (S/N) analysis with an ANTEK apparatus from FOLIO instrument, INC. (Kitchner 517-748, model number 900 HNS).

Moreover, the CRD sample was analyzed using the FTIR spectroscopy together with a commercial dye of known structure called acid red dye 27 (AR27) to get further detail about the functional groups present in the commercial red dye.

2.3.6 Adsorption experiments

Batch-mode adsorption experiments were performed at 298 K by adding 100 mg of a certain type of the aforementioned nanoparticles to a 10 mL aqueous solution containing a specific concentration of the CRD at a specified solution pH inside a 25-mL glass vials. After that, the vials were tightly closed to ensure that the concentration remains the same without losing water due to evaporation. Then, adsorption was allowed to take place by shaking the vials by a Wrist Action shaker (Burrel, Model 75-BB) for a predetermined time. For the pH-dependent study, CRD adsorption experiments were performed at 200 rpm for 24 h shaking by adding a 100 mg of the selected nanoparticles into a 25 mL-vials containing 10 mL of CRD at two different initial concentrations of 554 and 1108 mg/L. Each sample had a specific pH value, which was adjusted by adding NaOH or H_2SO_4 solutions within the pH range 2.5-11. For the adsorption isotherm study, a screening to select the best adsorbent (highest adsorption capacity) among the previously prepared nanoparticles and AC was conducted. In brief, five sets of 10 ml samples were prepared. Each set contained solutions with different initial concentrations of the CRD in each vial. In the first set 100 mg of the 0.8-PEI-PNPs was used; in the second set the same amount of the virgin PNPs was added. For the third and fourth sets, the same amount of functionalized and virgin magnetite nanoparticles (i.e., virgin INP and 0.8-PEI-INP) were added. In the last set, 100 mg of commercial AC was added. The pH in each of the 25-ml glass vials was kept constant at ~8.10 and the temperature was kept at 298 K. All the sets were shaken at 200 rpm for 4 h (enough time for the saturation). For the kinetic study, 2 sets of batch adsorption experiments using the screened

PNPs (adsorption isotherm experiments) at two different CRD initial concentrations of 1108 and 554 mg/L were performed at 200 rpm and solution pH of ~8.10 for specified time intervals in order to determine the time required for the adsorption equilibrium.

After the adsorption, in all experiments except the kinetic study, the samples were left on the lab bench overnight to allow settling of the nanoparticles. Subsequently, the nanoparticles containing the adsorbed CRD were centrifuged for 10 min at 5000 rpm in the Eppendorf Centrifuge 5804. The supernatant solution was decanted, and the residual concentration of the CRD in the supernatant was measured by UV-vis Spectrophotometry (UV-vis) using a Nicolet Evolution set at a wavelength of 511 nm. A calibration curve of UV-vis absorbance at 511 nm versus the CRD concentration (mg/L) was established using a standardized model solution of CRD. In order to normalize the concentration of the standard model solutions of the CRD in terms of TOC (mg/L), other calibration curve was established by using a Shimadzu Total Organic Carbon Analyzer (TOC-L CPH/CPN) to measure the TOC in each of the CRD samples. Then, the adsorbed amount of CRD, in terms of mg TOC/ g of dried adsorbent, was estimated by the mass balance analysis as per eq 1.2:

$$Q = \frac{C_o - C}{m} V \qquad (1.2)$$

where C_o is the initial concentration of CRD in the solution (TOC, mg/L), C is the final concentration of CRD in the supernatant (TOC, mg/L), *V* is the solution volume (L), *m* is the dry mass of adsorbent (g). For the equilibrium data, C replaced with C_e, *Q* replaced with Q_e in the eq 1.2.

2.3.7 Computational Modeling

Figure 2.1 shows a 2-D representation of the chemical structure of the repeat unit of the PEI polymer. The chemical composition was taken from the Sigma-Aldrich website and drawn with the ChemDraw v15.1 software [86]. To get some insights into the possible interactions of the selected PEI polymer with the surface of the pyroxene aegirine nanoparticles; pictorial representations were carried out using the BIOVIA Materials Studio Software v2017 [87]. The 10 nm pyroxene nanoparticle presented in Figure 2.1 was created using the Build Nanostructure module within BIOVIA Materials Studio and the structural parameters reported for aegirine by Cameron et.al [88]. The surface broken bonds were capped with hydrogen atoms, in this way, the hydroxyl groups presented in the real material can be taken into account. The 3-D representation of the PEI polymer shown in Figure 2.1 was created using the Build Polymers module within BIOVIA Materials Studio. The repeating unit was constructed within the Build Polymers module and a short polymer with five repeating units was generated and used to show some of the possibilities that the polymer can conform onto the surface of the pyroxene nanoparticle.

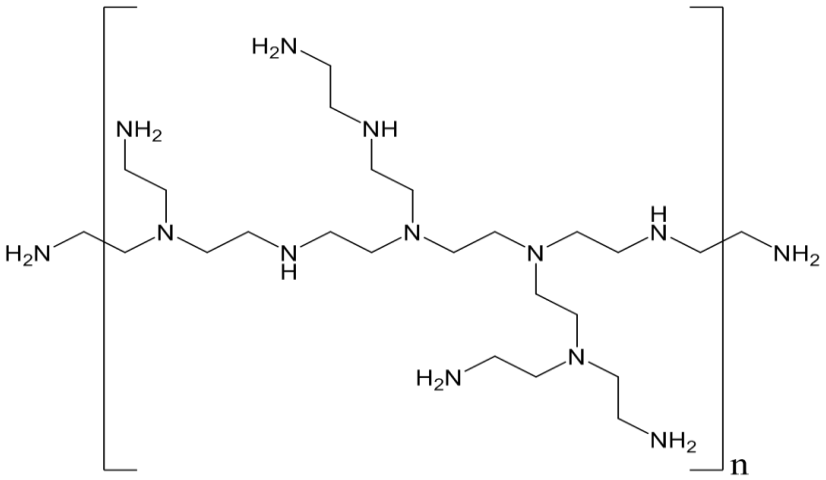

Figure 2.1. Chemical structure representation of the repeated unite of the used PEI polymer.

2.4 Results and discussions

Pyroxene nanoparticles (PNPs) were synthesized by the hydrothermal method and the polyethylenimine (PEI) was used for functionalization without the need for any binding agents or preliminary functionalization which was commonly used for surface modification of other types of nanoparticles, as published elsewhere [15,32,79,89]. The PEI was anchored on the surface of the pyroxene nanoparticles that are composed of sodium, silicon, iron and oxygen atoms with a silicon to iron atomic ratio (Si/Fe) of 2.0 [80,81]. The iron atoms in this structure impart negative charges to the framework and these negative charges are compensated by sodium cations (Na^+). Under aqueous conditions, the sodium cations present on the surface of the pyroxene nanoparticles can be ion exchanged (e.g., Na-PNP + $M^+ \Leftrightarrow$ M-PNP + Na^+; where M^+ is a cation moiety that can be exchanged with the sodium cation), and thus, the cationic amino group R-NH_3^+ present in the aqueous solution of the polymer (e.g., reaction R-NH_2 + $H_2O \Leftrightarrow$ R-NH_3^+ + OH^-), can be anchored on the surface by its electrostatic attraction to the negative site produced by the iron in the

framework close to the surface. The resulting PEI-functionalized pyroxene nanoparticles have long chains containing amino groups (R-NH_2 or R1-NH-R2); and these anchored long-chains containing amino groups would efficiently interact with organic contaminants present in the textile wastewater, such as dye. Figure 2.2 represents a 10 nm nanoparticle of the pyroxene aegirine (Figure 1.2a); a 5-repeated unit of PEI (Figure 2.2b) and possible ways that the PEI polymer chains can be anchored onto the pyroxene nanoparticles (Figure 2.2c). The latter figure also shows how the polymer can produce interacting sites/pockets that may allow the capture of components of the dye present in the textile wastewater.

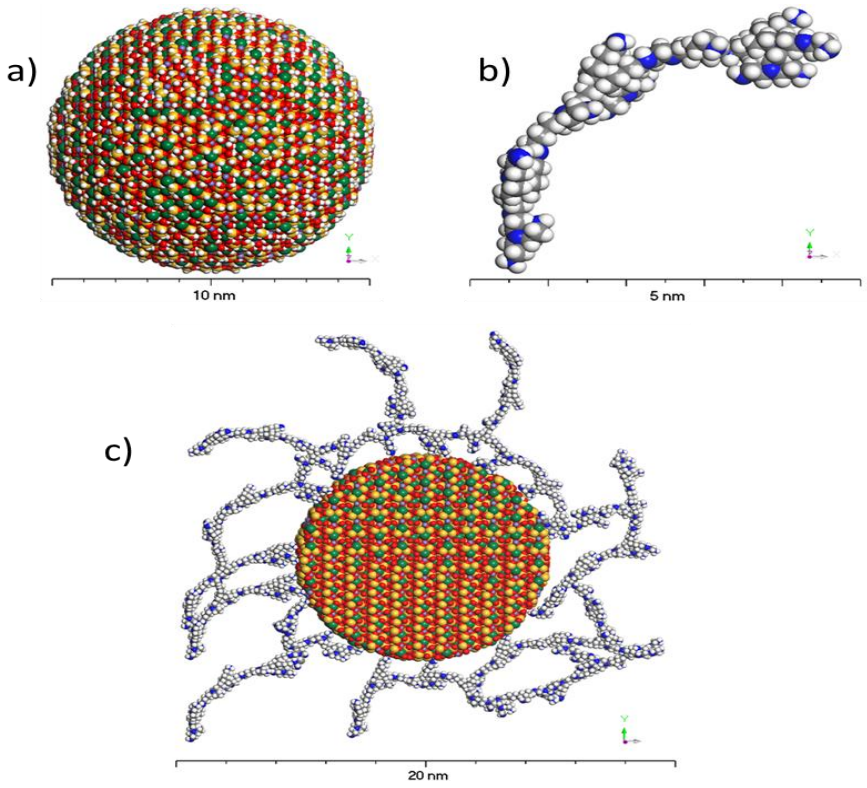

Figure 2.2. a) CPK representation of a 10-nm spherical nanoparticles of the pyroxene aegirine; b) CPK representation of a possible conformation of a PEI polymer chain; c) Cross sectional pictorial representation of the interaction of the PEI polymer with the surface of the pyroxene aegirine showing different ways the polymer can be anchored and how the polymer can produce interacting sites/pockets capture the due present in the wastewater. Red spheres represent oxygen atoms, yellow sphere represent silicon atoms; green spheres represent sodium atoms; light purple spheres

represent iron atoms; white spheres represent hydrogen atoms; grey spheres represent carbon atoms and blue spheres represent nitrogen atoms.

2.4.1 Characterization studies

2.4.1.1 HRTEM and XRD analyses

Figure 2.3a-d show the HRTEM images that were taken of the PNPs (Figure 2.3a), 0.8-PEI-PNPs (Figure 2.3b), INPs (Figure 2.3c), and 0.8-PEI-INP (Figure 2.3d). These images demonstrate some differences between the two types of nanoparticles in terms of shape and size before and after the functionalization. As seen, PNPs and 0.8-PEI-PNPs appear to be formed by aggregates of smaller particles forming granulated-like morphologies and with average sizes around ~10 nm, confirming the crystalline average demain size obtained by XRD, as will be discussed later. INPs and 0.8-PEI-INPs both were globular in shape with very low crystaline size (12 nm), in agreement with reports in literature [15].

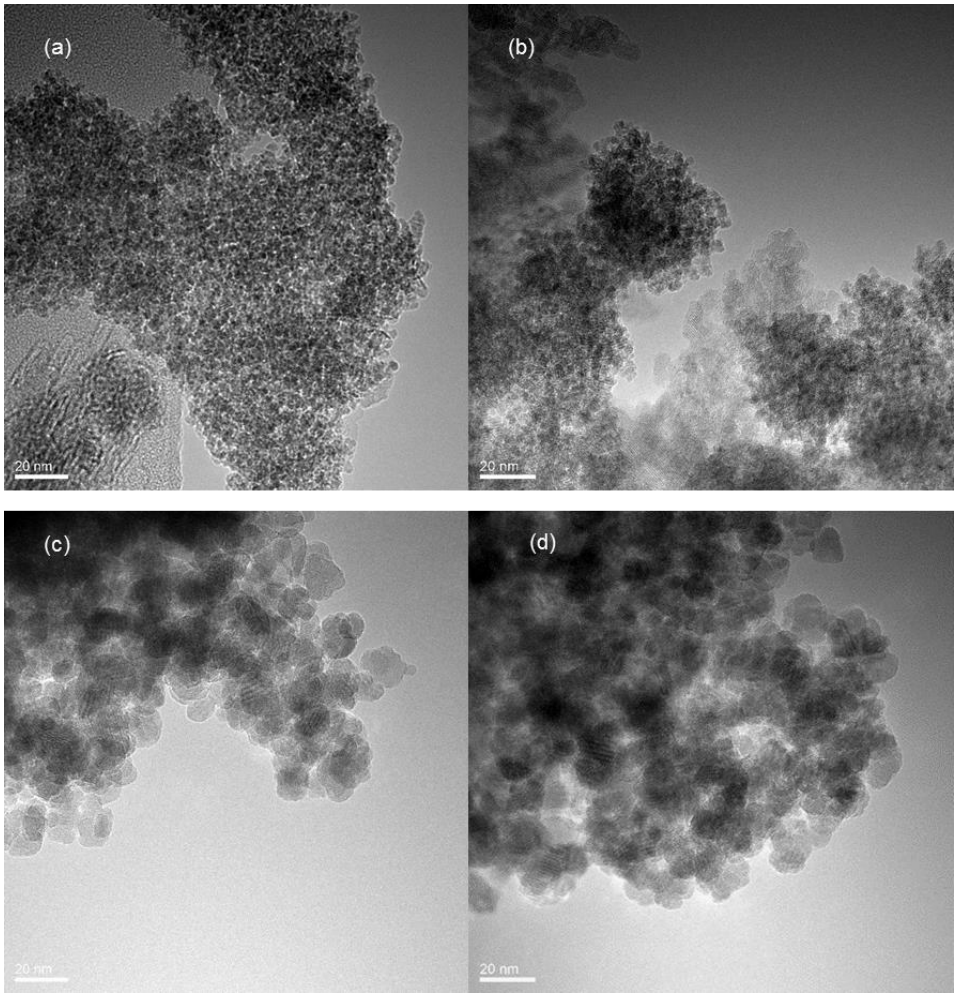

Figure 2.3. HRTEM images for (a) PNPs, (b) 0.8-PEI-PNPs, (c) INPs, and (d) 0.8-PEI-INPs (line mark in the image corresponds to 20 nm).

Figure 2.4 shows the X-ray diffraction patterns of the synthesized PNPs and PEI-PNPs. The obtained patterns of the prepared PEI-PNP's materials confirmed the formation of the pyroxene structure known as aegirine [80,81], having the powder diffraction file (pdf) card #01-076-2564 (2005 International Center for the Diffraction Data base included in the program JADE V. 7.5.1Materials Data XRD Pattern Processing Identification and Quantification). This result indicates that the PEI-PNPs have been successfully synthesized without damaging the crystal structure of PNPs core during coating or surface functionalization [37]. However, the broadening

observed in the patterns clearly indicates the formation of materials with very small crystalline domain sizes [82]. The obtained patterns for the different functionalized PNPs showed no significant changes in signal intensities and broadening. This is expected since the PEI has a very low crystallinity that cannot be detected by the XRD scans. Therefore, the functionalization and the amount of polymer added to the PNPs did not alter the crystallinity of the prepared PNPs. Accordingly, the determined average crystallite sizes were found to be around 10 nm for the PEI-PNPs and the virgin sample; which is in very good agreement with the particle size obtained by the HRTEM.

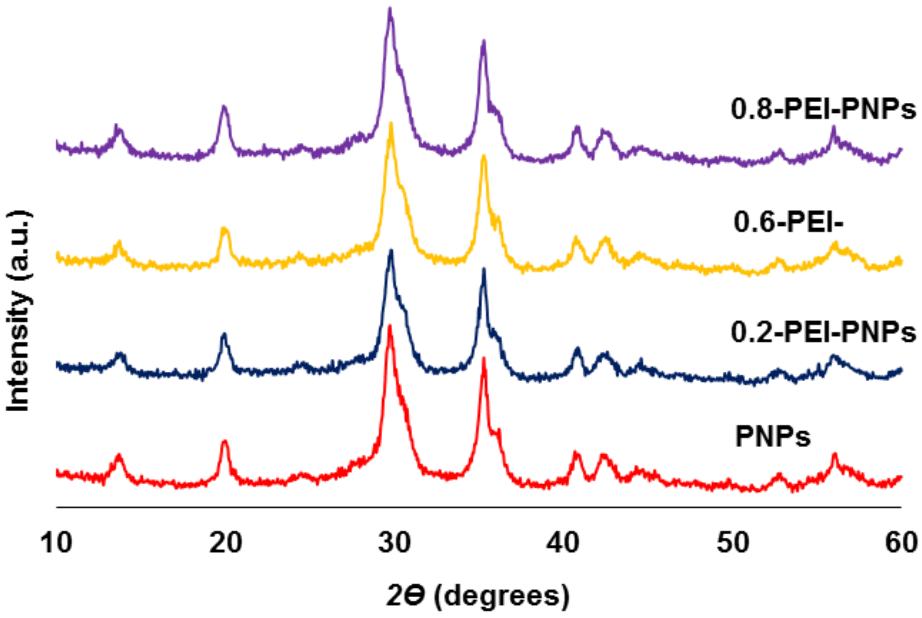

Figure 2.4. X-ray diffraction powder in the region of 10-90^{o} for the synthesised PNPs and PEI-PNPs.

2.4.1.2 Textural properties

PNPs and PEI-PNPs were essentially non-porous, which was discerned by examining the similarities between surface area obtained through the BET and that obtained by the *t*-plot methods [85,90]. Furthermore, the particle size of the aforementioned nanoparticles, assuming they had a

spherical shape, was estimated by using the measured specific surface area and the derived equation d =6000/(S_A ρ_{PNPs}); where d is the particle size in nm, S_A is the experimentally measured specific surface area (m^2/g), and ρ_{PNPs} is the density of pyroxene (3.57 g cm^{-3}) [81]. Table 2.1 lists the BET surface area, the estimated particle size (nm) and the crystalline demined size obtained by the XRD on the functionalization of PNPs that have various concentrations of PEI. As seen, using increasing amounts of the PEI polymer concomitantly there was a reduction of the surface area when the material is dried. This occurred because when drying, the polymer will cover the pyroxene particles acting like a plastic bag trapping the particles inside, and thus, the nitrogen could not access and estimate the surface area of the exposed active sites/pockets formed under the aqueous conditions. It should be expected that under aqueous conditions, the polymer chains will not embed the nanoparticles of pyroxene, and thus, active sites/pockets should be observed and surface area exposed should increase. Moreover, the BET and XRD both confirmed the particle size of the non-functionalized PNPs was the same (~10 nm). However, the two tests indicated differences in the particle size in the different concentrations of the PEI in the PEI-PNPs. As discussed above, the BET showed that the estimated particle size seems bigger than the crystalline domain size obtained by the XRD because the polymer is embedding many crystalline sizes, and thus, reducing the exposed surface area. In order to have a more realistic perception of the PEI-PNPs surface area and porosity, it was important to lyophilize one of the PNPs by sublimating the trapped water after its functionalization and not drying it as before [91,92]. This process allowed the particles to conserve the configuration presented in the aqueous solution, and thus, after lyophilizing a sample prepared in the same way to the 0.8-PEI-PNPs, but using freeze drying instead of conventional drying. The measured BET surface area increased from 16 to 118 m^2g^{-1}. This is not surprising. Figure 2.5 also explains the fact of reduction the surface area of the

normally dried 0.8- PEI-PNPs that was occurred due to covering the mesoporous area. Therefore, the distribution of the pore size was low around the region of 30-35 Å. However, the freeze-dried sample (0.8-PEI-PNPs-FD) similar to the PNPs, had both a significantly major size distribution around 30-35 Å, which was due to exposing the mesoporous area to the nitrogen during this test. Interestingly enough, this result indicated that under the aqueous conditions required for the use of the functionalized nanoparticles, the polymer should be anchored on the surface of the particles but the chains extended allowing the formation of pockets that produce porosity which allows to anchor and trap the organic components present in the textile wastewater.

Table 2.1. BET surface area, particle size and XRD crystalline size of different-functionalized PNPs.

Sample	**BET surface area (m^2g^{-1})**	**Particle size by BET (nm)**	**Crystalline domain size by XRD (nm)**
PNPs	179	9	10±1
0.2-PEI-PNPs	37	40	11±1
0.4-PEI-PNPs	24	70	10±2
0.6-PEI-PNPs	20	86	11±2
0.8-PEI-PNPs	16	104	12±2
0.8-PEI-PNPs-FD	118	15	10±2

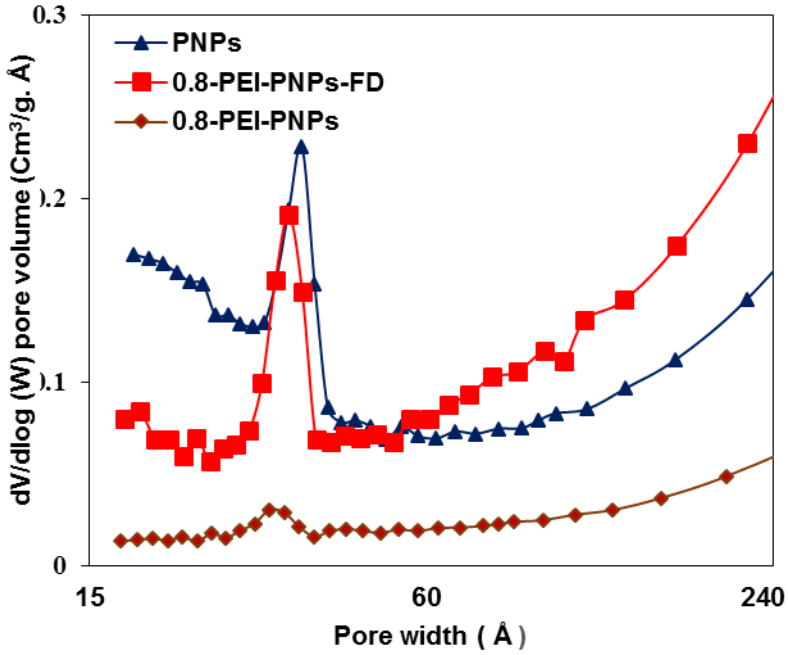

Figure 2.5. Pore size distribution of PNPS, 0.8-PEI-PNPs, and 0.8-PEI-PNPs-FD.

2.4.1.3 Functionalization study of PEI-PNPs

FTIR measurements were carried out for PNPs to confirm the PEI functionalization on the surface of the PNPs at frameworks of 500-1800 cm^{-1}(Figure 2.6) and 2700-4000 cm^{-1}(Figure 2.7). Each figure represents the obtained signals for the pyroxene nanoparticles (Figures 2.6a and 2.7a), the polymer (PEI) (Figures 2.6b and 2.7b), and the functionalized pyroxene nanoparticles (Figures 2.6c and 2.7c). The functionalized pyroxene nanoparticles included 0.4-PEI-PNPs, 0.6-PEI-PNPs, and 0.8-PEI-PNPs. Before the functionalization, it was excepted to show a wide stretching hydroxyl band around 3300 cm^{-1} that observed due to the hydrothermal preparation of the nanoparticle of pyroxene [80,81]. Anchoring the PNPs with PEI reduced the broadness of this band that might occur due to the interaction between the polymer and the nanoparticles. However, the same band became broader when the nanoparticles were loaded with more PEI since the band of 3300 cm^{-1} also attributed to N-H stretching [15]. Furthermore, NH_2 bending and C-N stretching

were assigned at around 1500 cm^{-1} for the PEI and the functionalized nanoparticles [93] .Interestingly, by increasing the concentration of the PEI, the bands became broader which confirms the successful anchoring of PEI on the PNPs.

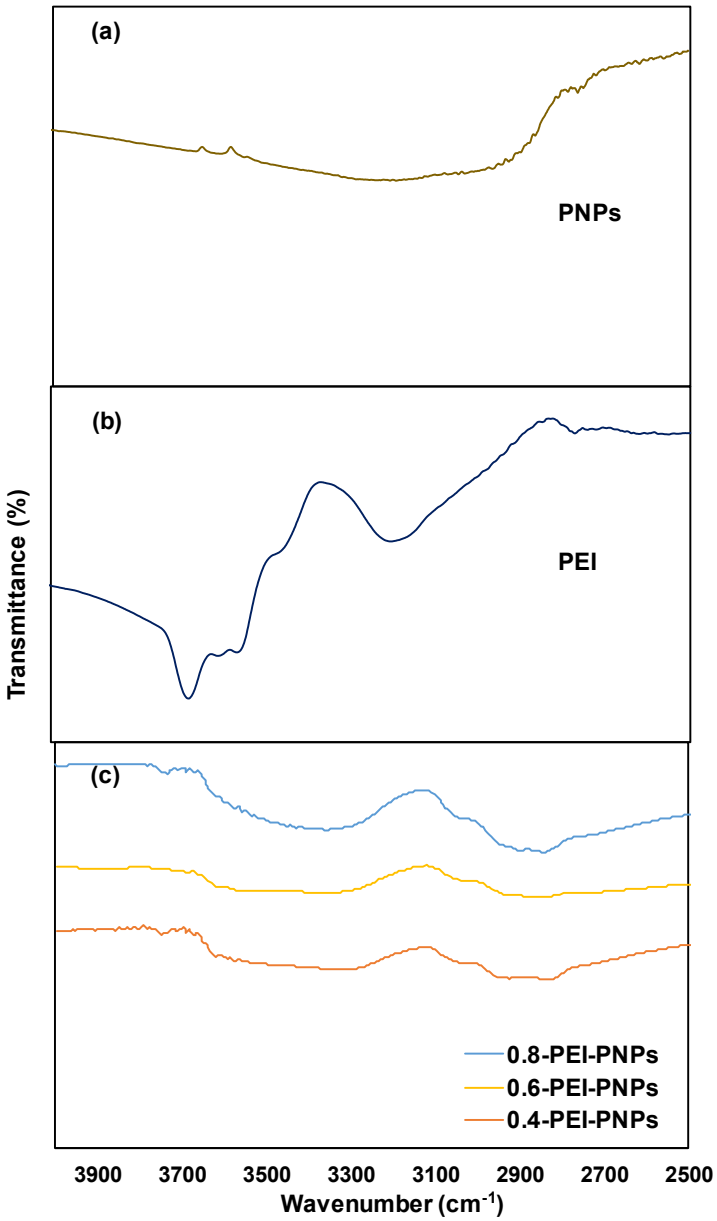

Figure 2.6. FTIR spectroscopy for (a) PNPs, (b) PEI, and (c) functionalized nanoparticles (0.4-PEI-PNPS, 0.6-PEI-PNPs, and 0.8-PEI-PNPs) at framework region of 2500-4000 cm^{-1}.

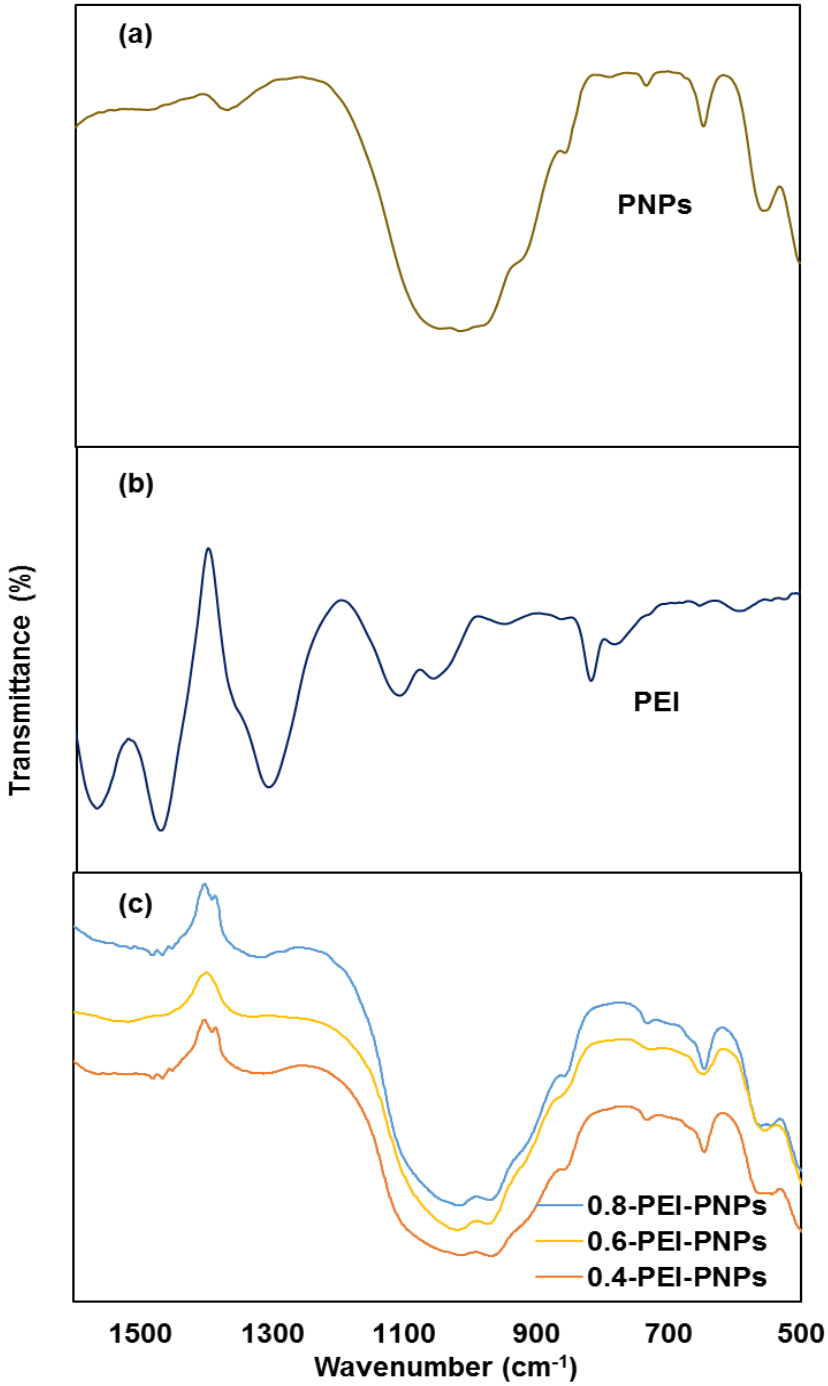

Figure 2.7. FTIR spectroscopy for (a) PNPs, (b) PEI, (b) functionalized nanoparticles (0.4-PEI-PNPs, 0.6-PEI-PNPs, and 0.8-PEI-PNPs) at framework region of 500-1600 com^{-1}.

TGA analysis on the other hand was applied to the PEI-PNP samples to gain insight into its organic content. Figure 2.8 shows the obtained thermograms from burning the different concentrations of PEIs that were anchored onto the nanoparticles. The analysis revealed that the PNP sample lost around 4-5 wt% while the total weight loss from 0.4-PEI-PNP, 0.8-PEI-PNP, 1.2-PEI-PNP, and 1.6-PEI-PNP samples were 9, 12, 12, and 10 wt%, respectively. For all samples, the weight loss occurring below 473 K was attributed to the water in the sample. For the functionalized nanoparticles, the weight loss occurring between 473 K and 933 K was attributed to the organic matter in the sample. The weight loss that occurred in the non-functionalized sample (PNPs) was due to the dehydroxilation (OH^-) that resulted from the heating process [81,94]. In the case of the PEI-PNPs, the weight loss corresponded to the amount of PEI anchored to functionalize the samples. The weight loss in the cases of 0.4-PEI-PNPs and 0.8-PEI-PNPs corresponded to the amount of loaded PEI that bounded to the surface of the nanoparticles in the functionalization process. However, in the case of the 1.2-PEI-PNPs and 1.6-PEI-PNPs, the estimated total weight loss values were ~12 wt% and ~10 wt%, respectively. These results seem to indicate that there is a saturation limit to anchor the polymer under the studied conditions with the optimal loaded amount of polymer being 0.8-PEI-PNPs. After this saturation point, the extra polymer does not anchor on the nanoparticle surfaces, and thus, it is lost in the aqueous solution. Furthermore, the TGA of the lyophilized sample (0.8-PEI-PNPs-FD) resulted in a total weight loss equivalent to 19 wt%.

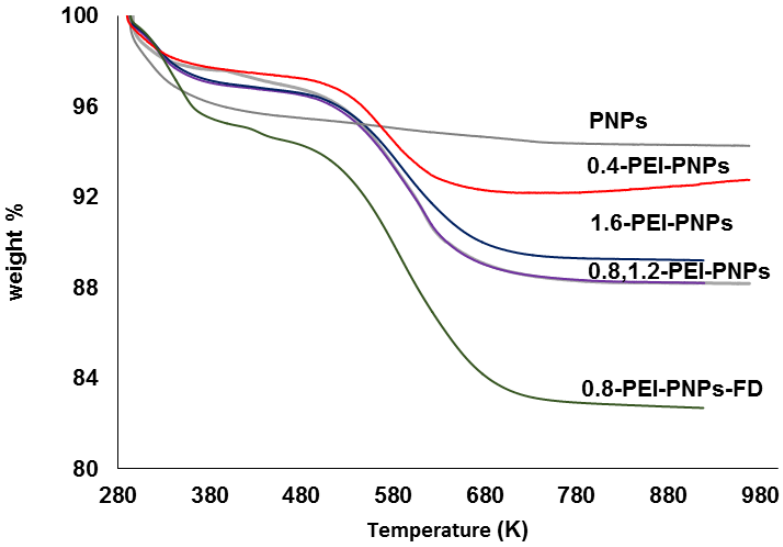

Figure 2.8. TGA thermograms of different PEI-functionalized PNPs with varying PEI concentrations.

2.4.2 Chemical analysis of the considered commercial red dye (CRD)

The results of ICP-AES and S/N tests to analyze the elemental composition of the CRD are listed in Table 2.2. As shown, sodium constituted the majority of the composition of the CRD at ~61 wt%. There were very low concentrations of Mg, K, N, and Fe. In addition, the XRD confirmed that 82.8 wt% of the CRD was halite NaCl (Fig. S1, Supporting Information). Using C, H, N analysis, the organic content (i.e., carbon, hydrogen, and nitrogen) constituted around 10 wt% of the CRD.

Table 2.2. Elemental analysis of considered commercial dye (CRD)**.**

Element	**wt%**
Na	61.11
Mg	0.02
K	0.01
Fe	0.03

N	1.13
C	7.97
H	0.7
N	1.17

Due to the high concentration of NaCl, the FTIR scans did not reveal exclusive organic bands. Thus, the CRD sample was extracted using methanol to reduce the NaCl in the sample to ~ 24 wt%. Thereafter, the main organic functional groups were observed under the FTIR analysis and the results were compared to a sample of AR27, which has known organic functional groups. Figure 2.9 shows the spectra for both samples at frameworks of 500-1800 cm^{-1} (Figure 2.9a) and 2700-4000 cm^{-1} (Figure 2.9b). In addition, the figures include the chemical structure of the AR27 as drawn with ChemDraw software. The results of the AR27 were compared to the extracted CRD (Ext-CRD) sample. The comparison confirmed the absence of aromatics in the extracted CRD sample as no visible signals were observed in around 3030, 1700-1500 cm^{-1}, and 860-680 cm^{-1}, which are assigned to aromatics C-H stretch, aromatic C=C stretch, and aromatic C-H bending [95], respectively. However, these bands were observed clearly in the spectrum of AR27. Further, bands around 1487-1311cm^{-1} pointed to C=N double bond stretching vibration, while bands around 1010-1250 cm^{-1} pointed to C-N, and C-O stretching vibration [28]. However, sufficiently large bands around 2850-2950 cm^{-1} were detected for C-H stretching vibration in the extracted CRD sample compared with AR27 that had a very low intensity bands since the commercial AR27 has a purity of 90% [15]. Also, a band was observed around 3300 for both spectra of AR27 and CRD that assigned to OH stretching. This band was sufficiently large for the AR27 in contrast to that one obtained for the CRD. This suggests that CRD has a lower content of OH, more of alkyl type structure and it has a spectrum close to that for the Dodecane.

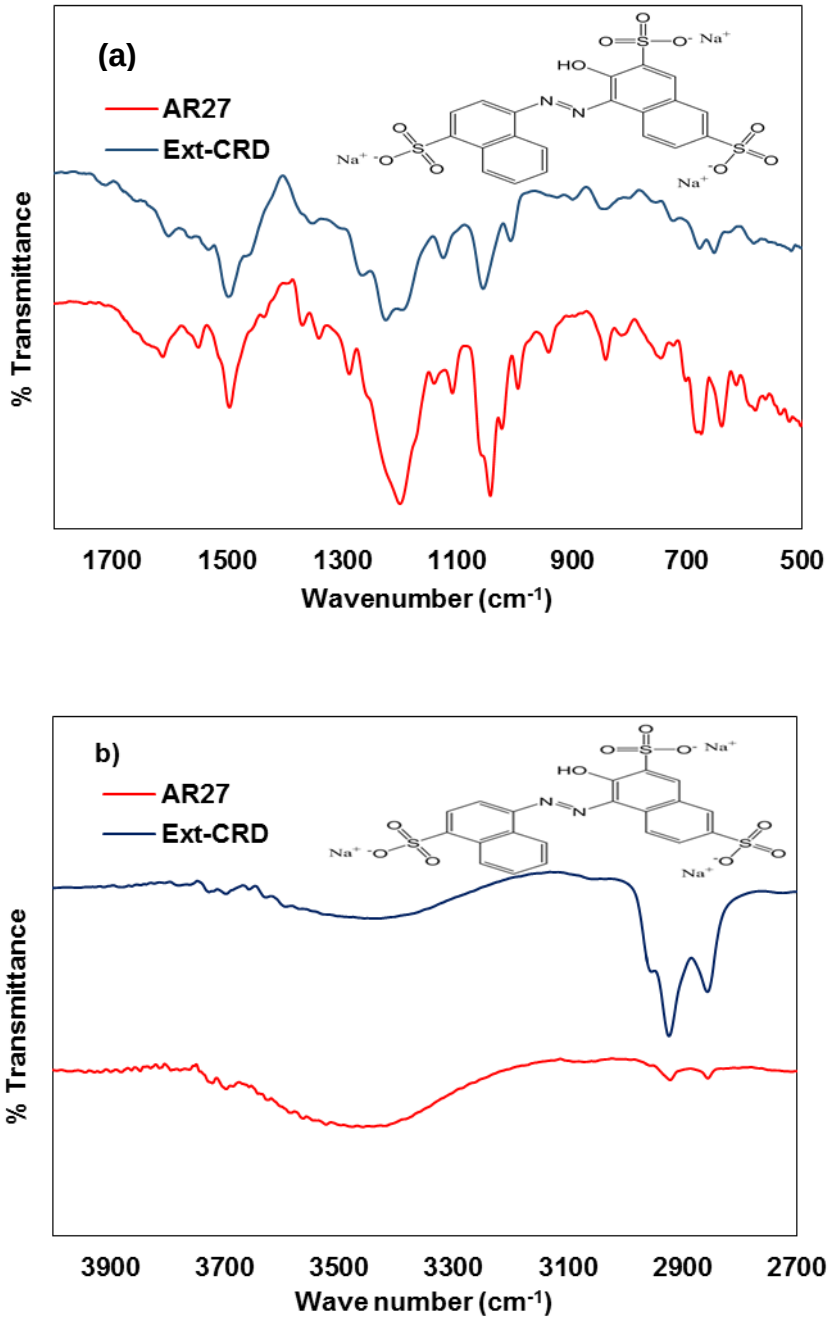

Figure 2.9. FTIR spectra for the extracted dye (Ext-CRD) and the AR27 samples: (a) framework region (500-1800 cm^{-1}) and (b) framework region (2700-4000 cm^{-1}).

2.4.3 Adsorption experiments

2.4.3.1 Effect of solution pH

Figure 2.10 illustrates the sorption capacity (mg/g) of the 0.8-PEI-PNPs at a constant temperature of 298 K and with CRD initial concentrations of 1108 and 554 mg/L with a wide range of pH levels in the sample solution (the pH range was from 3.7 to 11). The results showed no significant influence of the pH level on the ability of the PEI-PNPs to adsorb the CRD in the wastewater sample. PEI, as previously reported, has a very wide range of buffering capacity [96], due to the presence of N at every third backbone atom that allows for a wide range of pKa values. Additionally, the PEI has the possibility to form zwitterion compounds [97] that might be occurring after the interaction with the negative surface of the used pyroxene nanoparticles, which subsequently, transforms the PEI-pyroxene into a pH-switchable structure which responds favorable to the surrounding pH changes, and thus, the adsorption of the CRD dye is the same in the whole studied pH range. However, the exact structure of this CRD dye is not known, but it may be possible that this dye has also multifunctional groups that can be trapped in the synthesized PEI-PNPs at different values of pH [98].

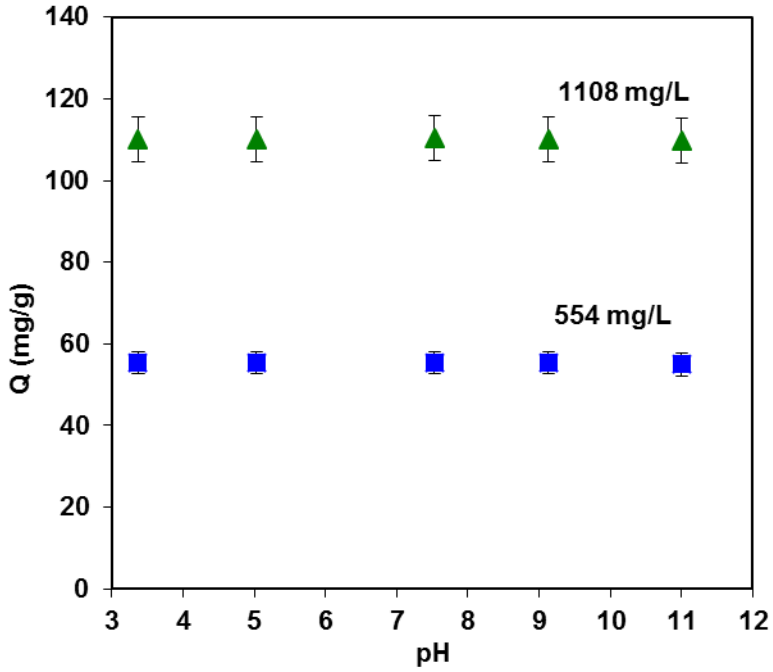

Figure 2.10. Effect of solution pH on the adsorption removal of CRD onto 0.8-PEI-PNPs at CRD initial concentrations of 1108 and 554 mg/L. Adsorbent dose:10 g/L; shaking rate: 200 rpm; T: 298 K.

2.4.3.2 Adsorption isotherm

The adsorption isotherm of different types of adsorbents considered in this study is shown in Figure 2.11. For all cases, the adsorption behavior was described by fitting the experimental data to the Sips model, commonly known as Langmuir-Freundlich model, represented by eq 2.3.

$$Q_e = \frac{K_s\, Q_m\, {C_e}^n}{1 + K_s\, {C_e}^n} \tag{2.3}$$

where Q_m is the maximum monolayer adsorption capacity (mg/g), K_s is the equilibrium adsorption constant related with the affinity of adsorbent-adsorbate binding force ((L/mg)^n), and n is the Sips dimensionless heterogeneity factor that indicates the surface-heterogeneity (unitless).

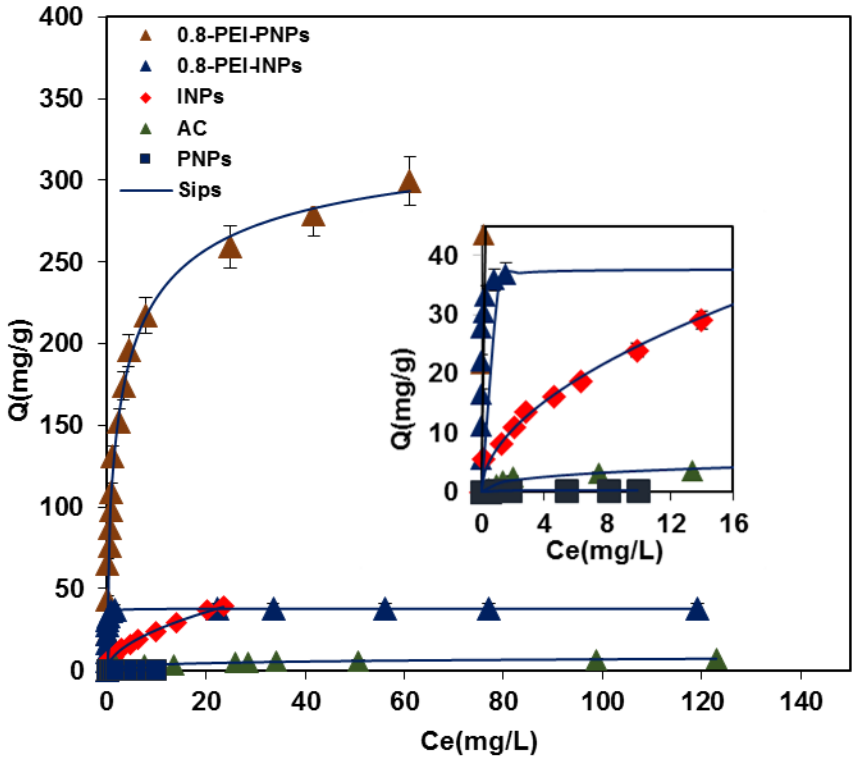

Figure 2.11. Adsorption isotherms of CRD onto different adsorbents. Adsorbent dose: 10g/L; shaking rate: 200 rpm; pH:8, Temperature:298 K. The symbols are experimental data, and the solid lines are from the Sips model [eq 2.2].

The degree of fitting the experimental data was evaluated statistically using the non-linear Chi-square analysis (χ^2) by minimizing the sum of squares of the differences between the experimental values and the predicted ones using OriginPro 8 SR4 software Version 8.0951 [99]. Table 2.3 summarizes the estimated Sips model parameters and the values of χ^2. As indicated by the χ^2 values, for all cases, the experimental data are adequately described by the Sips model. Clearly, the 0.8-PEI-PNPs had the highest adsorption capacity for the CRD. The value of Q_m was 342.5 mg/g, which is much greater than the Q_m values of the other adsorbents. The Q_m values of the considered adsorbents are ranked as follows: 0.8-PEI-PNPs > INPs > 0.8-PEI-INPs > AC > PNPs. Although the 0.8-PEI-PNPs had smallest surface area compared with INPs, 0.8-PEI-INPs, AC,

and PNPs, it had the highest uptake; such that INPs, 0.8-PEI-INPs, AC, and PNPs had a surface areas of 79, 83, 250 (non-microporous surface area), 180 m^2g^{-1}, respectively. This indicates that the adsorption capacity of PEI functionalized pyroxene nanoparticles goes beyond the surface area and involves the interactions of PEI with CRD molecules.

This is also confirmed by the obtained values of the *n* parameter of the Sips model. As seen in Table 2.3, the values of *n* for the 0.8-PEI-PNPs, INPs, and AC are $0 < n < 1$, which indicates the heterogeneity of their surfaces. However, 0.8-PEI-INPs had a fully Langmuirian surface (n=1) indicating there was a monolayer adsorption, and non-fully Langmuirian was for PNPs indicating a heterogeneous surface.

Table 2.3. Estimated Sips isotherm parameters obtained at temperature 298 K and pH 8.0.

Nanoparticle Symbol	Sips parameters			Error analysis
	Q_m (mg/ g)	K ((L/mg)^n)	n (unitless)	χ^2 (unitless)
0.8-PEI-PNPs	342.50	0.01	0.61	0.094
0.8-PEI-INPs	37.74	26.5	1.00	0.006
INPs	40.13	0.001	0.53	1.164
AC	12.79	0.13	0.47	0.089
PNPs	0.31	1.80	1.63	0.001

4.4.3.3 Adsorption Kinetics

The rate of removing the CRD from the wastewater sample was determined using the kinetic experiment. In the experiment, the best adsorbent 0.8-PEI-PNPs was used at a constant temperature of 298 K and a solution pH of 8.0 at two different initial CRD concentration of 554 and 110 mg/L.

Figure 2.12 shows the change in concentration of the CRD in its solution as a function of contact time. For both initial concentrations, the concentration decreased rapidly during the first 15 min and remained unchanged after 30 min of contact, suggesting that equilibrium was nearly reached within 15 min. These results were expected since the 0.8-PEI-PNPs are non-porous as indicated by the BET and *t*-plot analysis. As a result, the external adsorption determined the rate of adsorption as there is no any porous diffusion that could slow the adsorption rate. In general, the process of adsorbing the molecules onto a non-porous adsorbent occurs as follows: (1) bulk diffusion of the molecules in the solution; (2) diffusion of the molecules into a film layer surrounding the adsorbent surface; and (3) adsorption of the molecules onto an adsorption active sites [33,98]. In this experiment, the first step did not occur due to the stirring of the nanoparticles in the solution during the adsorption experiment. In addition, last step was fast and equivalent to the equilibrium reaction [33]. Therefore, the only step that could be considered as the rate-limiting step in the kinetic study is the film diffusion. Hence, the model for the rate of diffusion was determined by using an external mass transfer model as per eq 2.4:

$$\frac{dC}{dt} = -K_m a\,(C - C_s) \tag{2.4}$$

where K_m is the external mass transfer coefficient in liquid phase (m/min), a is the specific surface area of the nanoparticles for the surface per unit volume (m^2/m^3), C is the concentration of the wastewater solution at time t (min), and C_s is the concentration of wastewater at the interface (wastewater-nanoparticles) assuming equilibrium conditions are available on the interface. In detail, the value of C_s can be estimated from reforming the Sips model as per eq 2.5:

$$C_s = \left[\frac{Q}{K_s\,[Q_m - Q]}\right]^{\frac{1}{n}} \tag{2.5}$$

Also, Q can be obtained from mass balance as described in eq 2.2 By substituting eqs 2.2 and 2.5 into 2.4, the following differential equation is obtained:

$$\frac{dC}{dt} = -K_m a \left[C - \left(\frac{(C_o - C)\, V}{K_s\, m\, (Q_m\, - (C_o - C)\, V)} \right)^{\frac{1}{n}} \right] \tag{2.6}$$

eq 1.6 represents a first order ordinary differential equation that can be solved numerically at initial conditions of $C = C_o$ at $t = 0$, and the Sips constants (i.e., K_s, Q_m and n) can be obtained from Table 3 in case of 0.8-PEI-PNPs. The Wolfram Mathematica 10 was used for estimating the $K_m a$ values at different initial concentrations by fitting the obtained experimental data to eq 2.6. As shown in Figure 2.12, the model fit well to the experimental data and described the adsorption kinetics very well. Thus, the estimated $K_m a$ values for both initial concentrations were 0.30 and 0.31 (min^{-1}), respectively. These values agree well with the values reported in literature for the adsorption of heavy hydrocarbon molecules onto silica-based nanoparticles [100]. These results are interesting as the prepared PEI-PNPs outperformed the commercial adsorbents, like AC, which have major shortcoming pertaining to its pore disordered structure that leads to slow adsorption kinetics and low adsorption capacity for large molecules [101], as the case of CRD. In fact, it is common for AC to take days to achieve its adsorption mass transfer equilibrium [24–26,65].

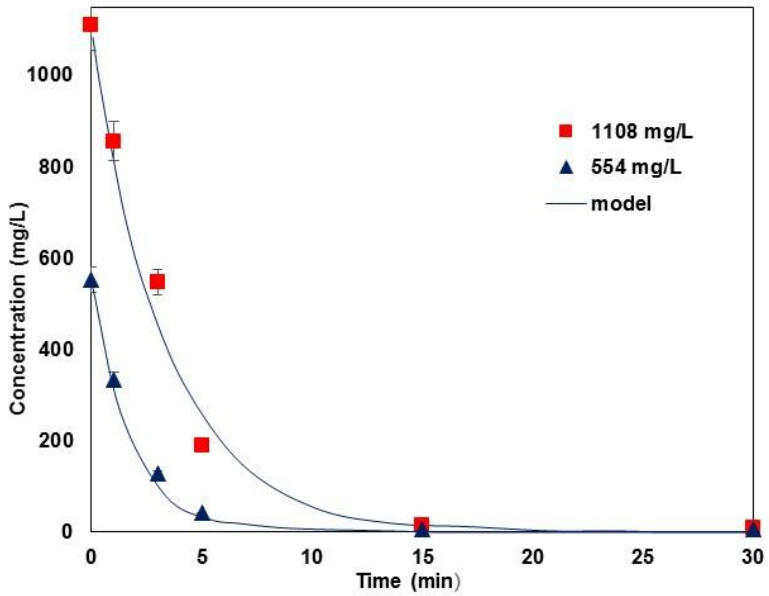

Figure 2.12. Adsorption kinetics of CRD onto 0.8-PEI-PNPs at CRD initial concentration s of 1108 and 554 mg/L. Adsorbent dose: 10 g/L; shaking rate: 200 rpm; pH: 8; T: 298 K. Points are experimental data, and the solid lines are from the external mass transfer model [eq 2.6].

2.5 Conclusion

This study is the first effective attempt to synthesize environmentally friendly and poly(ethylenimine)-functionalized pyroxene nanoparticles at mild conditions for targeting the cleanup of textile wastewater. The prepared PEI-PNPs were sheet-like and spherical like in shape, had a low BET surface area (~ 18 m^2/g) that increased reasonably to ~119 m^2g^{-1} by drying using Lyophilizing method instead of conventional drying of the synthesized materials. The prepared inorganic part of the PEI-PNPs had a small crystalline domain size around 10 nm. The PEI functionality was confirmed using FTIR and TGA analysis. Also, during batch-mode adsorption, the adsorption isotherm was described using Sips model and the PEI-PNPs had a very high adsorption capacity and affinity to dye compared with other adsorbents like activated carbon and iron oxide, without being affected with respect to the medium pH. Moreover, fast adsorption was

obtained (< 15 min) and the kinetic external mass transfer model fit well with the kinetic experimental data and reasonably described the rate of adsorption.

Chapter Three

Poly(ethylenimine)-Functionalized Pyroxene Nanoparticles Embedded on Diatomite for Adsorptive Removal of Dye from Textile Wastewater: Batch and Fixed-Bed Studies

This chapter is adapted from the following publication

A. Hethnawi, N. N. Nassar, G. Vitale, A. D. Manasrah, Poly(ethylenimine)-Functionalized Pyroxene Nanoparticles Embedded on Diatomite for Adsorptive Removal of Dye from Textile Wastewater: Batch and Fixed-bed Studies, Chemical Engineering Journal, (under review), (2017)

3.1 Abstract

In this study, poly(ethylenimine)-functionalized pyroxene nanoparticles (PEI-PNPs) were embedded into Diatomite (D4500), a commonly used filter aid, at < 5 wt% to remove a dissolved commercial textile red dye (CRD) from wastewater in a continues fixed-bed column setup. An array of characterization techniques, such as XRD, BET, HRTEM, and SEM were carried out for the diatomite embedded nanoparticles. The characterization results showed that the filter aid was mainly composed of amorphous diatomaceous earth, its adsorption surface area and capacity toward the CRD were improved significantly via embedding more nanoparticles. CRD uptake over the diatomite embedded with 1.5, 3, and 5 wt% of PEI-PNPs has been investigated in batch equilibrium adsorption study, with isotherms being fairly explained by the Sips model. After that, the adsorption performance of fixed-bed column was tested for D4500 before and after embedding it with virgin and PEI-functionalized nanoparticles of pyroxene, iron oxide, and activated carbon (AC) to determine the breakthrough curves under different operational conditions (e.g., inlet concentration of CRD, inlet flow rate, bed height, and nanoparticle concentration in diatomite, %nps). The convection-dispersion transport equation was used to describe the obtained breakthrough curves, which enabled the determination of the axial dispersion coefficient (D_L) and the Peclet number (Pe). Additionally, the breakthrough data was analyzed using the equivalent length of unused bed (H_{UNB}) approach. In this approach Pe was correlated with H_{UNB} with a good accuracy with the correlation: $H_{UNB} = 0.013\,Pe + 1.25$ when Q and C_o are the control operational parameters, while the correlation: $H_{UNB} = 4.08\,\mathrm{e}^{-0.002\,\mathrm{Pe}}$ when Z and *%nps* are the control operational parameter. These correlations can be helpful and useful for scaling up our proposed process for real industrial applications.

3.2 Introduction

With an increased demand for textile products, textile wastewater has become a major issue because it contains a variety of pollutants and toxic substances including organic loads, salts, surfactants, and dyes [48,102,103]. Dyestuff, however, are often the most difficult substances to treat, and therefore, they have received a lot of attention over the last few decades [41,104,105]. Biological treatment technology, for example, removes a significant amount of the organic content, but it is ineffective in removing dyes, and it generates high sludge amounts[21,41]. Similarly, coagulation/ flocculation, advanced oxidation, and membrane filtration [106] are effective but generally limited by high operational costs [107]. Therefore, adsorption is involved as one of the most effective physical processes for the decolourization of textile wastewater [107–109]. Conventional adsorbents like activated carbon (AC) showed a satisfactory result in the fixed bed column studies when followed by the biological treatment [4,18,110]. However, AC has recently been replaced with other adsorbent materials that have a higher adsorption affinity for various types of pollutants and are more environmentally friendly [2,111,112]. In addition, AC has major shortcoming pertaining to its pore disordered structure that leads to slow adsorption kinetics and low adsorption capacity for large molecules.

Alternatively, several researchers have been studying the use of nanoadsorbents either as powder nanoparticles or functionalized with some active species, in which the latter performed well in removing heavy metals and some organic substances from the wastewater [15,27,28,33,35,98,113–117]. For instance, iron oxide type nanoparticles when functionalized with different polymeric materials its removal efficacy of organic and trace pollutants has been improved outstandingly, especially in batch adsorption processes [15,118,119]. Nevertheless, the batch mode is limited when it comes to real wastewater treatment processes. Moreover, the data

obtained in the batch studies cannot be applied to wastewater treatment plants where the contact time is not sufficient for attaining equilibrium. Thus, from an industrial practice point of view, continuous flow fixed-bed column studies are needed [4,16,18,113]. This column is usually simple to operate by packing it through a stationary bed of a specified adsorbent. However, for the case of nanoparticles, using powder nanoparticle as filter medium in a packed bed column is challenging as it will result in low loading rate with high head loss. To overcome these challenges, some studies integrated nanoparticle technology with sand bed filtration in different ways in treatment of various types of wastewater [9,68,98,120]. Nassar et al. [13], for instance, tested decolourizing olive mill wastewater in a continuous-mode process using the column experiment after combining sand filtration with adsorption using iron-oxide nanoparticles (INPs). The INPs-embedded sand performed much better than the standalone sand. In addition, Reddy et al. [68,120], used adsorption integrated with filtration in their set up by developing a point-of-use filter. This filter compressed sand layers that were placed above a suspended solution of cupric oxide nanoparticles. This design provided adsorption using cupric oxide nanoparticles for the arsenic removal. In addition, the sand was used to trap the cupric oxide nanoparticles after adsorption and to provide further filtration to treat wastewater. Although, the point-of-use- filter is an efficient design in arsenic removal, however, it is not scalable to an industrial application as an adsorption integrated technology with sand bed filtration.

In our previous study [121], we used poly(ethylenimine) (PEI) to functionalize earth abundant pyroxene nanoparticles (PNPs) to remove commercial red dye (CRD) from textile wastewater in a batch process . The results showed a high removal efficiency and rapid kinetics of the adsorption process for PEI-PNPs (donated for functionalized-pyroxene with PEI) compared with that of magnetite nanoparticles and commercial activated carbon. Hence, this work aims at exploring the

possibility of utilizing the novel nanoparticle adsorbents of PEI-PNPs in a continuous mode using a fixed bed column. The PEI-PNPs nanoparticles were embedded into diatomite (D4500), a commercial filter aid, at low concentration (< 5 wt%). Afterwards, the adsorptive removal of CRD column operation was conducted. The influence of bed depth (Z), inlet CRD concentration (C_o), flow rate (Q), and the concentration of the embedded nanoparticles (%nps) in D4500 were all investigated. Further, the column experimental results under different test conditions (Z, C_o, Q, and nanoparticle concentration in D4500) were fitted with the convection-dispersion equation to describe the breakthrough curves. Batch adsorption experiments were also conducted to determine the adsorption capacity as well as kinetic parameters, which later used to estimate the breakthrough profiles for the adsorption column operation. The modeled breakthrough profiles along with the operational parameters of the column tests and the batch adsorption data were successful in describing the adsorption behavior of PEI-PNPs nanoparticles embedded into diatomite in fixed-bed column.

3.3 Materials and Methods

3.3.1 Chemicals and reagents

Chemicals with different purities were purchased from Sigma Aldrich, Ontario, Canada: sulfuric acid (95-98%), iron tri-chloride (97%), sodium silicate solution ((10.6%) Na_2O, and (26.5%) SiO_2), iron sulfate hexa-hydrate (≥99%), ammonium hydroxide (28-30% NH_3), hydrogen peroxide (30-35%), and polyethylenimine (PEI) (99%). The sodium hydroxide beads (99.99%), and the GAC (90%) were bought from VWR International, Edmonton, Canada, and from the CABOT Company, Estevan, Saskatchewan, Canada, respectively. All the mentioned materials were used as received without any further purifications. Executive Mat Ltd, Calgary, Canada, supplied a commercial red dye sample (CRD), which is used as an adsorbate in this work. The following

types of filter aids (Diatomite) were also provided by Executive Mat Ltd: D4500, D5000, D6000, EP-powder, and RD-silica.

3.3.2 Synthesis of embedded nanoparticles in Diatomite

Pyroxene and magnetite, types of nanoparticles, were synthesised, functionalized, and then embedded into diatomite (D4500) for comparative purposes. In detail, pyroxene nanoparticles were prepared from a hydrothermally treated gel as reported from the previous study [80,81]. This gel was synthesized by a reaction between acidic and basic solutions; experimentally, the acidic solution was prepared by adding 18.067 g of sulfuric acid in 90 g of deionized water; then, 20.793 g of iron tri-chloride was gradually added to the solution, which was continuously stirred (300 ppm). The basic solution, on the other hand, on the other hand was formed by adding 21.413 g of sodium hydroxide to 60.0 g deionized water; 30.707 g of sodium silicate was then added while the solution was stirred. Then the acidic solution was added gradually to the basic solution while magnetic stirring for 15 min. The magnetic stirring provided a homogenous orange-yellowish gel. The gel was crystalized hydrothermally by a 300- ml reactor vessel (A2230HCEB, Parr Instrument Company, Moline, I1, USA). This reactor contains a heating mantle, which is connected to a temperature controller loop. Also, it has a gauge pressure and mechanical stirrer with a speed controller. Then, the reactor was heated to 433 K at 300 rpm for 72 h (time for crystallization). After that, the reactor was cooled down for 4 h and the resulting gel was removed from the reactor vessel. Then, the gel was filtered, washed with deionized water, and eventually was left over night at room temperature for drying.

Magnetite nanoparticles, on the other hand, are other types of nanoparticles that were synthesized as reported by the previous study [121]. In detail, a solution of ferrous sulfate was prepared by dissolving 6 g of ferrous sulfate hexa-hydrate into 100 ml of deionized water. 15 ml of ammonium

hydroxide was added to the solution. Then, a 15 drops of hydrogen peroxide were added as an adjustable amount to obtain a specific blackish color indicating the formation of magnetite. Finally, the solution was filtered, washed, left overnight, and the magnetite nanoparticles (INPs) were recovered for further usage.

After synthesizing pyroxene and magnetite nanoparticles, both were separately functionalized with PEI following the same reported procedure in the first study [121]. Briefly, two solutions A, and B were prepared. Solution A was a 0.8 wt% of PEI. Solution B was 1 wt% of suspended nanoparticles. Solution A was added to solution B drop by drop to at room temperature. After that, the solution was magnetically stirred for 2 h. Then it was filtered, and washed to remove the unbounded PEI. Finally, the PEI-nanoparticles were dried and recovered. All the previously synthesized nanoparticles of pyroxene, magnetite, PEI-functionalized pyroxene, and PEI-functionalized magnetite were donated as PNPs, INPs, PEI-PNPs, and PEI-INPs, respectively. After that, the prepared nanoparticles were embedded on a selected filter aid of D4500. A suspended 5 wt% of sand was prepared first. Then, the nanoparticles were added to the suspended solution under stirring for 15 min. The suspended was filtered, and dried. Finally, the product was recovered for the batch and column adsorption studies. The embedded diatomite with the nanoparticles of PNP, INPS, PEI-PNPs, and PEI-INPs at 5 wt% were donated by 5D-PNPs, 5D-INPs, 5D-PEI-PNPs, and 5D-PEI-INPS. The previously functionalized diatomite was used to conduct fixed-bed column studies to select one, which had the best adsorption capacity for CRD (longest breakthrough time). Then the screened diatomite was used to perform breakthrough dynamic study. In this study, D4500 was also embedded with 1.5 wt%, and 3 wt% of the selected nanoparticles to study the influence of embedding various concentration of nanoparticles on D4500.

3.3.3 Characterization of embedded nanoparticles in Diatomite

3.3.3.1 X-ray diffraction (XRD)

To identify the structure of the provided types of filter aids, X-ray diffraction (XRD) analysis was conducted, providing Diatomite crystalline structural identity. XRD was also performed to estimate Diatomite crystalline size domain. This analysis was conducted by an Ultima III Multipurpose Diffraction system (Rigarku corporation, The woodlands, TX, the USA), which operates with Cu Kα radiation as the X-ray source at 40 kV and 44 mA with a θ-2θ goniometer. The analyzer had a glass top-loaded sample holder that has a cavity of 0.5 mm in depth, where the sample for the analysis was placed and uniformly distributed with help of a microscopic slide. The analyzer provided scans in the range of 3-90° 2-θ degrees using a 0.02° step and a counting time of 1.0° per min. The results were shown as peaks forming a specific pattern. The obtained peaks computed the crystalline size domain by calculating the full width at half maximum (FWHM). The calculations were implemented in the software JADE after applying Scherer equation. Also, JADE used to fit the experimental profile to pseudo-Voigt profile function [83].

3.3.3.2 Textural properties

Sorption surface area and porosity of the provided filter aids was determined by Brunear–Emmett-Teller (BET) surface area and porosity analysis (TriStar II 3020, Micrometrics Instrument Corporation, Norcross, GA). Also, the influence of embedding D4500 with 1.5, 3, and 5 wt% of PEI-PNPs was tested. The BET analysis was conducted by exposing a pretreated amount (< 200 mg) of each sample to liquid nitrogen, which works as a probe molecule, under investigation at 77 K, which allows to submit the adsorption-desorption isotherms. Then, the BET surface area was estimated using BET equation. This analysis was conducted for the samples after pretreating them

inside sample holder cells. The pre-treatment was done by heating the sample overnight to 423 K with flow of nitrogen gas, simultaneously.

3.3.3.3 Scanning electron microscopy (SEM)

A field emission Quanta 250 electron microscope was a type of scanning electron microscopy (SEM), which was manufactured by FEI was used to confirm the successful embedding of the D4500 with PEI-PNPs in 5D-PEI-PNPs. The sample for the analysis was prepared by placing very small quantity of each powder over a carbon tape sample holder. The carbon tape sample holder then was taped to allow for the extra amount of the powder to release.

3.3.3.4 High resolution transmission electron microscopy (HRTEM)

High-resolution transmission electron microscopy (TEM) analysis was performed for D4500 and its embedded with PET-PNPs type of nanoparticles in 5D-PEI-PNPs to test the presence of nanoparticle on D4500 and their interaction. The sample was prepared as follows: 0.5 mg of the sample was suspended in around 4 ml of ethanol. The suspended solution was sonicated. Then, for the analysis, few drops were deposited into a Formvar/carbon copper grid sample holder and allowed to dry. Finally, the images were collected by FEI Tencnai F20 FEG TEM with an accelerating voltage of 200 kV.

3.3.4 Adsorbate

A commercial red dye sample (CRD) was used as adsorbate, which was analyzed in our previous study[121] using X-ray diffraction, thermogravimetric analysis (TGA), carbon, hydrogen, and nitrogen (C, H, and N) elemental analysis, inductively coupled plasma-atomic emission spectroscopy (ICP-AES), sulfur/nitrogen analysis, and infrared spectroscopy(IR). The reported

results showed that CRD sample had a composition of 83 wt% NaCl (halite), nearly 12 wt% organic (carbon, hydrogen, and nitrogen) with absence of both sulfur and aromatic rings.

3.3.5 Batch adsorption experiments

Batch-mode adsorption was conducted at constant temperature of 298 K and pH of 8.10 for one selected type of embedded nanoparticles on Diatomite at mass percentages of 1.5, 3, and 5 wt%. First, 100 mg from one type of the previously mentioned powders was added to a 10-ml aqueous solution that contained a specific concentration of the CRD inside a 25-ml glass vials. Afterward, the vials were closed very well to avoid the change in the concentration of the CRD solution during the experiment. Then, batch adsorption for the CRD was carried out by shaking the glass vials by a Wrist Action shaker (Burrel, Model 75-BB) for a specific time for the equilibrium to occur. Then, all the samples were left on the lab bench overnight, which allows for adsorbent settling. After that, the samples were centrifuged for 10 min at 5000 rpm in the Eppendorf Centrifuge 5804 to separate the residual after the adsorption. The separated supernatant solution was measured by UV-vis Spectrophotometry (UV-vis) using a Nicolet Evolution set at a wavelength of 511 nm. UV-vis allows to determine the various concentrations of CRD via establishing a calibration curve at wave length of 511 nm using as standardized model solutions of CRD. The concentrations of the standardized model solutions were measured in terms of TOC (mg/L) by using a Shimadzu Total Organic Carbon Analyzer (TOC-L CPH/CPN). Then, other calibration curve was established to relate the obtained concentration by the TOC analyzer with the absorbance that obtained by UV-vis. The adsorbed amount of CRD, in terms of mg TOC/g of dried adsorbent, was estimated by the mass balance analysis as per eq 3.1**:**

$$Qe = \frac{C_o - C_e}{m} V \quad (1)$$

where C_o is the initial concentration of CRD in the solution (TOC, mg/L), C_e is the equilibrium concentration of CRD in the supernatant (TOC, mg/L), *V* is the solution volume (L), *m* is the dry mass of adsorbent (*g*).

3.3.6 Column adsorption study

Column experiments were implemented to study the performance of D4500 after integrating it with nanoparticles. Figure 3.1 demonstrates the setup of the fixed bed column for this experiment at 298 K. The column system contained a vertical glassy column of internal diameter of 0.9 cm and 15 cm in length. Before each experiment, the column was packed with an approximately 1 cm of cotton layer at the bottom to provide closely packing. Then, certain amount of adsorbent was packed and tightly closed to avoid the fluctuation on inlet flow rate. A uniform flow rate was flowed downward to the column system by a 50-ml high pressure stainless steel syringe pump with 1/8" Swagelok fitting (HARVARD). The effluent samples were collected periodically from the bottom of the column during the experiment. Then, each sample concentration was measured using UV-vis and TOC analyzer. In fixed-bed study, 6 individual experiments with different type of adsorbents were conducted. These adsorbents were D4500, AC, 5D-PNPs, 5D-INPs, 5D-PEI-INPs, and 5D-PEI-PNPs. Then, the best one from the previously mentioned adsorbents was selected. The screening was performed based on long period time of breakthrough. Afterward, the kinetic parameters of inlet flow rate (*Q*), inlet dye concentration (C_o), bed height (*Z*), and the embedded nanoparticle concentration in diatomite (%*nps*) were all investigated for the screened adsorbent by one factor at one time (OFAT) design of experiment method. In detail, the effect of inlet dye concentration study was performed by running 3 experiments with predetermined concentrations of 49, 74, and 99 mg/L. The inlet flow rate study, on the other hand, was performed by running other 3 experiments with flow rates of 0.8, 1.2, 1.5 ml/min. The effect of nanoparticle

concentration study carried out by running 3 experiments with nanoparticle concentrations of 1.5, 3, and 5 wt%. Finally, the bed depth effect study was occurred by running 3 experiments with bed heights of 2.5, 3.7, and 7.3 cm.

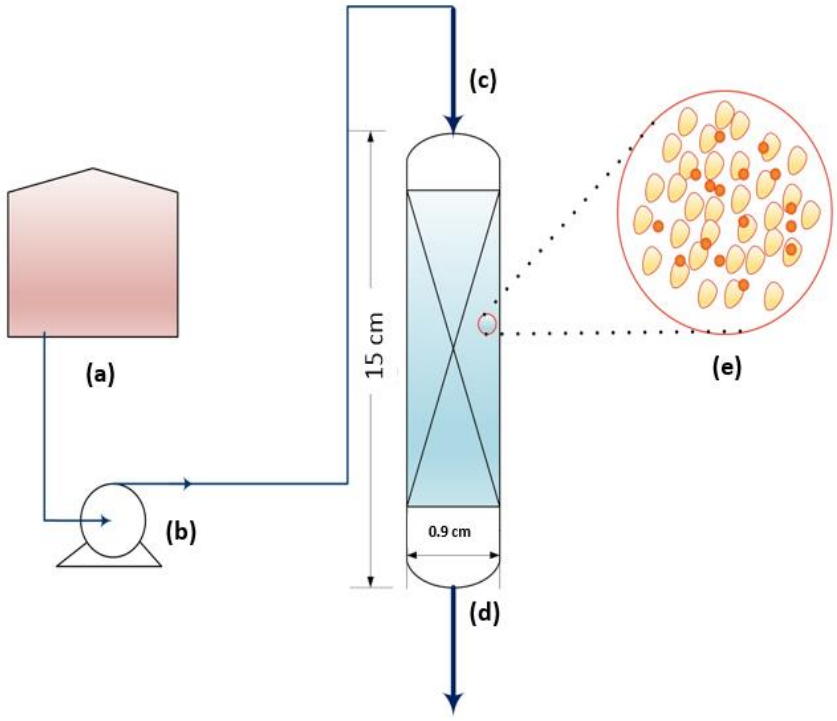

Figure 3.1. Schematic representation of the fixed-bed experimental set up. (a) Dye feed tank, (b) syringe pump, (c) inlet flow rate, (d) outlet flow rate, and (e) nanoparticle embedded on D4500.

3.4 Theoretical background

3.4.1 Batch equilibrium adsorption

In accordance with the adsorption mechanism of CRD, several currently reported adsorption isotherms are used to fit the experimental batch adsorption results in order to illustrate the equilibrium characteristics. Among these is the Sips model. This model is a combination of the Freundlich and Langmuir isotherms, which represents systems for which one adsorbed molecule could occupy more than one adsorption site [81,122]. It also takes into account the interaction

between the adsorbed molecules, in contrast to Langmuir theory, which assumes that the surface of the adsorbent is homogenous, and therefore the adsorption is localized and constant over all active sites, such that each active site can accommodate only one molecule. The Sips equation can be expressed by eq 3.2 [123]:

$$Q_e = \frac{Q_m K C^{n_s}}{1 + K C^{n_s}} \quad (3.2)$$

where Q_m is the maximum monolayer adsorption capacity (mg/g), K is the equilibrium adsorption constant that is related with the affinity of adsorbent-adsorbate binding force ((L/mg)^n), and n_s is the Sips dimensionless heterogeneity factor (unitless), which indicates the adsorbent heterogeneity and the interaction mode.

3.4.2 Break through curve (BTC) and mass transfer zone (MTZ)

Estimation of breakthrough curve shape (BTC) is one of the most important factors in designing the ideal fixed-bed column. This is because BTC provides information concerning the feasibility of using an adsorbent in a continuous process [62,124,125]. The BTC for the given fixed-bed column is essentially established by plotting the exit concentration from the fixed-bed versus lapse time or reacted volume throughput [126,127]. The BTC of the concentration gradient with respect to time depends on the designed dynamic parameters, namely: the characteristics of adsorbent in the fixed-bed column (mass or bed-depth, particle size), the adsorbate inlet concentration, flow rate, and length over diameter (L/D) of the fixed-bed column [126,128]. The breakthrough time (t_b) is arbitrarily chosen when the effluent concentration approaches 5% of C_o (influent adsorbate concentration). Saturation time (t_s), on the other hand, is chosen when the adsorbent is exhausted [126,129]. Time equivalent to stoichiometric capacity, can mathematically be expressed as:

$$t_t = \int_{t=0}^{t=\infty} (1 - \frac{C_t}{C_o})\, dt \quad (3.3)$$

while the time equivalent to usable capacity can be expressed as:

$$t_u = \int_{t=0}^{t=tb} (1 - \frac{C_t}{C_o})\, dt \tag{3.4}$$

The unused bed height is given from the usable capacity of the bed up to t_b. Thus, the value of t_u is approximately equal to the value of t_b. The value of t_u/t_t is the fraction of the total bed capacity or the utilized length up to break point. Mass transfer zone (MTZ) is formed when the adsorption takes place, which can be controlled by the dynamic parameters [126,128]. All the aforementioned dynamic parameters in the section "column study" can influence the life time of the column, which is expressed in terms of unused bed length (H_{UNB}) or MTZ. H_{UNM} or MTZ can be calculated as [126]:

$$H_{UNB} = \left(1 - \frac{t_u}{t_t}\right) H_T = \left(1 - \frac{t_b}{t_t}\right) H_T \tag{3.5}$$

where H_T is the total bed height (cm). Used bed length H_B up to break point is also estimated as:

$$H_B = \left(\frac{t_b}{t_t}\right) H_T \tag{3.6}$$

The adsorbed quantity of CRD (q_{total}) in mg for given dynamic conditions is equal to the product of the area under the breakthrough plot and the flow rate. It can be calculated by applying the mass balance such that the absorbed concentration (C_{ads}) represents the difference between inlet (C_o) and outlet (C_t) concentrations ($C_{ads} = C_o - C_t$), where C_o, C_t, and C_{ads} are in mgL^{-1}. Thus, q_{total} is calculated as follows [128–130]:

$$q_{total} = \frac{Q\ A}{1000} = \left(\frac{QC_o}{1000}\right) \int_{t=t_{to}}^{t=t_{total}} C_{ads}\ dt \tag{3.7}$$

where Q is the flow rate (ml/min), A is the area under the BTC and t (min) represents the time that can be t_{total}, t_s, and t_b. Therefore, the total CRD sent to the column (m_{total}) is as follows [126,130]:

$$m_{totol} = \frac{C_o\, Q\, t_{total}}{1000} \tag{3.8}$$

then, the total removal (%) of the CRD (*% Removal*) can be calculated from the equation [130]:

$$\%\, Removal = \left(\frac{q_t}{m_{total}}\right) \times 100 \tag{3.9}$$

3.4.3 Modelling of column dynamic adsorption

Developing a general mathematical model that predicts the time dependent concentration profiles of adsorbed organic compounds on nanoadsorbents embedded on diatomite in the fixed bed column under isothermal conditions is needed. The principle of the theoretical model is to determine the dynamic capacity of the adsorbent bed without any need for time and capital intensive experimentation [131]. Hence, the model response must match the experimental data by employing suitable prediction tools for various solid adsorbents. Moreover, the theoretical model of breakthrough curves allows us to link the experimental data of batch adsorption, and thus, achieving a successful description behavior of adsorption mechanism within a continuous fixed-bed adsorption process [3,132].

In a fixed-bed adsorption column shown in Figure 3.1, the adsorption process begins when the fluid (wastewater influent) moves through the bed, the concentration of the adsorbate in the feed decreases along the bed (i.e., in the axial direction). In this model, the fluid concentration is assumed to be uniform at all points on the cross section of the bed at any axial position. As such the adsorbate concentration does not depend on the radial position in the bed. At any point of the bed, adsorbate molecules are transported from the bulk to the surfaces of nanoadsorbents

integrated with diatomite by convective mass transfer through a film around the particle. Hence, most of the adsorbate molecules get adsorbed on the outer surfaces of the nanoadsorbents [133,134]. The following assumptions are made in the theoretical derivation of our developed convection-dispersion mathematical model [135,136]:

- The fixed-bed column operates under isothermal condition.
- No chemical reaction occurs in the column.
- Axial dispersion is considered along with the longitudinal axis of the column.
- Concentration gradients profile due to the radial flow are neglected.
- The nanoadsorbent-embedded Diatomite (D4500) are considered to be spherical in shape and homogeneous in density and size.
- The axial velocity is assumed to be constant along the column.
- The adsorption equilibrium is described by the Sips isotherm model.

Based on these assumptions, the dynamics behavior of a fixed-bed column is described by a set of convection-diffusion equations, coupled with source terms due to adsorption and diffusion inside the nanodsorbent particles. Hence, the mass balance of the adsorbed component in a cross-section of the column is governed by eq 3.10**:**

$$-D_L\frac{\partial^2 C}{\partial z^2}+v\frac{\partial C}{\partial z}+\frac{\partial C}{\partial t}+\frac{1-\epsilon}{\epsilon}\frac{\partial q}{\partial t}\ =0 \qquad (0<z<L, 0<t<\infty) \tag{3.10}$$

where, C is the bulk adsorbate concentration in the fluid flowing through the bed (mg/L), D_L is the axial dispersion coefficient (m/s^2), v is the interstitial velocity (m/s), q is the adsorbed mass of adsorbate per unit mass of solid, z is the distance (m), t is the time (min) and ϵ is the porosity (unitless). In this equation, the first term of this model is accounted for axial dispersion with the effective diffusivity (D_L) that accounts to Eddy diffusion. The axial variation of fluid velocity is described by the next two terms and the last term is the volume-average adsorbate loading per unit

mass. This term ($\frac{\partial q}{\partial t}$) accounts for the variation of adsorbed amount throughout the nanoadsorbent-embedded Diatomite, due to external mass-transfer resistance, by averaging the rate of adsorption over the adsorbent particles [137].

The following initial and boundary conditions are considered:

$$C(z,0) = 0 \qquad (0 < z < L) \tag{3.11}$$

$$at\ z = 0,\ C_{in} = C - \left(\frac{D_L}{v}\right)\left(\frac{dC}{dz}\right) \qquad (0 < t < \infty) \tag{3.12}$$

$$at\ z = L,\ \frac{\partial C}{\partial z} = 0 \qquad (0 < t < \infty) \tag{3.13}$$

This model is usually coupled with various adsorption equilibrium model and/or kinetics adsorption to model experimental data in different applications [138,139]. This adsorption models describes the concentrations of adsorbate in the liquid and solid phases through an adsorption equilibrium or kinetics at the solid-liquid interface. In this study, the equilibrium isotherm adsorption model is used to describe the uptake rate ($\frac{\partial q}{\partial t}$) using the Sips model as described in the previous section eq 3.2**.** It is expressed on the basis of unit adsorbent volume, in terms of the intra-particle diffusion which can be obtained from the solution of the appropriate intra-particle diffusion equation. However, other isotherm models such as Langmuir and Freundlich are used to describe the uptake rate [138,140,141]. In our model, we are implementing the Sips model which includes the heterogeneity factor of nanoadsorbent-embedded Diatomite surface (n_s) and stems from the adsorbent or the adsorbate or a combination of both. The values of n_s are varying from 0.5 to 0.6 based on the batch adsorption results. This mean that our model is sensitive to these values (i.e., n_s) which may affect the steepness of breakthrough profile. Thus, the batch adsorption process is used to determine the adsorption equilibrium constant (K), maximum uptake (Q_m) as

well as the kinetic parameters, which were later employed to calculate the breakthrough profiles in fixed-bed adsorption column. Differentiating eq 3.2 with respect to time yields eq 3.14:

$$\frac{dq}{dt} = \frac{n\,K\,Q_m C^{n-1}}{(1+KC^n)^2}\frac{dC}{dt} \tag{3.14}$$

After combining eq 3.14 and eq 3.10**,** the final fluid phase balance equation is presented in eq 3.15:

$$-D_L\frac{\partial^2 \mathrm{c}}{\partial z^2} + v\frac{\partial \mathrm{c}}{\partial z} + \frac{\partial \mathrm{c}}{\partial t} + \frac{1-\epsilon}{\epsilon}\left(\frac{n\,K\,Q_m c^{n-1}}{(1+Kc^n)^2}\frac{dc}{dt}\right) = 0 \tag{3.15}$$

Since nonlinear adsorption equilibrium is considered, an exact solution to eq 3.15 is basically impossible [142]. However, the preceding set of partial differential equations **(eqs 3.10-3.14)** are solved numerically using method of lines technique [143,144]. This technique is common for solving non-linear partial differential equations. Indeed, many authors have used this method for the discretization of this phenomenon [143,144]. In this method, the feed concentration in the bed is discretized (N =100 sections) in the spatial direction. The bed length is divided into (N-1) grids which are numbered from 1 to N through varying the length (Z) from 0 at entrance to L at the exit. Then, the concentration of feed is modeled through ordinary differential equations and evaluated with time at each node [145]. A mathematical algorithm is developed and implemented into a computer program with Mathematica (v.10.2) software to solve these couple of equations using NDSolve code [146,147].

Flow experiments were conducted using information from batch isotherms. For each experiment specified parameters, including; mass of nanoadsorbents, influent adsorbate concentration, flow rate, and length of fixed bed was studied. Each of these parameters had a significant impact on the shape of the generated breakthrough curve. For each breakthrough curve one parameter, effective diffusion coefficient (D_L), was fit with experimental data using Manipulating code in order to get

the proper value of D_L that minimizes the square root of the sum of the squares of residual between the numerical values and experimental data [148]. Hence, the simulated breakthrough curve using the above model with the least squares gave a goodness-of-fit to the experimental data.

It is worth mentioning that the solution of this model allows to determine the time of the breakthrough appearance, which is recognized as the time at which the outlet concentration reach the $C/C_0 = 0.05$ value. Also, the shape of the breakthrough curves is related to the height of the mass transfer zone. In other words, the breakthrough time is proportional to the nanoadsorbents capacity, however, it is inversely proportional to the height of the mass transfer zone value [3,149].

3.5 Result and discussion

3.5.1 Characterization of embedded nanoparticles in Diatomite

3.5.1.1 X-ray diffraction (XRD) and textural properties

Figure 3.2 shows the obtained XRD patterns of filter aids of D4500, D5000, D6000, EP-powder, and RD-silica. The figure shows that all obtained patterns confirm the structure of cristobalite-SiO_2 which was as the provided raw data sheets discloses. The cristobolite-SiO_2 structure was identified by comparing the experimental signals with a background signals that reported in the file (pdf) card #01-076-2564 (2005 International Center for the Diffraction Data base included in the program JADE V. 7.5.1Materials Data XRD Pattern Processing Identification and Quantification).

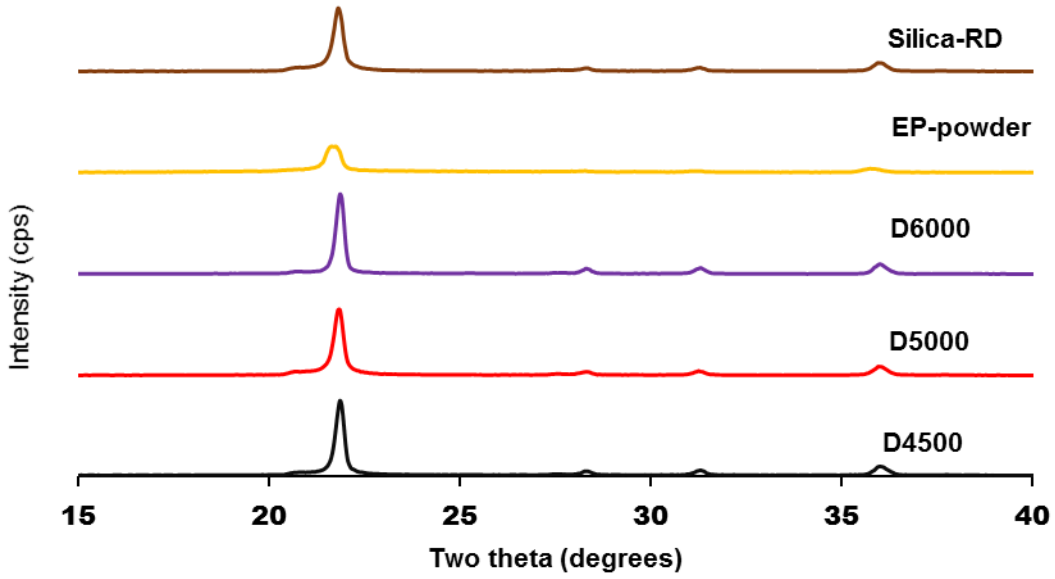

Figure 3.2. X-ray diffraction powder in the region of 15-40 for the commercial filter aid samples.

BET surface areas for the previously mentioned filter aids and the corresponding particle sizes that can be obtained from BET surface area assuming spherical-like particles were accomplished by using the equation $d = 6000/S_A \rho$; where, d is the particle size in nm, S_A is the experimental specific surface area in m^2/g, and ρ is the average density for filter aids (1.39 g/cm^3) display in Table 3.1. As seen clearly, surface areas of the commercial filter aids are less than 0.7 $m^2\ g^{-1}$ and the estimated particle sizes for the filter aids using BET equation do not agree with that obtained by XRD. It is not surprising, cristobalite-SiO_2 structure is mainly composed of amorphous silica that is naturally occurring and is composed of shells of microscopic diatoms of Diatomaceous earth (DE). DE, as reported, has a very week adsorption capacity but excellent absorption power [40,150]. This might be explained because of its macroporous structure. Figure 3.3 also explains this fact. The figure shows both the adsorption/desorption isotherms and the pore size distribution of D4500. As seen, the patterns of adsorption/desorption isotherms belong to type II based on BDDT classification [40], indicating that D4500 should be macroporous, which also confirmed by the distribution of

the pore size that is in macroporous region (>500 Å). Due to the affinity of amorphous silica of water molecules, it is widely used as a filter aid in the filtration of suspended solids but it is ineffective in the adsorption of the dissolved solids especially the dissolved dyes [11,39]. Thus, in this application D4500 (most widely used type of the previously mentioned filter aids at industrial scales) was embedded with nanoparticles that has a very high affinity to adsorb the dye from the textile wastewater.

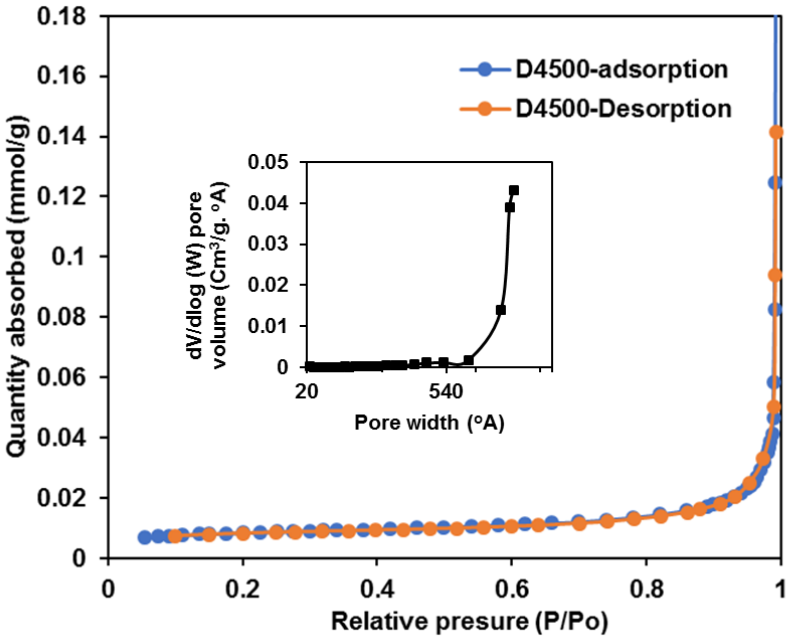

Figure 3.3. Nitrogen physiosorption isotherms and pore size distribution of D4500.

Table 1. BET surface area for different types of commercial sand.

sample name	BET surface area (m^2/g)	Particle size by BET (nm)	Particle size by XRD (nm)
D4500	0.31	8225	25.50 ± 3
D5000	0.63	3974	22.25 ± 5
D6000	0.67	3759	28.62 ± 4
EP-powder	0.36	8230	17.12 ± 7
RD-silica	0.05	49121	20.75 ± 4

After embedding D4500 with 1.5, 3, 5 wt % of PEI-PNPs, the BET surface areas were 5.21, 8.80, and 12.04, respectively. Obviously, the BET surface areas of the resulting solids tend toward gradual increase with increasing the percentage of the embedded nanoparticles in D4500. Interestingly enough, the adsorption capacity for the DE can be enhanced by embedding them with low percentages of nanoparticles without modifying the structure during etching reaction by strong acid or strong base, as typically the case reported in literature [39,40].

3.5.1.2 HRTEM and SEM

Figures 3.4a and 3.4b show the HRTEM images that were taken for D4500 before and after embedding with the 5 wt% of PEI-PNPs, respectively. In the standalone D4500 as anticipated, one cannot distinguish any crystallization or short range of order. However, a significant structural change was occurring after embedding PEI-PNPs. Similarly, SEM micrographs of the same samples are illustrated in Figures 3.5a and 3.5b, respectively. As seen, the D4500 sample reveals a variety of rigid shapes and macrospores/open voids. On the other hand, 5D-PEI-PNPs image shows a good distribution of nanoparticles on the D4500 structure. SEM results confirms a high ability of the D4500 structure to trap solids or residue for separation from clear liquids.

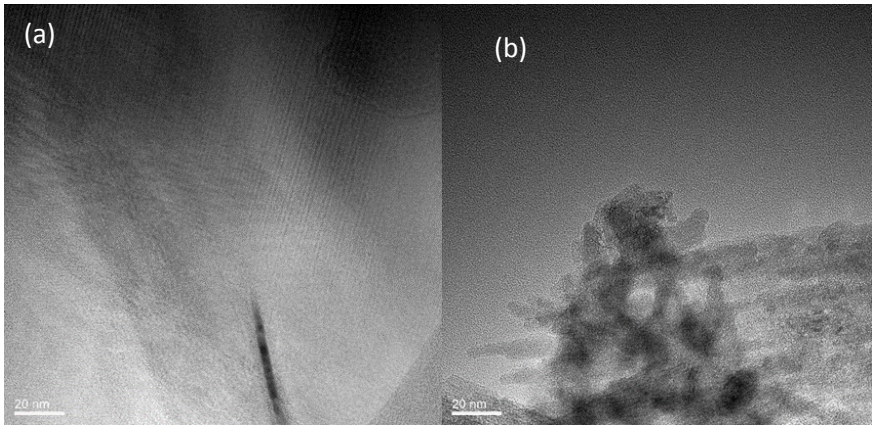

Figure 3.4. HRTEM images for (a) D4500, and (b) 5D-PEI-PNPs (line mark in the image corresponds to 20 nm).

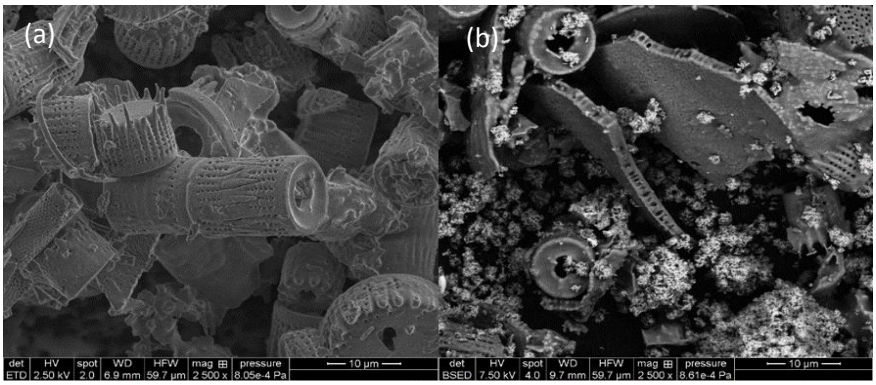

Figure 3.5. SEM images for (a) D4500, and (b) 5D-PEI-PNPs (line images corresponding to 10µm)

3.5.2 Batch equilibrium adsorption

Figure 3.6 presents the adsorption isotherms of 5D-PEI-PNPs, 3D-PEI-PNPs, and 1.5D-PEI-PNPs at 298 K along with their fitting with Sips model. The corresponding parameters of Sips model were obtained from non-linear regression of the experimental data and are displayed in Table 3.2

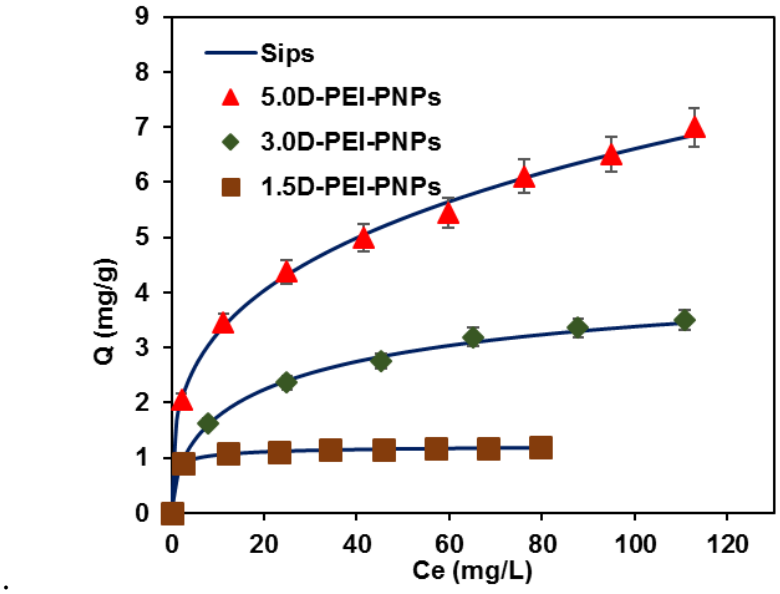

Figure 3.6. Adsorption isotherms of CRD onto adsorbents of 5D-PEI-PNPs, 3D-PEI-PNPs, and 1.5 D-PEI-PNPs. Adsorbent dose:10g/L; shaking rate:200 rpm; T:298 K. The symbols are experimental data, and the solid lines are from the Sips model [eq 3.2]

The goodness of Fitting Sips isotherm with the experimental data was evaluated statistically by minimizing the sum of squares of the differences between the experimental values and the predicted ones using OriginPro 8 SR4 software Version 8.095. This software allows us to evaluate χ^2 that was low in all cases, which indicates an agreement between Sips isotherm and the achieved experimental data [99]. The Q_m values showed that embedding D4500 with 5 wt% of PEI-PNPs nanoparticles have the highest adsorption uptake. In addition, the n_s values for all adsorbents were $0 < n_s < 1$, which corresponds to the surface heterogeneity [81].

Table 3.2. Estimated Sips isotherm parameters obtained at temperature 298 K and pH 8.0.

Adsorbent type	Sips parameters			Error analysis
	Q_m (mg/ g)	K ((L/mg)^n)	n (unitless)	χ^2 (unitless)
5D-PEI-PNPs	10.67	0.095	0.61	0.013
3D-PEI-PNPs	5.003	0.138	0.59	0.0047
1.5D-PEI-PNPs	1.52	1.3	0.52	4.2 X10^{-5}

3.5.3 Column adsorption

3.5.3.1 Effect of type of adsorbent

The breakthrough curves (BTC) for the D4500 before and after embedding it with 5 wt% of PNPs, INPs, PEI-INPs, and PEI-PNPs are shown in Figure 3.7. The figure also shows the BTC for AC for comparison purposes. Evidently, BTCs have S-shape, which is the typical shape of the BTCs [5]. Also, the best attainment breakthrough point was obtained for D4500 that embedded with PEI-PNPs (~250 min) compared with the other cases (< 40 min). This is expected because in the previous study PEI-PNPs showed the highest adsorption capacity in the batch experiment [121]. Hence, D5-PEI-PNPs has the highest uptake and the maximum percentage removal of CRD. For this reason, the PEI-PNPs was selected to perform the column dynamic study.

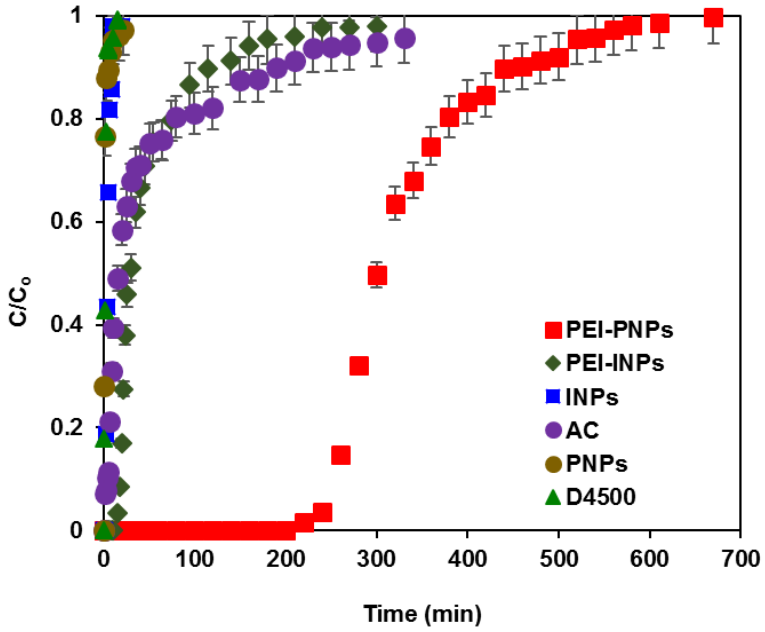

Figure 3.7. Breakthrough curves (BTCs) of fixed-be column for the different nanoparticle types embedded on D4500 at 5 wt.% as well as for the activated carbon, temperature of 298 K and pH of 8 for the removal of CRD at flow rate, influent concentration, and bed height of 0.8 ml/min, 50 mg/L, and 7.5 cm, respectively.

3.5.3.2 Dynamic parameters study

Figures 3.8-3.11 show the BTCs obtained for the CRD adsorption from the textile wastewater by embedding PEI-PNPs on D4500 under different operational conditions. For all the curves shown in the Figures 3.8-3.11**,** the experimental data were identified by points having different shapes, whereas the continuous solid lines of the curves represent plotting of the proposed numerical model for the mass balance of the fixed-bed column (eq 3.15). As seen, the experimental BTCs have a S-shape, which is the typical shape of the BTC for column operation, indicating the effect of the mass transfer parameters as well as the internal resistance within the column [5]. Also, the breakthrough time of the BTC was influenced by varying the dynamic parameters of influent flow rate (Q), inlet CRD concentration (C_o), bed height (Z), and concentration of nanoparticles embedded on D4500 (*%nps*). Table 3.3 displays the adsorption parameters in the column

experiments for all obtained BTCs, including the values of t_b, t_t, % removal, and MTZ. The table also lists the values of D_L and the corresponding Peclet numbers (*Pe*) and χ^2 values. Furthermore, the low values of χ^2 indicate that the proposed model cannot only reproduce an accurate value of the axial dispersion coefficient D_L, but also predicts an experimental breakthrough profile with a satisfactory determination of the operation behavior of the fixed-bed adsorber.

Table 3.3. Summary of the experimental breakthrough curves (BTCs) design parameters and the predicted parameters after fitting the experimental data with the dispersion-convection model together with standard error analysis of the fitting in terms of the values of χ^2 for CRD adsorption at 298 and pH= 8.

Experimental conditions			**Designed parameters**				**Modeling parameters**			
***Q* (ml/min)**	***C*$_o$ (mg/L)**	***Z* (cm)**	***%nps* (wt%)**	***t*$_b$ (min)**	***t*$_t$ (min)**	***% Removal***	***H*$_{UNB}$**	***D*$_L$×10^7 (m^2/s)**	***Pe***	**χ^2**
0.8	50	7.5	5	210	360	70.5	3.1	1.07	147	0.10
1.2	50	7.5	5	112	221	67.1	3.7	4.81	33	0.11
1.5	50	7.5	5	78	174	64.4	4.1	7.54	21	0.15
0.8	75	7.5	5	130	260	66.6	3.75	5.55	42	0.16
0.8	100	7.5	5	96	189	66.3	3.8	9.51	32	0.16
0.8	50	3.5	5	85	198	63.7	2	1.27	63	0.10
0.8	50	2.5	5	45	122	61.4	1.6	1.85	25	0.11
0.8	50	7.5	3.5	87	196	64.2	4.17	0.75	209	0.07
0.8	50	7.5	1.5	31	87	60.8	4.82	0.55	283	0.19

3.5.3.2.1 Effect of the flow rate

Figure 8 shows the effect of varying the feed flow rate (0.8, 1.2, 1.5 mg/L) with a constant bed-depth of 7.5 cm and inlet CRD concentration of 49 mg/L on the adsorption of CRD using 5D-PEI-PNPs. This effort was performed to achieve maximum removal of CRD and to investigate flow rate effect as an important parameter on the pilot or an industrial scale. The flow rate is an important parameter since the length over diameter of the column was so small that characteristics of dispersion are strongly affected via changing the velocity distribution [155,156]. The trend of the obtained BTCs as presented in Figure 3.8 can be observed by three steps; in the first step, the

BTCs showed that the adsorption was rapid at the beginning, which refers to presence of sorption sites able to capture CRD molecules. The next step was occupancy of these sorption sites by CRD molecules, which reduces the uptake. The final step was progressive accumulation of CRD even after occurring the breakthrough on the obtained BTCs [126].

As seen in the figure, with the increased flow rate the BTC became steeper, with which the breakpoint time and the adsorbed CRD concentration decreased. The reason behind this is that when the residence time of CRD in the column is not enough for adsorption equilibrium to be reached at that flow rate, the adsorption zone quickly saturates the top of the column, then, CRD left the fixed-bed column before the equilibrium. Therefore, the contact time of CRD is very short at a high flow rate. That subsequently reduced the CRD removal efficiency. On the other hand, when the influent flow rate is low, the CRD had more time to contact the sorption sites of adsorbent that leaded to achieving a higher removal of CRD molecules in the column [126,156,157].

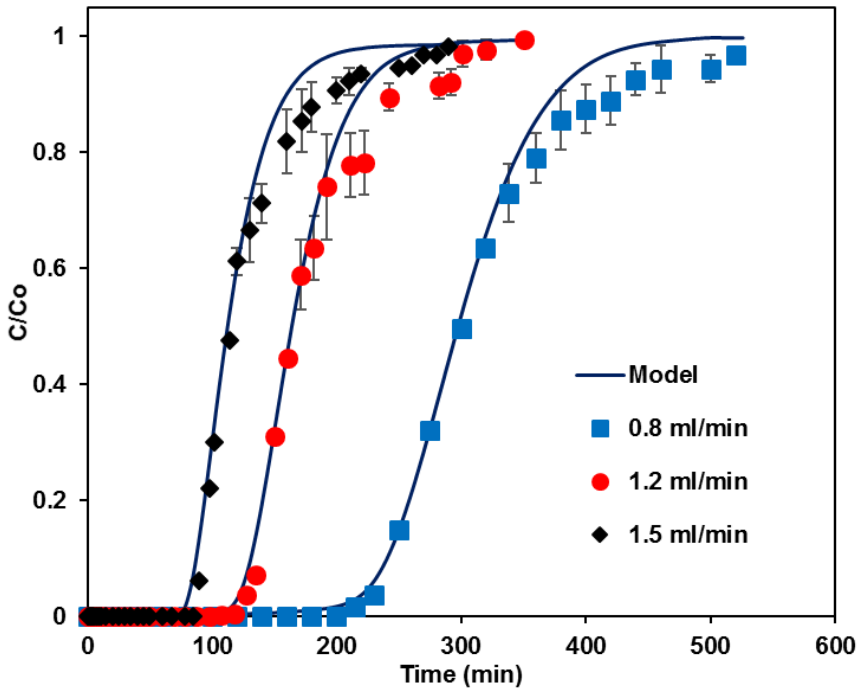

Figure 3.8. Breakthrough curves (BTCS) for adsorption of CRD into 5D-PEI-PNPs at different flow rate. the symbols represent the experimental data, and the solid lines are convection-axial dispersion model (eq 3.15). Experimental operational conditions: initial CRD concentration =50mg/L, bed height =7.5 cm, temperature=298 K, pH=8.

Thus, as Table 3.3 displays, the CRD percentage removal was decreased with increasing the flow rate. The table also shows that t_b values were deceased from 210 to 78 min for flow rate ranging between 0.8 to 1.5 ml/min, respectively, which is in a good agreement with the obtained trend of results that have been reported by the other researcher [126,156–158]. On the basis of mass transfer fundamentals, the slope of BTCs can also be explained. For instance, the amount of CRD adsorbed onto the bed height (MTZ) increased with increasing the flow rate, which led to faster saturation of bed at a higher velocity [126]. At a higher velocity also, the contribution of the convective dispersion becomes the dominant over the molecular diffusion [159]. But the molecular diffusion is significant for the Reynold numbers (*Re*) of 0.0016-55 [160]. Since Re values here were 0.356, 0.54, and 0.67 at the flow rates of 0.8, 1.2, and 1.5 ml/min, respectively, therefore, it is very convenient to develop this model, which takes into account the molecular diffusion that was

represented by the axial dispersion term (eq 3.15**).** Consequently, the proposed model was able to predict the dispersion coefficients values (D_L) and the corresponding Peclet numbers (*Pe*) values that are given in Table 3.3. As illustrated, D_L values increased and *Pe* decreased with increasing flow rate. This is expected, because with increasing the flow rate causes less time for the molecular diffusion to occurred and subsequently the dispersion significantly increases [3,126].

3.5.3.2.2 Effect of adsorbate inlet concentration

Figure 3.9 illustrates the sorption BTCs obtained for different inlet CRD concentrations of 50, 75, and 100 mg/L at bed height of 7.5 cm and flow rate of 0.8 ml/min. This series of experiments aimed to study the effect of varying the inlet concentration on the performance of BTC in the column experiment. In the figure, it is observed that as inlet CRD concentration increased from 50 to 100 mg/L, the breakthrough was steeper because of lower mass transfer-flux from the bulk to the adsorbent surface. This is due to the weaker driving force in mass transfer process [126,161]. In addition, more CRD molecules can be available at higher concentration, which led to higher uptake then it followed more quickly saturation in the column, leading to earlier breakthrough time [3,62,161].

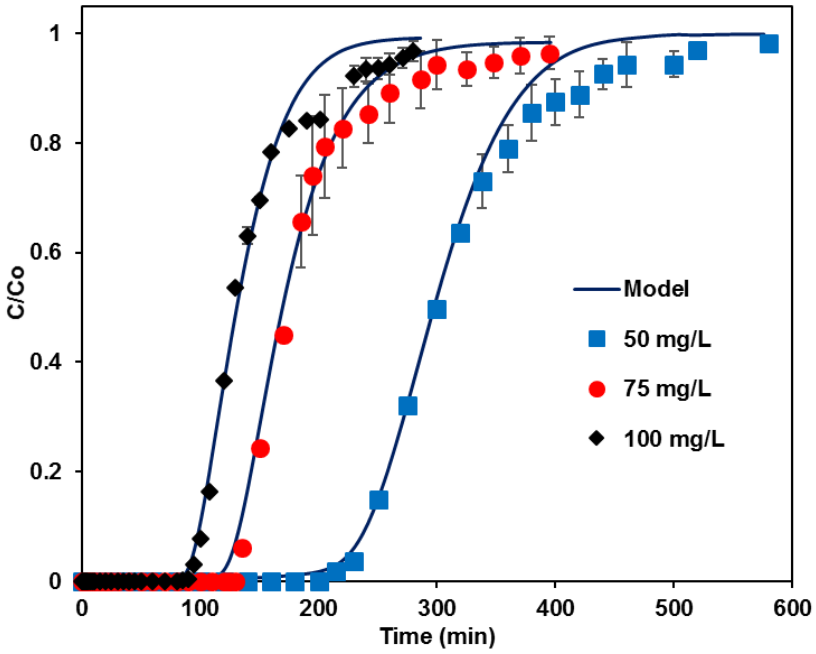

Figure 3.9. Breakthrough curves (BTCs) for adsorption of CRD onto 5D-PEI-PNPs at different initial CRD concentration. The symbols represent experimental data, and the solid lines are the convection-axial dispersion model (eq 3.15). Experimental operational conditions: CRD flow rate=0.8 ml/min, bed height=7.5 cm, temperature=298 K, pH=8.

Table 3.3 presents the various BTCs parameters of the fixed-bed column for the plotted BTCs in Figure 3.9 The table shows that with an increase in the inlet CRD concentration, the percentage of removal of the CRD influent decreased from 70.5 to 66.3 % and the fitting parameter represented by the values of D_L were increased. This can be explained by the fact that all adsorbents have a limited number of binding sites, which were saturated at a certain concentration. Before this concentration, a higher driving force was provided that was enough to overcome the mass transfer resistance. After that, more CRD molecules were left unadsorbed, leading to decrease the percentage removal of CRD with increasing the CRD influent concentration and this is due to decreased the diffusion coefficient [3,18,73,159].

3.5.3.2.3 Effect of adsorbent bed height

The quantity of adsorbent that accumulates on the fixed-bed column is an important parameter in column design, this because the steepness of the BTCs is a strong function of bed height [126,161,162]. Therefore, the performance of the BTCs by varying the bed height at 7.5, 3.5, and 2.5 cm was investigated as shown in Figure 3.10. This study was implemented at influent CRD concentration and flow rate of 50 mg/L and 0.8 ml/min, respectively. The figure reveals that the breakthrough time increased from 45 to 210 min, with increasing the bed height from 2.5 to 7.5 cm. The explanation for this is that as the bed height increased, the residence time for the dye inside the column increased, which allows for the dye molecules to diffuse deeper into the adsorbate particles, resulting in high dye removal efficiency [126,128,156]. The removal efficiency as shown in Table 3.3 increased from 61.4 to 70.5% by increasing the bed height. The profile of the breakthrough curve at different bed height shows a similar shape regardless of the chosen bed height. This suggests that no any back-mixing problem or axial dispersion exist in the column. This assert is accordance with the approximately equal D_L values showed in Table 3.3 at different bed heights. A similar trend of results was reported by García-Mateos et al. for the removal of paracetamol on biomass-derived activated carbon [163].

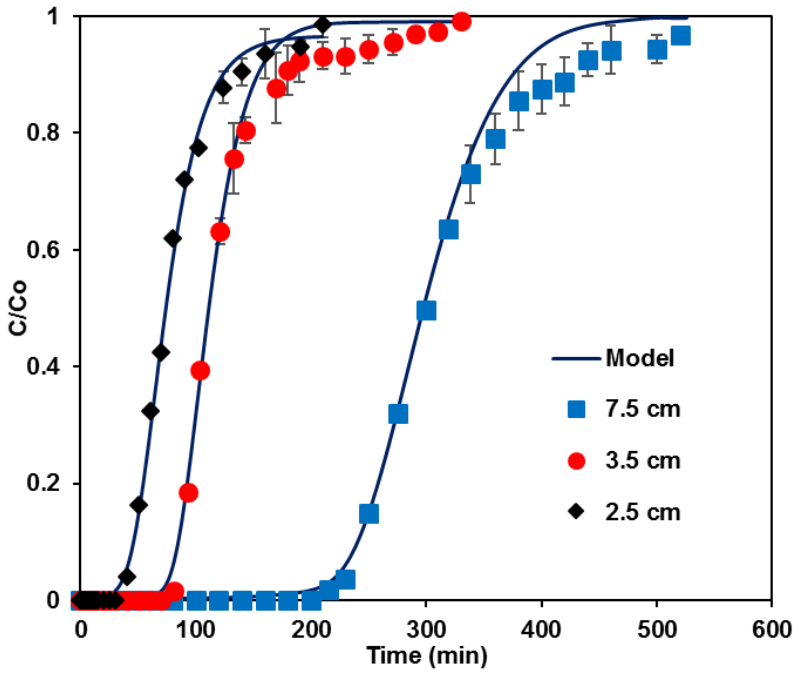

Figure 3.10. Breakthrough curves (BTCs) for adsorption of CRD onto 5D-PEI-PNPs at different bed heights, the symbols represent the experiments data, and the solid lines are the convection-axial dispersion model (eq 3.15). Experimental operating conditions: initial CRD concentration=50 mg/L, CRD flow rate=0.8 ml/min, temperature=298 K, pH=8.

3.5.3.2.4 Effect of the concentration of nanoparticles embedded into Diatomite

Concentration of the PEI-PNPs type of nanoparticles strongly effects the steepness of the obtained BTCs. As shown in Figure 3.11, with increasing the concentration of the embedded nanoparticles on D4500 from 1.5 to 5 wt%, the breakthrough time accordingly increased. This referred to the fact that more sorption sites must be available inside the fixed-bed column with increasing the concentration of nanoparticles. Then, more mass transfer surface area was provided, which subsequently, increasing the rate of diffusion [156,159,164]. Table 3.3 supports this fact. As seen clearly, the percentage of dye removal efficiency increased from 60.8 to 70.5% with increasing the concentration of nanoparticles from 1.5 to 5 wt%. However, the MTZ decreased from 4.82 to 3.14 with increasing the concentration of nanoparticles from 1.5 to 5 wt%. These obtained results reflect

the dependence of the rate of diffusion with increasing the number of sorption sites. This is also increased the D_L values, which is not surprizing, it was indicated that by more binding sites was provided with an increase in the nanoparticles embedded on D4500.

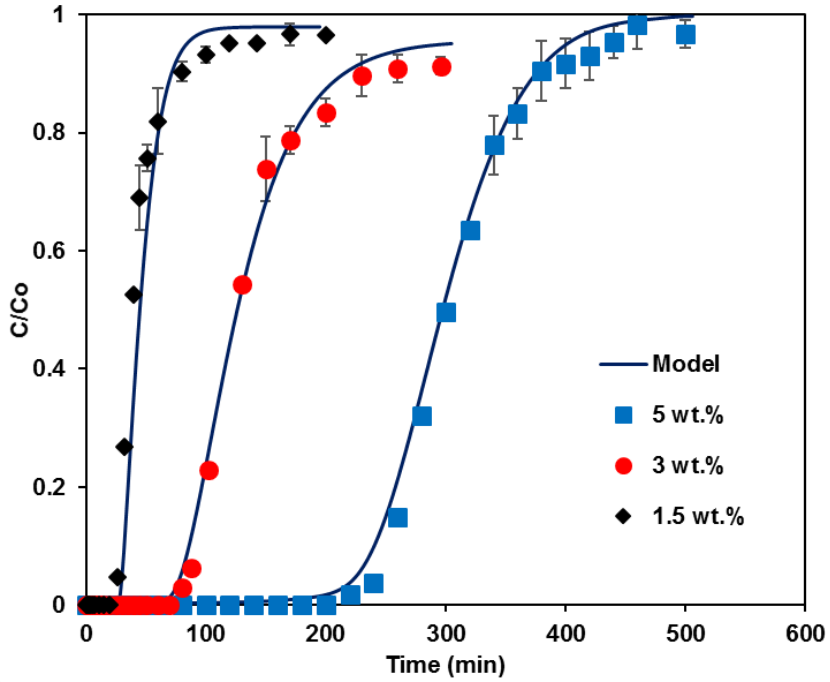

Figure 3.11. Breakthrough curves (BTCs) for adsorption of CRD at different weight of PEI-PNPs concentration (5 wt.%, 3wt.%, and 1.5 wt.%). The symbols represent experimental data, and the solid lines are the convection-axial dispersion model (eq 3.15). Experimental operating conditions: initial CRD concentration= 50mg/L, CRD flow rate=0.8 ml/min, bed height= 7.5 cm, temperature=298 K, and pH=8.

3.5.3.3 Length of unused bed (H_{UNB}) and Peclet number (Pe) correlations

The length of unused bed (H_{UNB}) or the length of mass transfer zone (MTZ) is considered an important design parameter [4] It is used to indicate the full-scale adsorbent bed as sum of the length of the ideal fixed-bed absorber. To produce a desired adsorption capacity, there is a dire need to take into account the stoichiometric length of the bed, based on the ideal-step function behavior as well as the additional length of unused bed (H_{UNB}) [4,165] Peclet number (Pe), on the

other hand, is a dimensionless number that dedicates the dominating of the process during the operation of the fixed-bed column [142,166]. For instance, the high value of *Pe* number with a very low value axial dispersion (D_L) suggests that the influence of the mass transfer phenomenon can be neglected [167]. Also, the sharpness of the breakthrough increased with decreasing *Pe*. These changes are very pronounced in low *Pe* (<100) [167]. Thus, it is worth to study H_{UNB} as a function of *Pe,* which can be accomplished by plotting H_{UNB} against the corresponding *Pe* value that are listed in the Table 3.3. Figure 3.12a and 3.12b represents this relation in two cases. The first case is the obtained correlation by changing the influent flow rate and CRD concentration (Figure 3.12a). The data obtained in this case was very well correlated with an exponential decay function with $R^2 = 0.92$. The resulting expression for the correlation is:

$$H_{UNB} = 4.08\, e^{-0.002\, Pe} \tag{3.17}$$

It is important to note that this correlation does not include the whole range of the experimental data especially when $Pe < 50$. This correlation explains the fact that as *Pe* becomes larger, H_{UNB} decreased exponentially and the adsorption column approaches plug flow behavior at high value of *Pe*. This correlation matches with that obtained in the literature at very low *Pe* [4,167]. The second case is the obtained correlation by varying the bed height and the concentration of the nanoparticles embedded on the Diatomite (Figure 3.12b). In this case, a very big change in *Pe* was obtained with changing H_{UNB} and the obtained data was very well correlated with a linear function that had $R^2=0.99$. The resulting expression for this correlation is:

$$H_{UNB} = 0.013\, Pe + 1.25 \tag{3.18}$$

This correlation suggests that H_{UNB} increased linearly by increasing *Pe*. Hence, *Pe* is strongly influenced by changing the bed height and the concentration of nanoparticles embedded on

Diatomite. This is expected due to presence of a direct relationship between the bed length and the *Pe* at constant flow rate and approximately equal values of D_L. However, the presence of more nanoparticles embedded on D4500 decreased sharply *Pe*. This was occurred because of increased the axial dispersion by increasing the nanoparticle concentration. Interestingly, the presence of nanoparticles embedded on Diatomite, as a dynamic parameter, considered as a best way to provide a column with less $H_{UNB.}$

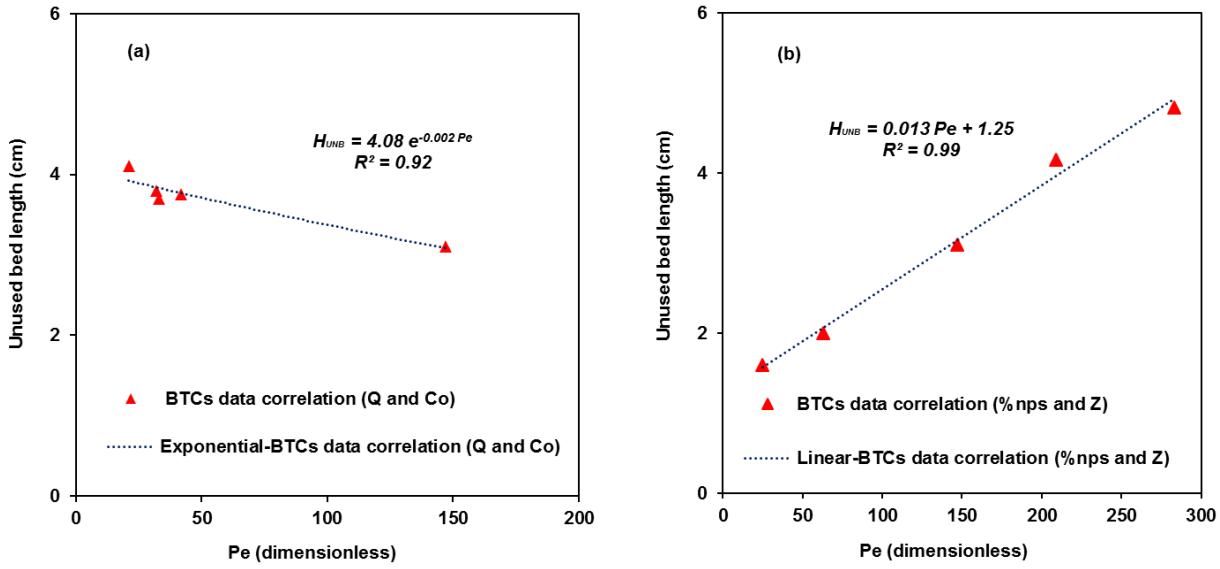

Figure 3.12. BTC data correlation between length of unused bed (H_{UNB}) and Peclet number (Pe). a) Varying influent flow rate (q) and CRD concentration (co), and (b) varying the bed height (Z) and the concentration of the nanoparticles embedded on the diatomite (% nps).

3.6 Conclusions

Poly(ethyleniminine)-functionalized pyroxene nanoparticles embedded into Diatomite (D4500), a commonly used filter aid, was prepared successfully, obtaining an active adsorbent with improved surface functionality. Adsorption of commercial red dye (CRD) has been studied in discontinuous (batch) and continuous flow column experiments. The adsorption isotherms were well described using the Sips model. Kinetic studies in the batch experiments have been employed to calculate

the breakthrough profiles in the fixed-bed adsorption column. In the continuous experiments, the effects of operational variables (e.g., inlet concentration of CRD, inlet flow rate, bed height, and nanoparticle concentration in Diatomite) have been analyzed using one factor at one time (OFAT) design of experiment method.

It was shown that adsorption performance of the CRD in continuous fixed-bed by using filter aid of D4500 that was functionalized by very low mass percentages (< 5 wt%) of functionalized-PEI pyroxene nanoparticles was improved very well. It is because this nanoparticle type had very high adsorption capacity toward the CRD, which led to improve the sorption surface area and subsequently the adsorption capacity of the D4500. In the fixed-bed column experiment, the breakthrough curves for CRD removal were very well represented using the convection-dispersion model, which enabled us to determine the axial dispersion coefficient (D_L) and Peclet number (Pe). The obtained fitting parameter values of D_L are in a good agreement with that obtained from the correlation available from the literature. Analysis of the breakthrough data using the equivalent length of unused bed (H_{UNB}) approach have shown that H_{UNB} is very well correlated with Pe using the relations: $H_{UNB} = 4.08\, e^{-0.002\, Pe}$ when the inlet flow rate and the inlet CRD are the operational parameters, while the relation: $H_{UNB} = 0.013\, Pe + 1.25$ was obtained when the bed height (Z) and concentration of nanoparticles embedded on Diatomite (%nps) are the operational parameters. To the best of our knowledge, our technique can be considered as a synergistic process as it could combine the adsorption and the filtration techniques into one process, and subsequently, it avoids the drawbacks of the previously reported techniques.

CHAPTER FOUR

Poly(Ethylenimine)-Functionalized Pyroxene Nanoparticles Embedded on Diatomite for Removal of Total Organic Carbon from Industrial Wastewater

This chapter is adapted from the following publication

A. Hethnawi, N. N. Nassar, G. Vitale, A. D. Manasrah, Poly(ethylenimine)-Functionalized Pyroxene Nanoparticles Embedded on Diatomite for Removal of Total Organic Carbon from Industrial Wastewater, Journal of Hazardous Materials, (to be submitted), (2017)

4.1 Abstract

In this study, the adsorption of total organic carbon (TOC) from an industrial wastewater using poly(ethylenimine)-functionalized pyroxene nanoparticles (PEI-PNPs) embedded into Diatomite (D4500) at <5 wt% was investigated. FTIR followed by ICP-AES, characterization methods, were used to gain insight into the main organic and metallic composition of the considered industrial wastewater. By FTIR and ICP-AES, it was obtained that the RWWT sample is mainly composed of an aromatic amine, alkyl benzene and small fractions of unknown functional groups in addition to very low concentrations of Fe, K, and Mg. The adsorption of TOC over the diatomite embedded with 1.5, 3, and 5 wt% of PEI-PNPS was conducted in a batch equilibrium adsorption that was very well presented using the Sips model. In the continuous fixed-bed column, the adsorption performance was investigated to determine the breakthrough behavior under different operational conditions (e.g., inlet concentration of CRD, inlet flow rate, bed height, and nanoparticle concentration in diatomite, %nps). A convection-axial dispersion model was applied to the experimental data to predict the breakthrough curves and to determine the characteristic parameters based on mass transfer phenomena. The axial dispersion coefficient (D_L) and group of dimensionless numbers include Renold number (Re), Schmidt number (Sc), and Sherwood number (Sh) were all determined and correlated by Wilson-Geankoplis correlation, which can be used at $0.0015<Re<55$. This correlation was used to find the external film diffusion coefficients (K_c) that followed by finding Biot number (Bi). The obtained values of Bi were able to describe the mass transfer process inside the fixed-bed column under various operational conditions. Thus, the values of Bi were all low, indicating that external film diffusion was the dominant for the mass transfer process inside the packed-bed column. Furthermore, the ability of reusing and

regenerating the spent adsorbent was studied and it was obtained that at low pH, incomplete and rapid kinetic of desorption were carried out for the considered industrial wastewater.

4.2 Introduction

Treatment of total organic carbon from industrial effluents has received a lot of attention in the last few decades [6,168–170]. Industries such as petroleum refining, petrochemical, pulp and paper, food, and textile involve processes that generate a wide variety of effluents [102,103,171]. This wastewater coming from these types of effluents typically has high levels of colloidal suspended and dissolved organic pollutants. These pollutants, which show a great difference in chemical composition, often need to be treated [172,173]. If these chemicals are not treated adequately, they can have a strong negative impact on water resources [10,174]. Synthetic dyes in textile wastewater, for instance, depending on the exposure time and concentration, can cause chronic and acute effects on exposed organisms [105,108,175,176]. Also, the presence of a small amount of these dyes in the textile wastewater limits the techniques that can be used for their treatment [41,47,104]. These techniques are effective in some cases but fail completely in others, especially if they are applied individually [9,21,47]. For example, biological treatment, on its own, did not show outstanding results in removing the color from the textile wastewater [22,47,102]. However, after integrating it with adsorption by activated carbon (AC) into one synergistic stage, the process significantly improved [22,177]. Likewise, coagulation/flocculation showed some very satisfactory results when it was followed by adsorption [23]. AC, even though it is a good adsorbent in many cases, has disadvantages [2,111,112]. Indeed, it has a low efficiency due to its slow mass transfer kinetics in adsorbing the heavy molecules, which lengthens the adsorption equilibrium time [24–26]. Furthermore, production and regeneration of the AC are not environmentally safe nor cost-effective in industrial applications [24–26]. Thus, numerous studies

focus on developing an adsorbent with unique properties that is able to provide better performance than AC [15,27,28,33,35,98,113–117]. Alternatively, nanoadsorbents offer good sorption efficiency, large surface area, and easily accessible sorption sites with organic contaminants. Hence, using nanoparticles may allow for better and more affordable wastewater process development [15,28,33,35,115–117]. Using nanoparticles in synergistic combination with other conventional techniques provides a greater possibility for large-scale applications of wastewater treatment [68,98,120]. For multi-functionality and stability purposes, nanoparticles, especially the magnetite, have been anchored during or after the synthesis with a wide range of stabilizers like polymers, surfactants, and inorganic materials [178,179]. Nevertheless, the magnetite type of nanoparticles need an initiator that primarily attaches to the surface of the nanoparticles [178,180]. This initiator works as a bridge or binding agent before the end-grafting [15]. This concept is a strong drawback of using the magnetite in the wastewater treatment fields. Thus, both the magnetite and AC should be replaced. Alternatively, pyroxene or iron silicate-based nanoparticle type occurs naturally, and is known as aegirine ($NaFeSi_2O_6$) [80,81]. The superficial ion exchange properties for the pyroxene allows it to do the interest in utilising it as an adsorbent [80,81]. It can be simply stabilized via direct end-grafting [121]. Our previous studies were successful in making this application effective and economical [121,181]. In details, by the first study, polyethyleneimine (PEI) was used to stabilize the pyroxene (PNPs) without modifying its surface via primary coating [121]. Also, the prepared PEI-PNPs showed an excellent adsorption removal and fast adsorption kinetics of a commercial red dye from a textile wastewater in batch mode of adsorption compared with that of magnetite nanoparticles and a commercial AC [121]. While in our second study, PEI-PNPs was embedded at <5 wt% on diatomite, a commercial filter aid, to test the dye adsorptive removal in continuous fixed-bed column and it was obtained that the

adsorption performance of the dye was greatly improved under the effect of variable dynamic conditions [181]. The objective of the current study is to investigate the possibility of utilizing our previous novel adsorptive technique in batch and contentious fixed-bed in cleaning-up a real and locally provided industrial effluent. Batch adsorption experiments for the removal of total organic carbon (TOC) were conducted to determine the adsorption capacity as well as kinetic parameters at equilibrium that are helpful to estimate the breakthrough profiles for the adsorption column operation. The adsorptive removal of TOC in a fixed-bed column was also conducted under influence of controlled operational parameters of bed depth (Z), influent TOC concentration (C_o), flow rate (Q), and the concentration of the embedded nanoparticles on the Diatomite. Then, the experimental results under different test conditions (i.e., Z, C_o, Q, and nanoparticle concentration in Diatomite) were fitted with the convection-dispersion model from our previous study to describe the breakthrough curves (BTCs) [181]. More efforts were made herein, which mainly consider the pH effect in the adsorption. Considering pH effect is beneficial because it not only shows a guidance to optimize the adsorption, but it also plays an important role in reusing the adsorbent by desorption. For this purpose, point of zero charge (PZC), or isoelectric point, was estimated experimentally by using Zeta-potential analyzer. After that, a regeneration study was accomplished by the back-wash of the spent adsorbent with an aqueous solution has pH at the minimum adsorption removal of TOC value.

4.3 Material and Methods

4.3.1 Adsorbate chemical analyses

An industrial wastewater sample was kindly supplied by Executive Mat Ltd, Calgary, Canada. To date, reviews have been unable to describe the exact structure of any real wastewater sample due to its complexity. This complexity did not permit to identify the exact pollutant and its effect on

the adsorption behavior. Therefore, it is advisable before conducting any adsorption experiment to apply as many independent methods as possible to gain insight into the structural information of the supplied wastewater sample. As mentioned, the industrial wastewater might contain plenty of suspended and colloids organic and metals and the presence of them has a negative impact on our focus study. Because of this negative impact, we filtered the mother wastewater sample to eliminate these suspended colloids and metals. Then, the filtrate was analyzed to get an indication about its organic and metallic compositions. Briefly, detecting the presence of metals was carried out by inductively coupled plasma-atomic emission spectroscopy, ICP-AES (IRIS Intrepid II XDL, Thermo-Instruments Canada, Inc., Mississauga, ON, Canada). In addition to that, the concentration of the total organic carbon (TOC) was estimated using a Shimadzu Total Organic Carbon Analyzer (TOC-L CPH/CPN). Then, the main organics in the industrial wastewater were determined by performing infrared spectroscopy (FTIR) analysis by a Nicolet 6700 FTIR instrument that was produced by the Thermo Electron Corporation. For FTIR analysis, the industrial wastewater from the mother solution was vacuum dried, resulting in powder. Then, approximately 5 mg of that powder was mixed with 500 mg of KBr. After that, the mixture was mounted in the DRIFTS sample holder. FTIR spectra were measured at the range of 400-4000 cm^{-1}, with a resolution of 2 cm^{-1} and the spectrum was the average of 128 scans.

4.3.2 Adsorbent preparation

The detailed description of the preparation of poly(ethylenimine)-functionalized pyroxene nanoparticles (PEI-PNPs) by a two-step preparation method is reported in our previous studies [121,181]. In the first step, a conventional hydrothermal synthesis at mild conditions was carried out to prepare the pyroxene nanoparticles (PNPs). In summary, iron and silicate solutions are A and B solutions. Solution A contained 18.067 g of sulfuric acid in 90 g of deionized water and

20.793 g of iron tri-chloride, while solution B comprised of 21.413 g of sodium hydroxide to 60.0 g deionized water and 30.707 g of sodium silicate. The iron solution was added slowly to the silicate solution while stirring for 15 min to produce a homogeneous orange-yellowish gel. Then, a hydrothermal crystallization for the produced gel was carried out at 433 K and 300 rpm for 72 h inside a 300-ml reactor vessel (A2230HCEB, Parr Instrument Company, Moline, Il, USA). The resulting gel was carefully discharged from the reactor vessel, filtered and washed with deionized water. Finally, the gel was left overnight, producing the pyroxene nanoparticles for further usage. In the second step, functionalization was accomplished by anchoring poly(ethylenimine) (PEI) onto a pyroxene suspended solution by adding 50 ml of a solution of the PEI having different concentrations to 1.0 g of nanoparticles suspended in 100 ml of water. The mixture was stirred for 3 h at room temperature to allow the anchoring of the PEI onto the surface of the nanoparticles. Finally, the suspension was filtered, washed, and dried by vacuum overnight at room temperature. Accordingly, PEI-PNPs were denoted for the anchored pyroxene with PEI. After that, PEI-PNPs were embedded on Diatomite. A suspended 5 wt% of Diatomite was prepared first. Then, the nanoparticles were added to the suspended solution under stirring for 15 min. The suspended solution was filtered, and dried. Finally, the product was recovered for the batch and column adsorption studies. Diatomite was also embedded with 1.5 and 3 wt% of PEI-PNPs to study the influence of embedding various concentration of nanoparticles on it, resulting in functionalized adsorbents of Diatomite that are donated as 5D-PEI-PNPs, 3D-PEI-PNPs, and 1.5D-PEI-PNPs for the Diatomite that was embedded with 5, 3, and 1.5 wt% of PEI-PNPs, respectively.

4.3.3 Adsorbent characterization

An array of characterization techniques including X-ray diffraction (XRD), high-resolution transmission electron microscopy (HRTEM), infrared (IR) spectroscopy, and thermogravimetric analysis (TGA) were reported in our prevoius study [121,181], followed by textural properties for the synthesized PEI-PNPs nanoparticles. The same was also carried out for the Diatomite before and after embedding it with 5 wt% of PEI-PNPs. As a result, PNPs were successfully functionalized by using the PEI. Also, they had granulated-like morphologies with average crystaline domain sizes around 10 nm and a low BET surface area (~18 m^2/g) that increased reasonably to ~119 m^2/g by drying using Lyophilizing as the solution instead of conventional drying of the synthesized materials [121]. Also, it was shown that the filter aid of Diatomite was mainly composed of amorphous diatomaceous earth; its adsorption surface area was improved significantly via embedding more nanoparticles [181]. Furthermore, the surface textures of the Diatomite sample were observed using a scanning electron microscope (SEM) with a field emission Quanta 250 electron microscope, which was manufactured by FEI. Figures 4.1a, 4.1b illustrate the SEM micrographs of the Diatomite, before and after embedding 5D-PEI-PNPs, respectively. Similar to our previous study [181], it is clearly shown that the PEI-PNPs were successfully embedded with diatomite without destroying the structure. It is also very obvious that the presence of the open voids plus the high adsorptive capacity of the PEI-PNPs led to an increase in the ability of Diatomite to trap TOC from the industrial wastewater solution.

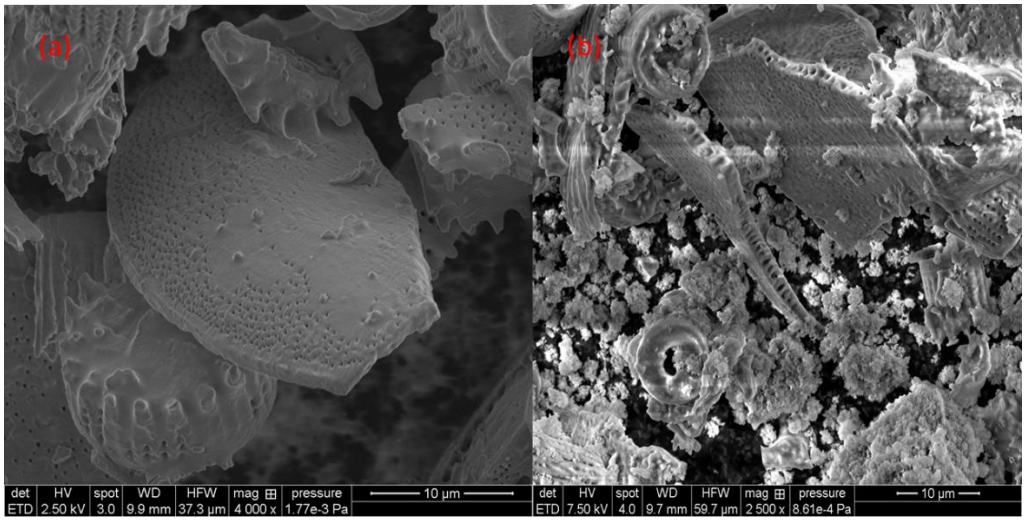

Figure 4.1. SEM images (a) Diatomite, and (b) 5D-PEI-PNPs (the line mark in the images corresponding to 10 µm).

In this work, the point of zero charges (PZCs) of the PEI-PNPs and the 5D-PEI-PNPs were also measured by using a Nano- Zetasizer (Nano-ZS) instrument that was manufactured by Malvern. In our present study, PZC was beneficial as evidence for the feasibility of the regeneration of the used adsorbent because desorption of the spent adsorbent can be maximized by selecting the proper pH, which provides a proper surface charge to attract opposite charge pollutants [117,182]. This can be indicated via creating an environment that has a surface charge or pH beyond the pH at PZC [68,117,120,182]. The analysis for PZC was as follows: 10 mg of each sample was suspended into 10 ml of deionized water inside a 20-ml vial. Then, sonication was carried out for 2 min to overcome any static aggregation that might occur. Then, each sonicated sample was injected into a disposable folded capillary cell. The analysis was done three times for each sample to ensure reproducibility. The pH was gradually adjusted using a few drops of NaOH or HCl; then, pH at PZC was recorded.

4.3.4 Batch adsorption experiments

The adsorptive removal of TOC from the industrial wastewater sample was tested for the adsorbents of 1.5D-PEI-PNPs, 3D-PEI-PNPS, and 5D-PEI-PNPs by a simple batch-mode of adsorption. Each experiment was carried out at 298 K by adding a fixed amount of adsorbent (100 mg) to a series of 25-ml glass vials filled with 10 ml of diluted solutions, resulting in different standard solutions having different initial concentrations of TOC. A batch adsorption was carried out for these solutions when the vials were sealed and placed in a Wrist Action shaker (Burrel, Model 75-BB) for 4 h, which is enough to attain equilibrium. After that, all of the vials were left overnight on the lab bench. After settling the adsorbents, all samples were centrifuged for 10 min at 5000 rpm in the Eppendorf Centrifuge 5804 to separate the residuals after adsorption. The supernatant was analyzed for the final TOC concentration by the same TOC analyzer as mentioned earlier. The adsorbed amount of TOC, in terms of mg TOC/g of dried adsorbent, was estimated by mass balance analysis as per eq 4.1**:**

$$Qe = \frac{C_o - C_e}{m} V \tag{4.1}$$

where C_o is the initial concentration of TOC in the solution (TOC, mg/L), C_e is the equilibrium concentration of TOC in the supernatant (TOC, mg/L), *V* is the solution volume (L), and *m* is the dry mass of the adsorbent (g). As the most important factor in the adsorption, the pH effect was tested following the same batch adsorption experiments for the stand-alone adsorbent of PEI-PNPs. This is because Diatomite works as an inert without containing binding sites. In this study, an undiluted standard solution of the textile wastewater mother solution was used for each sample after gradually pre-adjusting the pH of each sample with a few drops of HCl and NaOH. However, the industrial wastewater is very sensitive towards changing the medium pH [183,184]. This

sensitivity occurs because it contains various molecules that have different net charges and solubility that by varying the pH, both the net charge and the isoelectric point (IEP) of these molecules change. This often leads to minimize the solubility and precipitate them out of the solution [185]. This fact strongly hinders the adsorption by adsorbent particle. Therefore, filtration, as one more step, is required after pre-adjusting the pH before conducting any adsorption experiments. Hence, the removal efficiency of TOC after filtration or due to adsorption can be calculated as follows:

$$RE\ (\%) = \frac{C_i - C_f}{C_i} \times 100 \qquad (4.2)$$

where *RE (%)* is the removal efficiency of TOC, C_i (mg/l) and C_f (mg/l) are the TOC concentrations before and after filtration or adsorption experiments, respectively.

4.3.5 Column adsorption study

Figure 4.2 shows a schematic diagram of setup for the contentious adsorption study. The fixed-bed column was made of a glass tube with a length of 15 cm and internal diameter of 0.9 cm. The adsorbents of 1.5 D-PEI-PNPs, 3D-PEI-PNPs, and 5D-PEI-PNPs were packed inside the column until the desired bed height was obtained. The adsorbent for each experiment was supported and closed by packing with an approximately 1 cm of cotton layer at the bottom and the top of the column to improve the flow distribution and avoiding the scape of the adsorbent from the column. The uniform influent was fed to the column in an up-down mode by a 50-ml high pressure stainless steel syringe pump with 1/8" Swagelok fitting (HARVARD). The effluent samples were collected periodically from the bottom of the column during the experiment. Then, each sample concentration was measured using the TOC analyzer. The flow was continuously provided to the column until no further TOC adsorption occurred that is obtained when the outlet concentration

(C_f) is approached to the inlet concentration (C_i). To investigate the Dynamic parameters, 9 separated experiments were carried out at room temperature (298 K) by varying the operating conditions of flow rate (*Q*), inlet TOC concentration (C_o), bed height (*Z*), and nanoparticle concentrations (*% nps*) on the Diatomite following one factor at one time (OFAT) design of experiment method. Particularly, 3 experiments under various flow rates of 0.8, 1.2, 1.5 ml/min in addition to 3 experiments with predetermined TOC concentrations of 290, 195, and 145 mg/L. Also, 3 experiments with bed heights of 2.5, 3.7, and 7.3 cm. Finally, 3 experiments with nanoparticle concentrations of 1.5, 3, and 5 wt%.

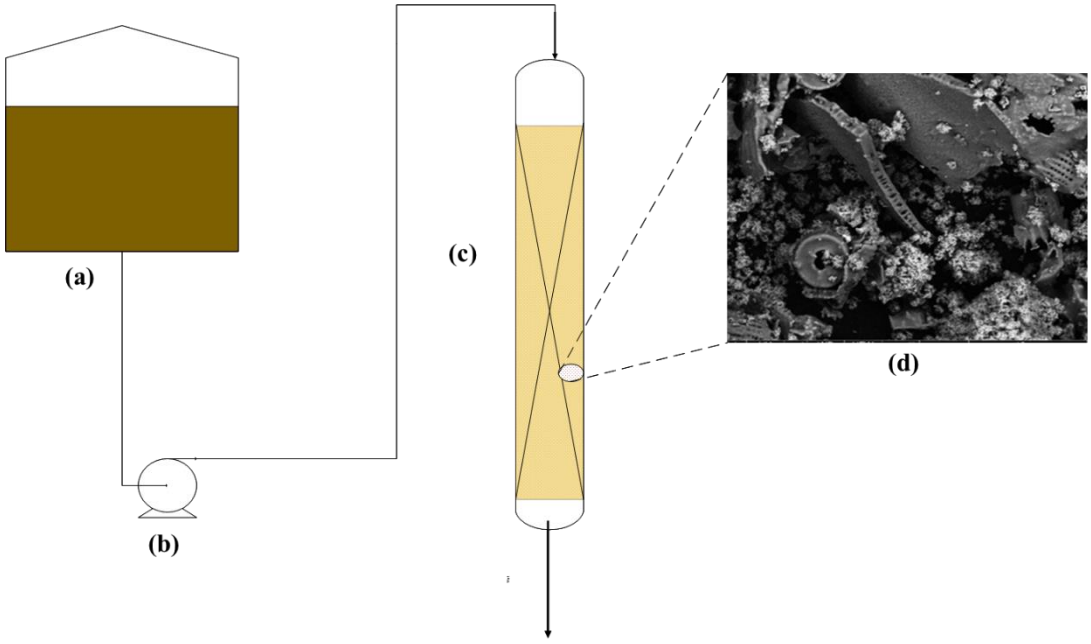

Figure 4.2. Schematic representation of the fixed-be experimental set up. (a) Influent feed tank, (b) syringe pump, (c) fixed-bed column, and (d) Nanoparticles embedded on Diatomite.

.

In order to ensure the feasibility of reusing the adsorbent, one exhausted bed from the previous experiments was regenerated to recover the adsorbent for further use. This experiment was done by using 0.5 M HNO_3 at a flow rate of 0.8 ml/min in down flow mode. It is worth it to mention that the back flow of H $NO_3$was conducted at the pH value < PH_{pzc}.

4.3.6 Breakthrough analysis and modeling

In the fixed-bed adsorption system, the breakthrough curve (BTC) behavior is affected by the operational parameters (*Q, C_o, Z,* and *% nps*) and the designed parameters (length over diameter) of the column as well as the characteristic of the adsorbent (size and shape) [126,127,161]. The performance of any obtained BTC can be indicated from its breakthrough time (t_b) and saturation time (t_s). t_b, and t_s are chosen when the influent and effluent and concentrations approach 5 and 95 % of C_o, respectively [110,163]. These times are useful to estimate the percentage removal of the TOC. Therefore, more equivalent parameters need to be calculated [126,162]. For instance, the time equivalent to stoichiometric capacity *(t_t)* can be expressed as follows:

$$t_t = \int_{t=0}^{t=\infty} (1 - \frac{C_t}{C_o})\, dt \tag{4.3}$$

The time equivalent to usable capacity *(t_u)* can be expressed as

$$t_u = \int_{t=0}^{t=tb} (1 - \frac{C_t}{C_o})\, dt \tag{4.4}$$

The equivalent length of unused bed (H_{UNB}) is calculated as follows:

$$H_{UNB} = \left(1 - \frac{t_u}{t_t}\right) H_T = \left(1 - \frac{t_b}{t_t}\right) H_T \tag{4.5}$$

where H_T is the total bed height (cm). Used bed length H_B up to break point is also

$$H_B = \left(\frac{t_b}{t_t}\right) H_T \tag{4.6}$$

Furthermore, the adsorbed quantity (q_{total}) of TOC, using the adsorbent particles inside the column, can be estimated under the given operational parameters for each BTC from multiplying the area under the BTC and the flow rate [126]. It can also be determined by calculating the adsorbed concentration (C_{ads}) against the effluent time (min). C_{ads} is the difference between the inlet (C_o) and the outlet (C_t) concentrations ($C_{ads}=C_o-C_t$), where C_o, C_t, and C_{ads} are in mg/L. Thus, q_{total} can be calculated as [126,162]

$$q_{total} = \frac{Q\ A}{1000} = \left(\frac{QC_o}{1000}\right) \int_{t=t_o}^{t=t_{total}} C_{ads}\ dt \tag{4.7}$$

where Q is the flow rate (ml/min), A is the area under the BTC, and t (min) represents the t_{total}.

Moreover, the total amount of TOC that was sent to the column can be calculated by eq. 4.8:

$$W_{totol} = \frac{C_o\ Q\ t_{total}}{1000} \tag{4.8}$$

Thus, the total removal percentage of TOC (% Removal) is the ratio of the maximum capacity of the column (q_{total}) to the total amount of TOC sent to the column (W_{total}). This is expressed in eq 4.9 as follows:

$$\%\ Removal = \left(\frac{q_t}{W_{total}}\right) \times 100 \tag{4.9}$$

The parameters t_t, t_u, H_{UNB}, H_B, q_{total}, $W_{total,}$ and %Removal describe the performance of the fixed-bed column through the experimentally obtained BTCs [62,126,129,186,187]. They are also very important characteristic parameters for determining the dynamic behavior of the adsorbent. However, calculating these parameters is insufficient for successfully designing a column

adsorption process since the column experiments require predicting the concentration-time profile as well as the breakthrough curve for the effluent [3,126,158]. Therefore, models like Adams-Bohart [188], Thomas [189], Bed depth service time (BDST) [190], and Clark [124] models have been developed to predict the dynamic behavior by considering the characteristic of the fixed-bed performance. Unfortunately, these models do not accurately describe the dynamic behavior of adsorption inside the column [3,191]. These reported models, though successful in some cases, sometimes led to errors when they were used to model the adsorption process in the fixed-bed column [3,192]. The Thomas solution [189], for instance, is limited due to being derived from a second-order reaction following Langmuir kinetics of adsorption under plug flow behavior in the bed. Because of these assumptions, the Thomas model neglects the axial dispersion in column adsorption [189,193]. The bed depth service time (BDST) model [190], on the other hand, considers surface reaction as the rate limiting step on adsorption. For this reason, it neglects intra-particular diffusion and the external mass transfer resistance [190,194]. Therefore, using a more suitable and descriptive model under the given dynamic conditions is necessary. A convection-axial dispersion model was suggested in our previous study [181] that showed a very satisfactory prediction of the dynamic behavior in the column experiment, as well as giving a good estimation of the axial dispersion effect in continuous fixed-bed removal of the organic pollutant from wastewater. In that model, the adsorption equilibrium is described by the Sips isotherm model. This is reasonable because the Sips model represents systems for which one adsorbed molecule could occupy more than one adsorption site while considering both the heterogeneity of the adsorbent surface and the interaction between the adsorbed molecules [81,122].The convection-axial dispersion model in combination with the Sips kinetic isotherm is presented in eq 4.10 [181]:

$$-D_L \frac{\partial^2 \mathrm{c}}{\partial z^2} + v \frac{\partial \mathrm{c}}{\partial z} + \frac{\partial \mathrm{c}}{\partial t} + \frac{1-\epsilon}{\epsilon}\left(\frac{n\,K\,Q_m c^{n-1}}{(1+Kc^n)^2}\frac{dc}{dt}\right) = 0 \qquad (4.10)$$

where, C is the bulk adsorbate concentration in the fluid flowing through the bed (mg/L), D_L is the axial dispersion coefficient (m/s^2), v is the interstitial velocity (m/s), q is the adsorbed mass of adsorbate per unit mass of solid, z is the distance (m), t is the time (min), ϵ is the porosity (unitless), Q_m is the maximum monolayer adsorption capacity (mg/g), K is the equilibrium adsorption constant that is related with the affinity of adsorbent-adsorbate binding force ((L/mg)^n), and n_s is the Sips dimensionless heterogeneity factor (unitless), which indicates the adsorbent heterogeneity. The following initial and boundary conditions are considered [181]:

$$C(z,0) = 0 \qquad (0 < z < L) \qquad (4.11)$$

$$at\ z = 0,\ C_{in} = C - \left(\frac{D_L}{v}\right)\left(\frac{dC}{dz}\right) \qquad (0 < t < \infty) \qquad (4.12)$$

$$at\ z = L,\ \frac{\partial C}{\partial z} = 0 \qquad (0 < t < \infty) \qquad (4.13)$$

Then, eq 10 was solved using a mathematical algorithm was developed using Mathematica (v.10.2) software to fit the experimental data with the partial differential equation (Eqn. 10) together with the initial and boundary conditions (eqs. 4.11-4.13). The NDSolve code coupled with method of lines technique was firstly used to solve the sets of partial differential equations (eqs 4.10-4.13) numerically. The proper value of effective diffusivity (D_L) for each breakthrough carve was then obtained by fitting the experimental data to the numerical solution using Manipulating code by minimizing the square root of the sum of the squares of residual.

4.4 Results and discussion

4.4.1 Characterization of adsorbate

Figure 4.3 shows the FTIR spectra of the vacuum-dried real industrial wastewater sample sample at framework rejoins of 500-1700 cm^{-1} (Figure 4.3a) and 2500-4000 cm^{-1} (Figure 4.3b). The FTIR analyzer detected significant bands at around 1700-1500 cm^{-1} and 860-680 cm^{-1}. These bands are

assigned to aromatic C=C stretch and aromatic C-H bending [28]. One visible band was obtained around 1487-1311 cm $^{-1}$, which is assigned to a N=C double bond stretching vibration [28]. An alkyl C-H stretch was assigned at the region of 2950 cm^{-1} [195], followed by a band obtained at 3030 that assigned to the aromatic C-H stretch. The O-H stretch was also assigned at the region of 3200-3300 cm^{-1} [178]. All the obtained bands suggest that the considered industrial wastewater sample is mainly composed of aromatic amine and alkyl benzene compounds. The presence of these compounds is expected because of their use in the textile processing industry. For instance, the presence of aromatic amines and alkyl benzene arises from the reduction of the azo bond of azo colorant through different processing mechanisms [196]. The sample also contained small fractions of unknown functional groups that could not be detected especially in the region of 900-1300 cm $^{-1}$.

The metals Fe, Ni, Pb, Cr, K, and Mg were detected by ICP-AES and the results showed the presence of Fe at 67 mg/L, K at 118 mg/L, and Mg at 218 mg/L. The metals Ni, Pb, and Cr could not be detected.

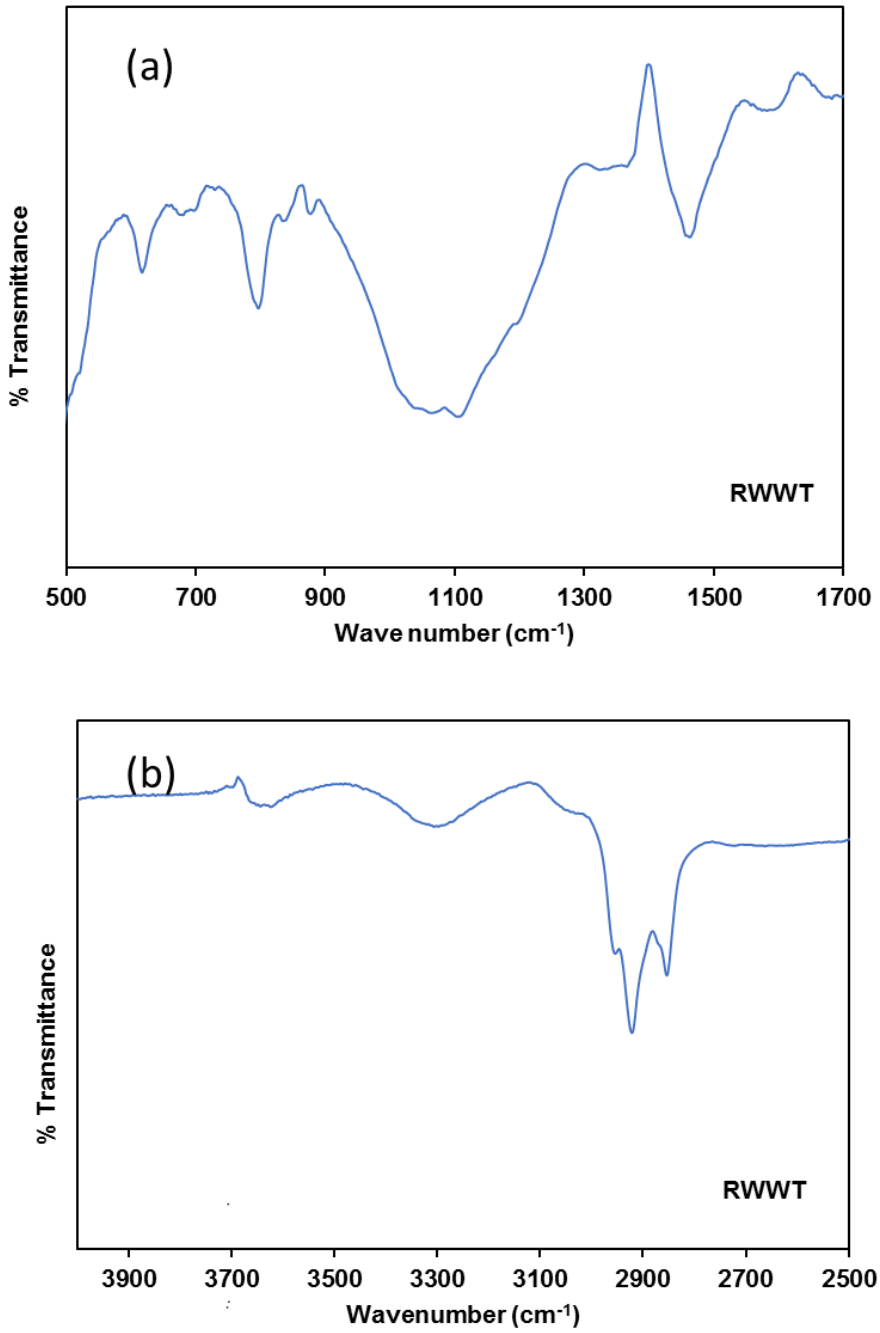

Figure 4.3. FTIR spectroscopy of dried powder of real industrial wastewater at framework regions of (a) 500-1700 cm^{-1} and (b) 2500-4000 cm^{-1}.

4.4.2 Batch adsorption experiments

4.4.2.1 Effect of pH

The initial pH value for a wastewater solution is very beneficial during any sorption study because the pH has an influence on both the surface charge of adsorbent and the solubility of the adsorbates [68,117,120,182]. Figure 4.4 describes the removal of TOC as the pH was changed from 6 to 11. No precipitation and colloid formation was observed at a pH of 9 but otherwise was observed as pH increased from 6 to 11 in the absence of specific trends because of the complexity of the industrial wastewater sample. This complexity, shown by FTIR, caused wastewater instability as pH varied. The presence of various complex organic pollutants also controlled the uptake TOC by the adsorbent, in contrast to our previous study[121] that showed constant uptake behavior as pH was changed in the removal of the dye molecules from the textile wastewater. It is important to mention the significance of PZC in the adsorption [68,120]. Through zeta potential analysis, PZC occurred at around a pH (pH $_{PZC}$) of 8 for PEI-PNPs and 5D-PEI-PNPs, which is in a good agreement with the obtained results from Figure 4.4. As shown, the obtained removal efficiency can be divided into two regions. The first region is at pH > pH_{PZC} and the second region is at pH > pH_{PZC}. Thus, the removal efficiency of the TOC was higher when the pH > pH_{PZC}. However, the removal efficiency of the TOC was lower at pH <pH_{PZC}. Based on that, at pH 9, the batch and continuous adsorption experiments were conducted and the desorption experiment was performed at pH 5.

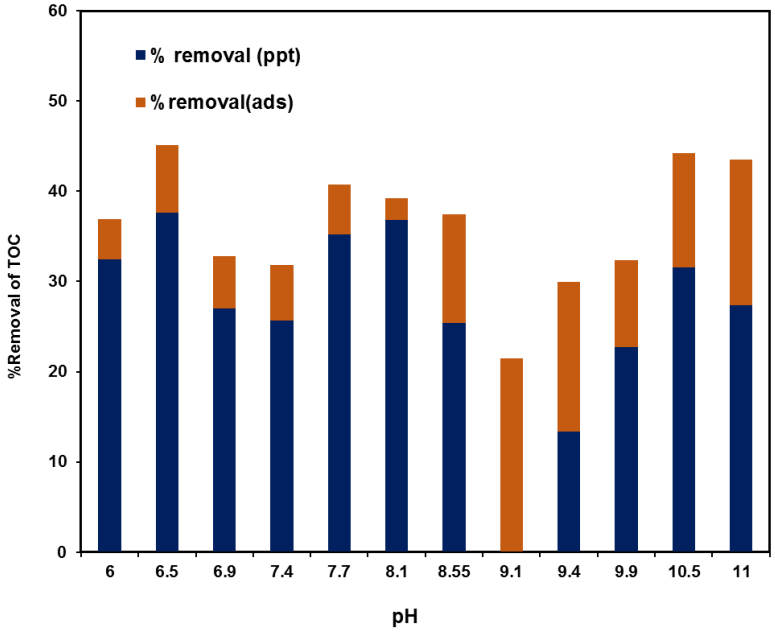

Figure 4.4. Effect of initial pH on TOC removal efficiency (% TOC removal) by adsorption (blue color) and solubility changing (red color) at range of 6-11 and the temperature of 298 K.

4.4.2.2 Adsorption isotherm

Testing the adsorption capacity for the adsorbents of 5D-PEI-PNPs, 3D-PEI-PNPs, and 1.5D-PEI-PNPs is very important. It allows us to construct adsorption isotherms, which are described by the Sips model as Figure 4.5 shows. This figure represents the experimental adsorption isotherm for the previously mentioned adsorbents at a constant temperature of 298 K along with their fit with the Sips model. Then, the corresponding fitting parameters, which were obtained from non-linear regression of the experimental data, were estimated as displayed in Table 4.1.

Statistical analysis was applied by minimizing the sum-squares of the difference between the experimentally obtained data and that expected from the Sips model by using OriginPro 8 SR4 software Version 8.095 to evaluate how well the data fits with the Sips model. This can be obtained by finding the value of Chi-square (χ^2), which was manipulated until the best fit was achieved

between the experimental data and the Sips model [99]. As illustrated in Table 4.1, the maximum adsorption capacity values (Q_m (mg/ g)) were in the order of 5D-PEI-PNPs> 3D-PEI-PNPs> 1.5D-PEI-PNPs. This is because embedding more sorption sites on Diatomite led to increasing adsorption capacity of the TOC. Furthermore, the heterogeneity coefficients (n) for all adsorbent particles were around unity, which indicated that the isotherms had a langmuirian trend [81].

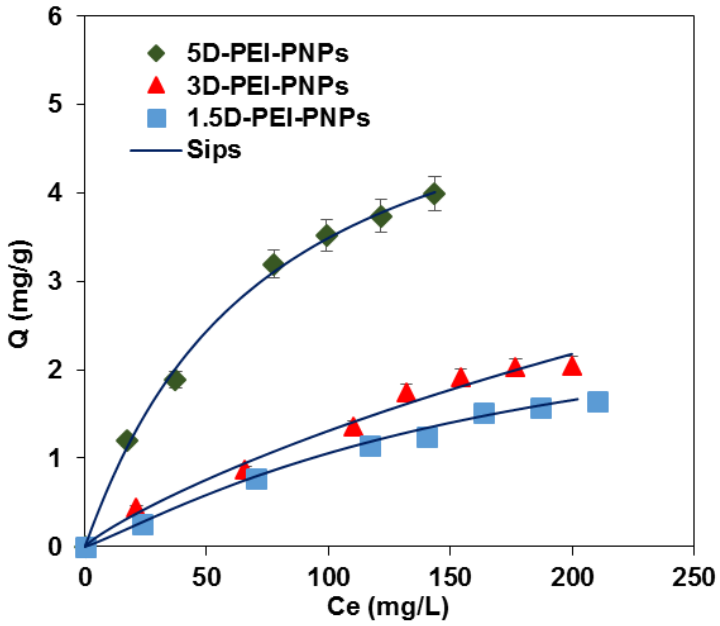

Figure 4.5. Adsorption isotherms of the TOC onto adsorbents of 5D-PEI-PNPs, and 3D-PEI-PNPs, and 1.5D-PEI-PNPs. Adsorbent dose: 100mg; shaking rate:200rpm; T:298 K. The symbols are experimental data and solid lines are from the Sips model.

Table 4.1. Estimated Sips isotherm parameters obtained at temperature 298 K and pH = 9.

Adsorbent type	**Sips parameters**			**Error analysis**
	Q_m (mg/ g)	**K ((L/mg)^n)**	**n (unitless)**	**χ^2 (unitless)**
5D-PEI-PNPs	5.95	0.012	1.03	0.0078
3D-PEI-PNPs	5.48	0.0039	1	0.0104
1.5D-PEI-PNPs	3.15	0.0034	1.15	0.0022

4.4.3 Column adsorption

Column experiments were successfully implemented for adsorption of TOC from the industrial wastewater sample in the D-PEI-PNPs fixed-bed under various dynamic conditions of influent flow rate (Q), inlet CRD concentration (C_o), bed height (Z), and concentration of nanoparticles embedded on Diatomite (%nps). During each column experiment, the experimental data followed the typical behavior of the BTC. Initially, all pollutants were adsorbed, resulting in zero solute concentration in the effluent. As column operations continued, an adsorption zone appeared and moved progressively downward through the bed. Eventually, the adsorption zone reached to the bottom of the column. In that moment, the effluent concentration began to increase gradually until attaining the saturation point. Then the experiment was stopped and the experimental data were plotted in the form of BTC profiles. Figures 4.6-4.10 show BTC profiles obtained from varying the values of various operational parameters. Each experimental BTC is identified by points having different colors, while the continuous solid blue lines represent the proposed numerical model for the mass balance of the fixed-bed column (eq 4.10). As can be clearly seen, these profiles have the typical S-shape of BTC, which is a good indication for mass transfer and internal resistance effects within the column [3,126]. In addition, the obtained data fit very well with the numerical solutions to eq 4.10. Table 4.2 lists the operational parameters during each column experiment as well as the calculated designed parameters of t_b, t_t, %Removal, and H_{UNB}. The table also displays the fitting parameter (D_L) and the corresponding dimensionless numbers of Renold (Re), Schmidt (Sc), and Sherwood (Sh), along with the Biot number (Bi) after estimating the external film coefficient (K_c) (m/s). As presented, axial dispersion coefficients (D_L) were computed, compared to some previous studies that neglected them [189,190,193,194]. In fact, neglecting this parameter may cause

considerable error in the evaluation of transfer coefficients while the fluid flows through the column, especially at low flow rates [159,166]. The fitting parameters ($D_{L's}$) were accurately described by the proposed model which can be indicated from the low values of χ^2 as displayed in Table 4.2. With respect to mass transfer phenomena, it is important to know which mechanism is dominant and controlling through the adsorbent particles. Therefore, it is beneficial to use an empirical correlation using a group of dimensionless numbers (Re, Sc, Sh, and Bi). Among these correlations is the Wilson-Geankoplis correlation [197,198], which can be used at $0.0015 < Re < 55$, and is given by the expression:

$$Sh = \frac{1.09}{\epsilon}\left(Re\ Sc^{1/3}\right) \tag{4.12}$$

This correlation can be used to estimate the film mass transfer coefficient (K_c). This coefficient has a sensitivity analysis in observing the overall effect of each parameter in the column because the obtained breakthrough curves have a significant response due to a small change in the K_c values [198,199]. The reason for the sensitivity of the film resistance is explained by using the Biot number (Bi), which is defined as

$$Bi = \frac{K_c R}{D_L} \tag{4.13}$$

where R is the adsorbent size (m). The Bi is a ratio between the intraparticle diffusion and the external film diffusion. As listed in Table 4.2, Bi values are low for all cases, indicating that film diffusion is the dominant step rather than the intrapaticular mass transfer [197,198]. This fact is in good agreement with the results obtained elsewhere [198].

Table 4.2. Summary of the experimental breakthrough curves (BTCs) design parameters and the predicted parameters after fitting the experimental data with the dispersion-convection model together with standard error analysis of the fitting in terms of the values of χ^2 for TOC removal for industrial wastewater sample at 298 and pH= 9.

Experimental conditions				**Designed parameters**			**Modeling parameters**							
***Q* (ml/min)**	***C*$_o$ (mg/L)**	***Z* (cm)**	***%nps* (wt%)**	***t*$_b$ (min)**	***t*$_t$ (min)**	***%* Removal**	***H*$_{UNB}$**	***D*$_L$×10^6 (m^2/s)**	***Re***	**Sc**	***Sh***	***K*$_C$ (m/s)**	***Bi***	χ^2
0.8	290	7.5	5	15	58	57	5.56	9.82	0.356	0.10	0.73	0.84	0.73	0.03
1.2	290	7.5	5	8	39	55	5.96	20.5	0.540	0.04	0.65	1.58	0.65	0.05
1.5	290	7.5	5	3.5	29	53	6.60	32.8	0.670	0.03	0.60	2.33	0.60	0.06
0.8	195	7.5	5	13	59	56	5.84	7.72	0.356	0.12	0.79	0.71	0.62	0.05
0.8	145	7.5	5	7	65	53	6.68	4.45	0.356	0.22	0.94	0.50	0.42	0.03
0.8	290	3.5	5	9	35.5	57	2.61	6.22	0.356	0.16	0.84	0.62	0.84	0.03
0.8	290	2.5	5	7	24	58	1.81	3.15	0.356	0.31	1.06	0.40	1.06	0.02
0.8	290	7.5	3	8.5	39.2	56	5.87	9.40	0.356	0.10	0.74	0.81	0.74	0.05
0.8	290	7.5	1.5	4.5	36.2	53	6.56	9.05	0.356	0.11	0.75	0.80	0.75	0.05

4.4.3.1 Effect of flow rate

The effect of the flow rate on adsorption of TOC from the industrial wastewater sample using 5D-PEI-PNPS was investigated by varying the flow rate (0.8, 1.2, 1.5 ml/min) with a constant adsorbent bed height of 7.5 cm and inlet TOC concentration of 290 mg/L. The break thought data is presented in Figure 4.6. As shown, it was found that as the flow rate increased (0.8-1.5 ml/min), the %Removal of TOC from the wastewater was decreased (57-53 %). The reason behind this is that at a high inlet flow rate, there is not enough residence time for adsorption equilibrium to be reached and the front adsorption zone rapidly moved to the bottom of the column, which saturates the column earlier, leading to less contact time of TOC with the adsorbent binding sites and subsequently a reduction in the removal efficiency of the TOC [126,156,186]. At a high flow rate, also, the rate of mass transfer increases such that a larger amount of TOC adsorbed onto unit bed height by increasing the flow rate [3]. This was indicated by increasing the value of H_{UNB} (Table 4.2). It is important to explain the breakthrough behavior by changing the flow rate in terms of mass transfer phenomena. As shown in Table 4.2, at high flow rate a larger value of K_c was obtained. Also, reasonable reduction in the values of Bi was obtained with increasing the flow rate. This is because at high flow rates and for short bed, film diffusion is the controlling mechanism [4,198].

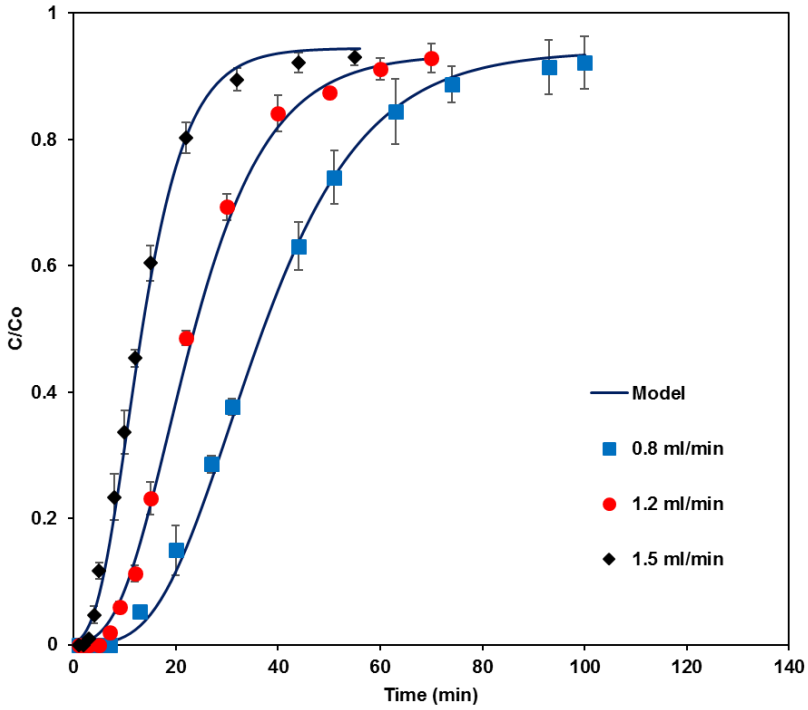

Figure 4.6. Breakthrough curves (BTCs) for adsorption of TOC onto 5D-PEI-PNPs at different influent flow rates. The symbols represent experimental data, and the solid lines are the convection-axial dispersion model (eq 4.10). Experimental operating conditions. Influent TOC concentration =290 mg/L, bed height=7.5 cm, temperature=298, pH=9.

4.4.3.2 Effect inlet wastewater concentration

Inlet pollutant concentration is a limiting factor due to the presence of a fixed number of binding sites for the adsorbent particles, which limits the adsorbed amount of pollutant inside the fixed-bed column. These binding sites treat a small volume of effluent when the inlet concentration is high [3,126,140,161,186]. Figure 4.7 illustrates the sorption BTCs obtained for adsorbate concentrations of 145, 195 and 290 mg/L at the bed height and the flow rate of 7.5 cm and 0.8 ml/min, respectively. As shown in Figure 6, late breakthrough occurred for low inlet TOC concentration and longer time required to saturate the surface of 5D-PEI-PNPS. In another contrary theory, with increasing the driving force of the mass transfer process inside the bed, the

equilibrium, as anticipated, is attained faster [3,4,126]. Table 4.2 shows that with increasing the inlet TOC concentration of pollutants (145-290 mg/L), H_{UNB} increased, while the %Removal of TOC decreased. This can be explained by the fact of increasing the uptake capacity of the adsorbent that might occur due to high inlet TOC concertation that provides a higher driving force to overcome the mass transfer resistance [16,126,198]. Thus, at lower TOC concentration, more TOC molecules present in the wastewater solution that interacts with the fixed number of binding sites. Hence, more TOC molecules left unbounded that subsequently led to decrease the removal efficiency [3,113,155,166,200].

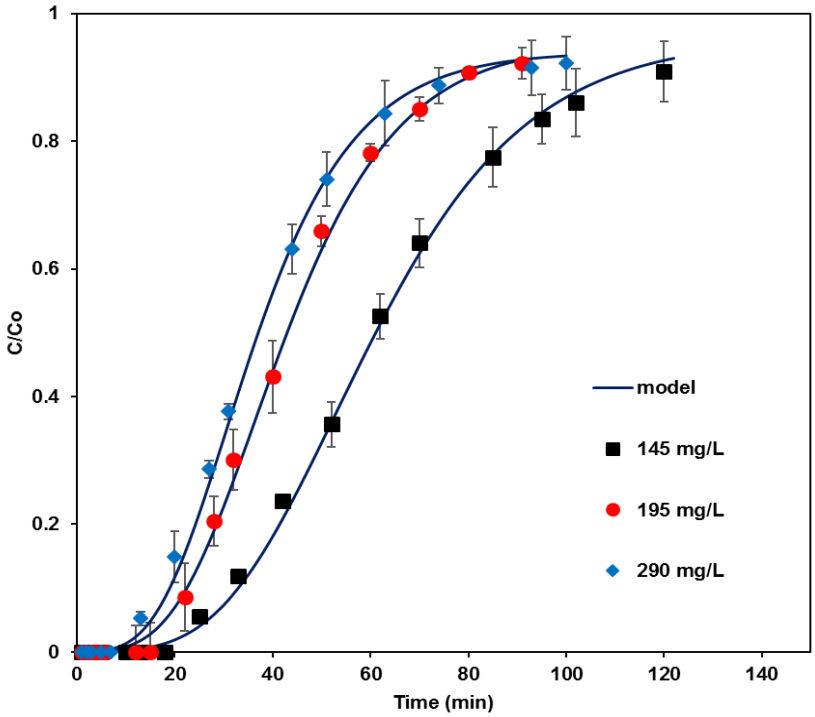

Figure 4.7. Breakthrough curves (BTCs) for adsorption of TOC onto 5D-PEI-PNPs at different initial TOC concertation. The symbols represent experimental data, and the solid lines are the convection-axial dispersion model (eq 4.10). Experimental operating conditions: influent flowrate= 0.8 ml/min, bed height= 7.5 cm, temperature=298K, pH=9.

4.4.3.3 Effect of bed height

Adsorbent amount or bed height is an important factor because it strongly influences the steepness on the BTCs. Therefore, this effort was done to investigate the performance of BTCs by varying the bed heights of 2.5, 3.5, and 7.5, wastewater had influent TOC concentration 290 mg/L, pH 9 and flow rate 0.8 mg/L. As depicted by Figure 4.8, the breakthrough time increased from 7 to 15 min, with increasing bed height from 2.5 to 2.5 cm. This occurred since by increasing the bed height, the residence time of the TOC molecules increased [3,126]. The presence of more residence time allows for more molecules to diffuse into the adsorbent particles that increased the removal efficiency. This behavior can be explained by the fact of increasing the surface area of the adsorbent particle via increasing the bed height, which provided more availability of binding sites that interact with more TOC molecules [3,62,126]. As listed in Table 4.2, longer breakthrough time was achieved as the bed height increased. This can be attributed to the fact that when there was a higher bed height, the better intraparticle phenomena was obtained, even though the intraparticle diffusion is function with some physical properties of the bed with bed porosity and tortuosity [201]. However, This trend is not agree with the prevoius studies [3,62,126] and our prevoius study in the adsorption of dye from the textile wastewater even though both studies occurred under the same conditions [121], because it was expected a reduction in the axial dispersion with increasing the bed height (Table 4.2). This trend might be explained due to presence of different adsorbed molecules in the considered industrial wastewater sample that had a significant contribution in changing the behavior inside the fixed-bed column while the bed height increased.

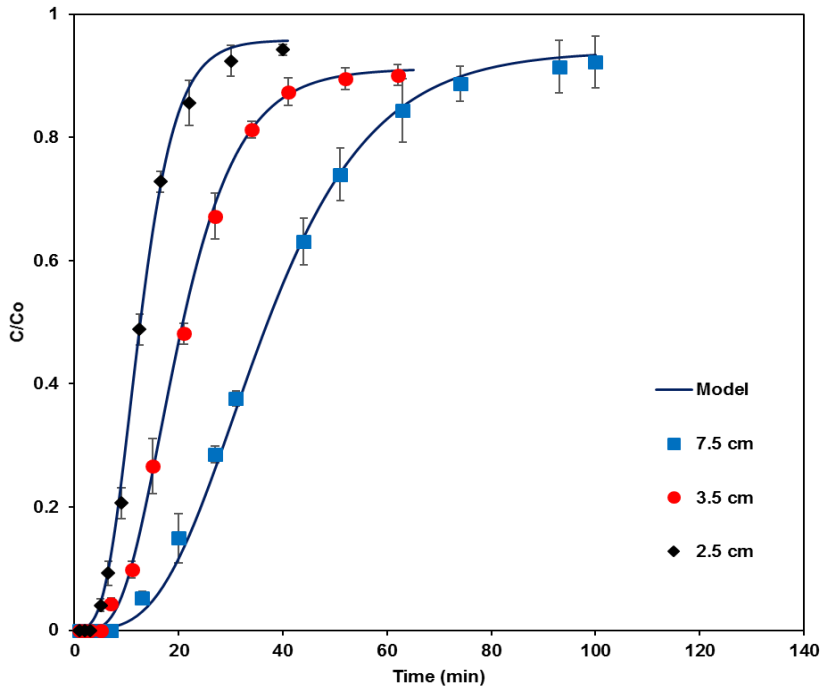

Figure 4.8. Breakthrough curves (BTCs) for adsorption of TOC onto 5D-PEI-PNPs at different bed-heights. The symbols represent experimental data, and the solid lines are convection-axial dispersion model (eq 4.10). Experimental operating conditions: influent TOC concertation =290 mg/L, influent flow rate =0.8 ml/min, temperature =298 K, pH=9.

4.4.3.4 Effect of the concentration of nanoparticles embedded into Diatomite

The amount of nanoparticles embedded on Diatomite has a strong influence on the breakthrough behavior[156,158,164,181]. Therefore, this study investigates the effect of embedding 1.5-5 wt% of PEI-PNPS at the constant influent flow rate of 0.8 ml/min, the influent TOC concentration of 290 mg/L, and the bed height of 7.5 cm. As shown in Figure 4.9, by increasing the number of nanoparticles embedded on Diatomite, longer breakthrough time was obtained due to the presence of more sorption sites with increasing PEI-PNPS on Diatomite, which led to providing more surface area to attract more TOC molecules from the influent wastewater [156,158,164,181]. As listed in Table 4.2, the %Removal of TOC was increased from 53 to 57% by increasing the

embedded nanoparticle on Diatomite. H_{UNB}, as an important design parameter, decreased from 6.65 to 5.65 when the nanoparticle concentration was from 1.5 to 5 wt%. This trend is similar to that obtained in our prevoius study [181]. In the phenomena of mass transfer, the obtained axial dispersion coefficients were slightly increased and the corresponding Bi was slightly decreased by increasing the nanoparticle concentration on Diatomite.

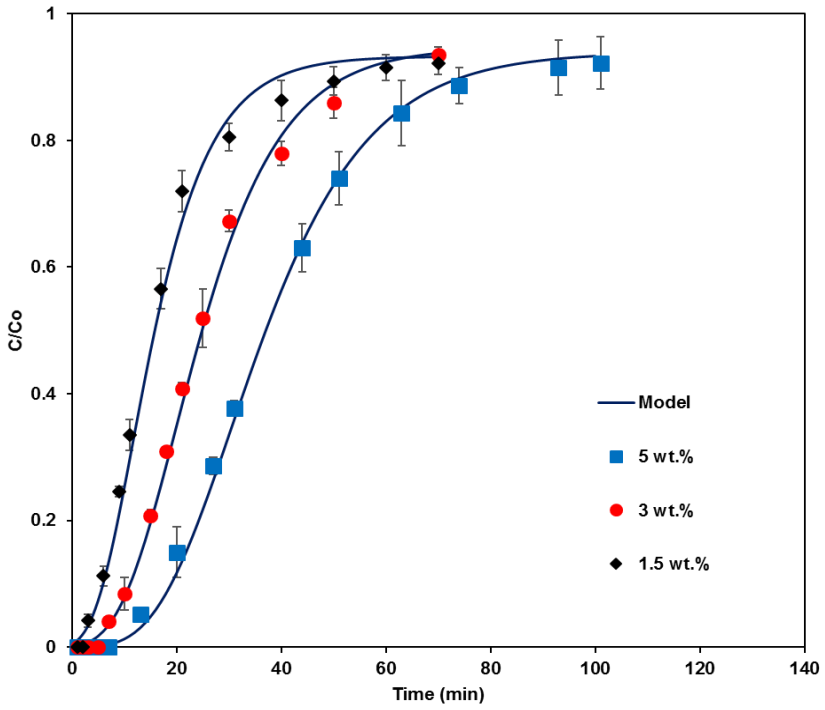

Figure 4.9. Breakthrough curves (BTCs) for adsorption of TOC at different weights of PEI-PNPs (5 wt.%, 3 wt.%, and 5 wt.%). The symbols represent experimental data, and the solid lines are the convection axial desperation model (eq 4.10). Experimental operating conditions: Initial TOC concertation =290 mg/L, influent flow rate=0.8mg/L, bed height=7.5 cm, Temperature=298, pH=9.

4.4.4 Desorption and regeneration study

Desorption or recovery is an essential concept, especially if the pH has a significant effect, in the sustainable manner of adsorption study [13,68,117,120]. But the regeneration process should not

damage the adsorbent inside the fixed-bed column otherwise their reuse will be inefficient [68,202]. Figure 4.10 shows desorption cycles that were obtained for the spent adsorbent of 5D-PEI-PNPs through 2 back-wash desorption cycles with 0.5 M of HNO_3 at pH 5. This pH and concentration, as indicated from the batch adsorption study, were selected to provide the opportunity to re-use or regenerate the adsorbent. Also, an efficient desorption only occurs in a acidic medium that provides protons, which efficiently compete with the pollutant ions on the amino sites of PEI [203]. As shown in the figure, a successful desorption was achieved by 2 back-wash cycles within 5 min, which indicates that the desorption occurred rapidly. In addition to that, the rapid desorption supports the fact that adsorption-desorption occurred at the external surface [33]. However, the desorption steps were not complete since the obtained desorption cycles are not identical (Figure 4.10). This suggest that the regeneration efficiency decreases with increasing the number of cycles. This is expected for the considered industrial wastewater sample because it contained various organic molecules that have different adsorption-desorption behavior, which led to saturate the sorption sites with molecules that have high affinity for adsorption at low pH.

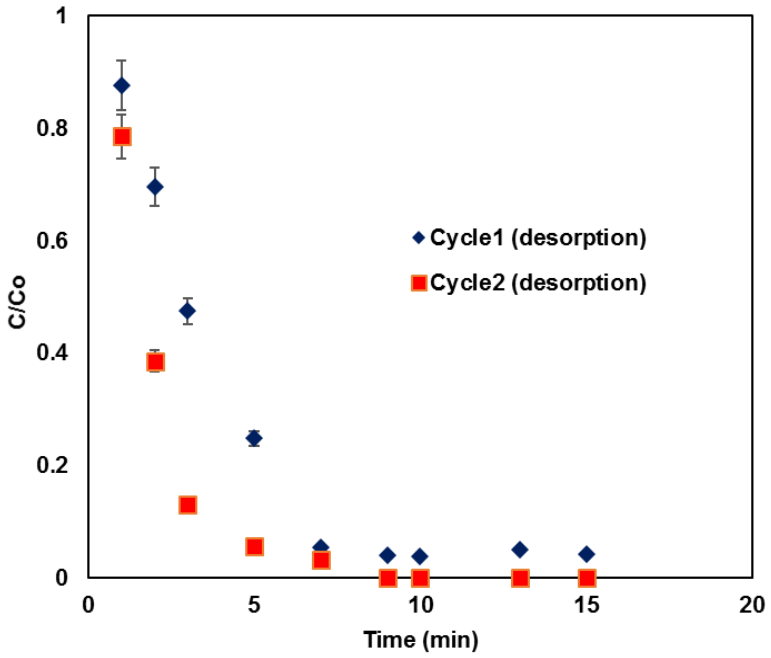

Figure 4.10. Desorption Cycles of 5D-PEI-PNPs with 0.5 M of HNO3 at pH of 5 and temperature of 298 K.

4.4 Conclusion

Diatomite (D4500), a type of filter aid, was successfully embedded with < 5wt % of poly(ethylenimine)-functionalized pyroxene nanoparticles, following our previously reported protocol. The Diatomite was then converted to a novel adsorbent, which had an active and a multifunctional surface. This novel adsorbent was tested in batch and continuous fixed-bed column experiments for cleaning up a real industrial wastewater sample under an optimal pH value and constant temperature. The obtained adsorption isotherms were well observed by the Sips model. Furthermore, kinetic study inside a column experiment was employed by using a convection-axial dispersion model to determine the breakthrough profiles in the fixed-bed column. The breakthrough profile was studied under the influence of various operational parameters that are the inlet flow rate, the influent total organic carbon concentration, the bed height, and the nanoparticles

concentration embedded on Diatomite. It was obtained that Diatomite, after embedding the functionalized nanoparticles, had an outstanding performance in removing the total organic carbon from the real industrial wastewater. In the fixed-bed experiments, the data obtained were represented very well by using the convection-axial dispersion model under the effect of various dynamic conditions. Fitting the obtained breakthrough data with the model allows us to determine the axial dispersion coefficient. This coefficient was able to observe the effect of dynamic conditions in terms of the mass transfer concepts together with a suitable correlation. This allowed us to determine the dominant of the mass transfer process inside the fixed-bed column under the effect of different operational parameters. Interestingly, it was obtained that external film diffusion is the dominant for the mass transfer phenomena inside the fixed-bed column experiments. Moreover, the ability of reusing and regenerating the spent adsorbent was studied and it was obtained that at low pH, incomplete and rapid kinetic of desorption was carried out for the real industrial wastewater.

CHAPTER FIVE

Application of Nanoparticles in Industrial-Level Field-Test Experiments:

Rotary Drum Filter Tests at Executive Mat Ltd

5.1 Introduction

Executive Mat Ltd, in Calgary, is using a conventional treatment method by a rotary drum filter (RDF) to remove the suspended solids and total organic carbon (TOC) from industrial effluents. As shown in Figure 5.1, RDF consists of a drum rotating in a tub of wastewater to be filtered. The drum is pre-coated with a filter aid, typically Diatomite. After applying the pre-coat, the wastewater is sent to the tub below the drum, which rotates through the wastewater liquid, applying a vacuum. The vacuum sucks the wastewater onto the drum's pre-coated surface, separating it into liquid and solid portions. The vacuum sucks the liquid portion through the filter media to the internal part of the drum, resulting in a filtrated liquid that is pumped away. Solids, on the other hand adhere to the pre-coated surface. The drum then automatically passes a knife through the adhered solid and part of the filter media (Diatomite), revealing a fresh surface media. Although RDF is effective in some types of wastewater, it is inefficient, especially when the wastewater contains a high level of dissolved total organic carbon. This is because the employed Diatomite has a very weak adsorption capacity but excellent absorption power. It is therefore widely-used as a filter aid in the filtration of suspended solids, but it is ineffective in the adsorption of the dissolved pollutants [39]. As a result, there is a dire need for an improvement in the filtration efficiency of the Diatomite. This is frequently accomplished by etching the Diatomite with a stronger acid or base to modify its adsorption efficiency [40]. Unfortunately, using strong acids or bases is environmentally unsafe and their action is corrosive to the RDF. There is therefore a need for an innovative and integrated technology to be used with the current one to overcome these problems. A practical novel technology was proposed and proven by embedding < 5 wt% of nanoparticles with Diatomite so that the nanoparticles, are improving the removal of suspended solids, also

increasing the adsorption capacity of the dissolved total organic carbon [181]. In this scalable application, we interpreted industrial-level field-test experiments of this proposed technique that aims at exploring the possibility of utilizing the novel nanoparticle adsorbents of magnetite (INPs) in a continuous mode using a RDF at Executive Mat Ltd. The INPs was prepared and embedded into Diatomite in the RDF at mass ratios of 0.5, 1, 2 wt%. Then the removal efficiency was tested and the effect of nanoparticle concentration, as one of the dynamic parameters, was investigated. To the best of our knowledge, there is no any real wastewater treatment process utilizing nanoparticle technology at industrial level.

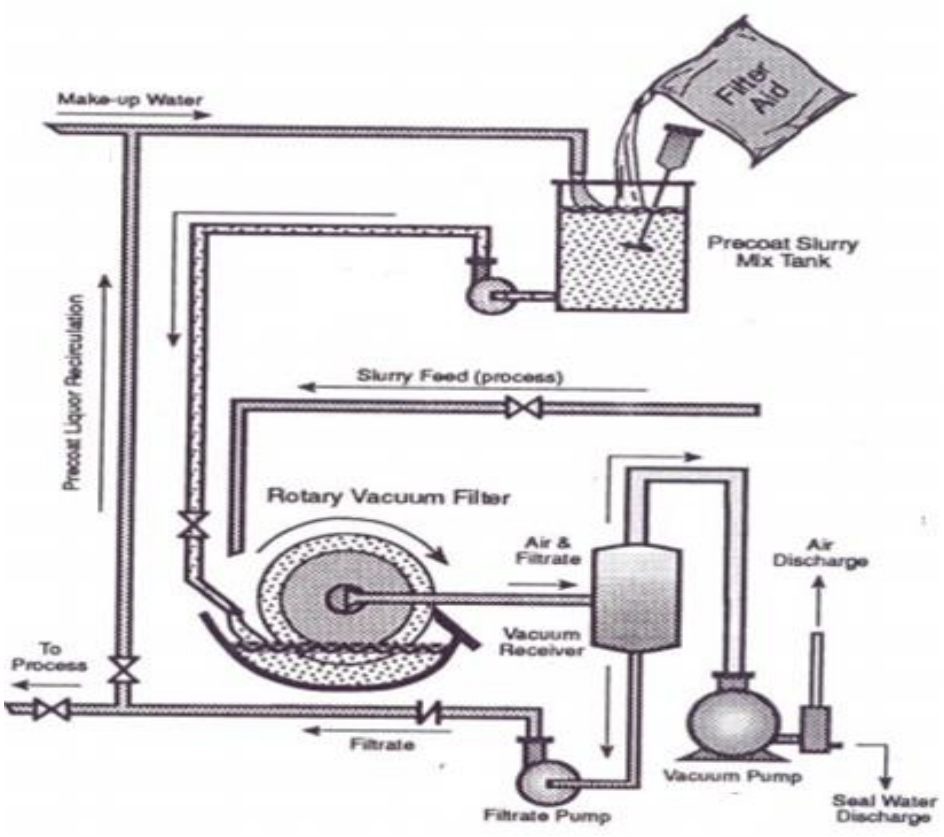

Figure 5.1. Schematic representation of typical design of rotary drum filter (RDF) process.

5.2 Materials and methods

5.2.1 Materials

The following chemicals were purchased from Univar Calgary, Alberta, Canada: Iron sulfate hepta-hydrate (≥ 99%), ammonium hydroxide (28-30% NH_3) and hydrogen peroxide (30-35%). While the Diatomite (filter aid) was supplied from Executive Mat Ltd, Calgary, Canada. All the previously mentioned chemicals were used as they are without any purification.

5.2.2 Methods

Concentration of nanoparticles, as an important operational parameter, was investigated with a RDF by running 5 experiments at concentrations of 0 wt% (standalone Diatomite), 0.5 wt%, 1 wt%, and 2 wt%, respectively, at Executive Mat Ltd, Calgary. These various mass ratios of nanoparticles were embedded in Diatomite by preparing them separately in the pre-coat slurry mix tank over a period of 65 min, following our modified protocol of preparing the magnetite nanoparticles [121]. The standalone Diatomite was pre-coated directly following the typical adapted method at Executive Mat Ltd, Calgary. The slurry solution of embedded nanoparticles in Diatomite then coated the rotary drum. Afterward, the vacuum sucked the contaminated wastewater onto the drum pre-coated surface and the effluent water was pumped to the discharge tank. Effluent samples were collected periodically as time proceeding from the tank during the experiment. Then, each sample concentration was measured using a Shimadzu Total Organic Carbon Analyzer (TOC-L CPH/CPN) to measure the TOC in the aqueous samples to estimate the removal efficiency and plot the breakthrough curves. In this application, the concentration of nanoparticles embedded on Diatomite was investigated under the same operational conditions for the all runs. This study allowed us to find the optimal ratio of nanoparticles embedded on the

Diatomite. The other operational parameters include influent flow rate, influent quality (TOC), knife cutting speed, and loaded amount of Diatomite were all fixed without being under our investigation.

5.3 Results and discussion

5.3.1 Total organic carbon (TOC) removal efficiency and breakthrough behavior

Figure 5.2 shows the experimental breakthrough curves (BTCs) obtained for the Diatomite before and after embedding various mass ratios of nanoparticles (0.5, 1, 2 wt% INPs) in a 22.7 kg of Diatomite. Each certain experiment was conducted at constant inlet flow rate, and knife cutting speed. As expected, with increasing the concentration of the embedded nanoparticles on Diatomite, the breakthrough time accordingly increased that refers to presence of more sorption sites that led to presence of more sorption surface area, providing better TOC removal efficiency. However, Figure 5.2 shows absence of specific trend in the shape of the breakthrough curve as the concentration of the nanoparticles was increased to 2 wt%.

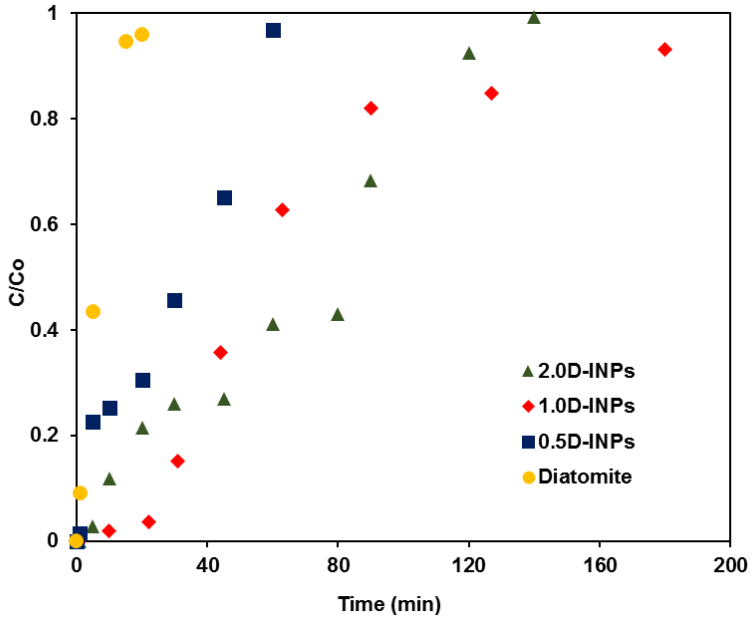

Figure 5.2. Breakthrough curves (BTCs) for adsorption of TOC at different weight of INPs (2 wt.%, 1 wt.%, and 0.5 wt.%). The symbols represent experimental data.

This behavior was observed due to formation of a serious crack at nanoparticle concentration of 2 wt%, because the presence of a high concentration of INPs embedded on Diatomite causes formation of pressure drop, leading to block the filter media. Based on that, it was suggested to perform other experiments at lower concentrations of INPs embedded on Diatomite. At 0.5 wt %, for instance, no crack was obtained but lower performance was achieved. Therefore, an experiment at 1 wt% INPs higher INPs was performed. At 1 wt% INPs, better performance in addition to formation of the typical breakthrough behavior. Accordingly, embedding 1 wt% of INPs was considered as the optimal concentration of the magnetite nanoparticles in the Diatomite. Figure 5.3a represents the obtained breakthrough curve of the standalone Diatomite, while Figure 5.3b shows that of 1.0D-INPs. Both figures also include selected samples, which shows the gradual changing in the color from colorless to dark as the time increased from colorless to dark in color. As seen, in absence of nanoparticles, very low efficiency in the TOC removal was obtained that can be indicated from the rapid changing in the color from colorless to dark. In presence of nanoparticle (1.0D-INPs), however, more efficient TOC removal was achieved that was indicated from the gradual changing of the samples color from colorless to dark.

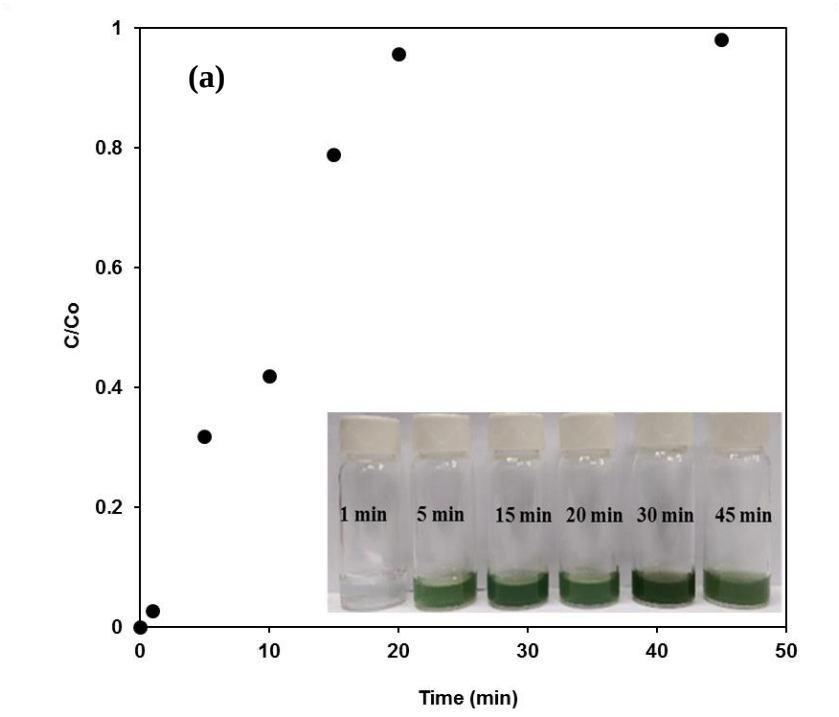

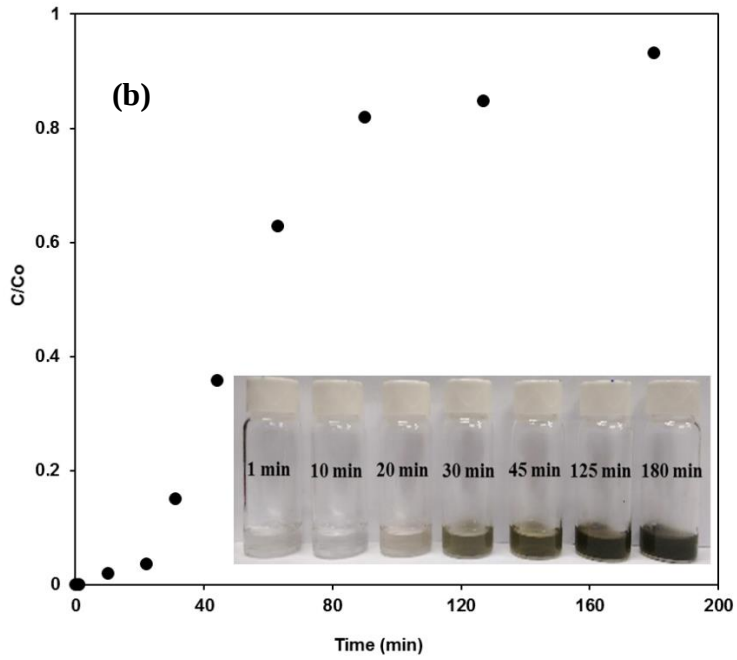

Figure 5.3. Breakthrough curves (BTCs) and photographs of selected samples for adsorption of TOC by (a) standalone Diatomite, and (b) 1 wt.% of INPs embedded into Diatomite. The symbols represent experimental data.

The operational parameters of influent wastewater quality (TOC), influent flow rate, amount of Diatomite, and knife speed cutting have a significant influence in the removal efficiency of the TOC and subsequently the obtained breakthrough behavior. The loaded amount of Diatomite, whether it's embedded with the nanoparticles or not, has a strong effect on the removal efficiency. The explanation for this is that as the bed depth increased, the residence time for the pollutant inside the bed increased, which allows for them to be adsorbed by the adsorbate particles, resulting in high TOC removal efficiency [3,126,181]. Increasing the influent flow rate and quality, in addition, have a strong effect on the obtained breakthrough behavior such that they increased the amount of TOC molecules, which led to higher uptake then it followed more quickly saturation, leading to earlier breakthrough time and lower removal efficiency [3,126,181]. Depth or speed of cutting, also, has a strong a substantial function in the breakthrough behavior because with increasing the cutting speed the saturation of the bed can be delayed. However, it reduces the loaded amount of Diatomite at the RDF, which impacts the removal efficiency of the TOC. All these operational parameters must be under investigation to provide more tangible and outstanding results.

5.4 Conclusion

As a summery, a real wastewater treatment technique using nanoparticle technology was implemented at Executive Mat Ltd, in Calgary, Canada. Magnetite nanoparticles at various mass ratios (0.5, 1, 2 wt%) were in-situ prepared and embedded into Diatomite at a rotary drum filter in order to improve the filtration efficiency of the industrial influents at Executive Mat Ltd. The concentration of nanoparticles embedded into the Diatomite, as an important dynamic parameter, was investigated and it was obtained that at mass fraction of 1 wt% of INPs embedded on diatomite, better performance in the removal efficiency was achieved without formation of any crack on the bed. The operational parameters of influent wastewater quality (TOC), influent flow rate, amount of Diatomite, and knife speed cutting were all figured out and their influence on the removal efficiency of the TOC was observed. Thus, and if successful, this work will be implanted industrially for the first time, as the preliminary filed test results confirmed the viability and the novelty of our technique.

CHAPTER SIX

Conclusion and Recommendation

6.1 Concluding remarks

Poly(ethylenimine)-functionalized pyroxene (PEI-PNPs) nanoparticles at mild conditions for targeting the cleanup of industrial effluents was successfully synthesized. The characterization result showed that the prepared PEI-PNPs were sheet-like and spherical like in shape, had a low BET surface area (~ 18 m^2/g) that increased reasonably to ~119 m^2/g by drying using Lyophilizing method instead of conventional drying of the synthesized materials. The prepared inorganic part of the PEI-PNPs had a small crystalline domain size around 10 nm. The PEI functionality was confirmed using FTIR and TGA analysis. Also, during batch-mode adsorption, the adsorption isotherm was described using Sips model and the PEI-PNPs had a very high adsorption capacity and affinity to organic species compared with other adsorbents like activated carbon and iron oxide, without being affected with respect to the medium pH. Moreover, fast adsorption was obtained (< 15 min) and the kinetic external mass transfer model fit well with the kinetic experimental data and reasonably described the rate of adsorption.

In our second study, PEI-PNPs were successfully embedded into Diatomite obtaining an active adsorbent with improved surface functionality. In addition to that, adsorption of commercial red dye (CRD) has been studied in discontinuous (batch) and continuous flow column experiments. The adsorption isotherms were well described using the Sips model. Kinetic studies in the batch experiments have been employed to calculate the breakthrough profiles in the fixed-bed adsorption column. In the continuous experiments, the effects of operational variables (e.g., inlet concentration of CRD, inlet flow rate, bed height, and nanoparticle concentration in Diatomite)

have been analyzed using one factor at one time (OFAT) design of experiment method. It was shown that adsorption performance of the CRD in continuous fixed-bed by using filter aid of Diatomite that was functionalized by very low mass percentages (< 5 wt%) of functionalized-PEI pyroxene nanoparticles was improved very well. Moreover, in the column experiments, the breakthrough curves for CRD removal were very well represented using the convection-dispersion model, which enabled us to determine the axial dispersion coefficient (D_L) and Peclet number (*Pe*). The obtained fitting parameter values of D_L are in a good agreement with that obtained from the correlation available from the literature. Analysis of the breakthrough data using the equivalent length of unused bed (H_{UNB}) approach have shown that H_{UNB} is very well correlated with Peclet number (*Pe*) under effect of various operational conditions.

In the third study, the Diatomite was successfully embedded with < 5wt % of PEI-PNPs, as a novel adsorbent, was tested in batch and continuous fixed-bed column experiments for cleaning up a real industrial wastewater sample under an optimal pH value and constant temperature. The obtained adsorption isotherms were well observed by the Sips model. Furthermore, kinetic study inside a column experiment was employed by using a convection-axial dispersion model to determine the breakthrough profiles in the fixed-bed column under the influence of the previously mentioned operational parameters. The results showed that Diatomite, after embedding the functionalized nanoparticles, had an outstanding performance in removing the total organic carbon from the real industrial wastewater. In the fixed-bed experiments, the data obtained were represented very well by using the convection-axial dispersion model under the effect of various dynamic conditions. Fitting the obtained breakthrough data with the model allows us to determine the axial dispersion coefficient. This coefficient was able to observe the effect of dynamic conditions in terms of the mass transfer concepts together with a suitable correlation. This

allowed us to determine the dominant of the mass transfer process inside the fixed-bed column under the effect of different operational parameters. Interestingly, it was obtained that external film diffusion is the dominant for the mass transfer phenomena inside the fixed-bed column experiments. Moreover, the ability of reusing and regenerating the spent adsorbent was studied and it was obtained that at low pH, complete and rapid kinetic of desorption was carried out for the real industrial wastewater.

In our last study, a real wastewater treatment technique using nanoparticle technology was implemented at Executive Mat Ltd, in Calgary, Canada. Magnetite nanoparticles at various mass ratios (0.5, 1, 2 wt%) were in-situ prepared and embedded into Diatomite at a rotary drum filter in order to improve the filtration efficiency of the influent wastewater at Executive Mat Ltd. The concentration of nanoparticles embedded into the Diatomite, as an important dynamic parameter, was investigated and it was obtained that at mass fraction of 1 wt% of INPs embedded on Diatomite, better performance in the removal efficiency was achieved without formation of any crack on the bed. The operational parameters of influent wastewater quality (TOC), influent flow rate, amount of Diatomite, and knife speed cutting were all figured out and their influence in the removal efficiency of the TOC was observed. Thus, and if successful, this work will be implanted industrially for the first time, as the preliminary filed test results confirmed the viability and the novelty of our technique.

6.2 Recommendations

The following recommendations are suggested for future studies in the field based on the obtained results:

- All the adsorption experiments were conducted for an in-house prepared pyroxene nanoparticles that have the same particles size under the same conditions. Considering

different nanosizes is worth investigating as nanosize effect plays role in adsorption. Furthermore, pyroxene, as reported, has a superficial ion exchange properties. It is excepted that functionalizing the pyroxene on acidic medium increases the loaded amount of the polyethyleneimine, which subsequently can increase the multi-functionality and the adsorption capacity for the functionalized nanoparticles.

- Separation prior all the batch and continuous adsorption experiments is considered as one of the drawback of using this type of nanoparticles, leading to use it as once-through process. Therefore, it is suggested to increase their magnetic properties by creating a magnetic core surrounded by shell of pyroxene nanoparticles that can be functionalized by the polyethyleneimine following our protocol.
- Polyethyleneimine, as reported, has a high adsorption capacity for the heavy metals like Pb (II), Cd (II), and Cu (II). Therefore, our innovative adsorption technology can be applied for heavy metal removal too.
- Our continuous fixed-bed column adsorption study was limited at very low flow rates. Therefore, increasing the influent flow rate might influence the validity of our proposed convection-axial dispersion model.
- At the rotary drum filter (RDF), the operational parameters of influent wastewater quality (TOC), influent flow rate, amount of Diatomite, and knife speed cutting should be all under investigation and their influence in the removal efficiency of the TOC. Thus, and if successful, this work will be implanted industrially for the first time, as the preliminary filed test results confirmed the viability and the novelty of our technique.
- Our promising results indicated that our innovative technique can be used as an integrated technique with sand-bed filtration for suspended and dissolved solids removal so our technique can be more mimicable to the industrial application.

References

[1] G. Water Intelligence, Industrial Water Technology Markets 2015, Water Supply. (2015). Https://Www.Globalwaterintel.Com/Client_Media/Uploaded/Emma/Toc Gwi_Industrial_Water_Technology_Markets_V1.Pdf.

[2] X. Qu, P.J.J. Alvarez, Q. Li, Applications Of Nanotechnology In Water And Wastewater Treatment, Water Res. 47 (2013) 3931–3946. Doi:10.1016/J.Watres.2012.09.058.

[3] F.J. García-Mateos, R. Ruiz-Rosas, M.D. Marqués, L.M. Cotoruelo, J. Rodríguez-Mirasol, T. Cordero, Removal Of Paracetamol On Biomass-Derived Activated Carbon: Modeling The Fixed Bed Breakthrough Curves Using Batch Adsorption Experiments, Chem. Eng. J. 279 (2015) 18–30. Doi:10.1016/J.Cej.2015.04.144.

[4] Y.A. Alhamed, Adsorption Kinetics And Performance Of Packed Bed Adsorber For Phenol Removal Using Activated Carbon From Dates' Stones, J. Hazard. Mater. 170 (2009) 763–770. Doi:10.1016/J.Jhazmat.2009.05.002.

[5] J. Lalley, C. Han, G.R. Mohan, D.D. Dionysiou, T.F. Speth, J. Garland, M.N. Nadagouda, Phosphate Removal Using Modified Bayoxide[Registered Sign] E33 Adsorption Media, Environ. Sci. Water Res. Technol. 1 (2015) 96–107. Doi:10.1039/C4ew00020j.

[6] C.Y. Teh, T.Y. Wu, J.C. Juan, Potential Use Of Rice Starch In Coagulation-Flocculation Process Of Agro-Industrial Wastewater: Treatment Performance And Flocs Characterization, Ecol. Eng. 71 (2014) 509–519. Doi:10.1016/J.Ecoleng.2014.07.005.

[7] Industrial Water Use, Stat. Canada. Catalogue (2011).

[8] Industry Canada Report, The Canadian Water Industry, Environ. Buisness Journal, Environ. Buisness Int. Inc. (2008) 1–14.

[9] J. Altmann, D. Rehfeld, K. Träder, A. Sperlich, M. Jekel, Combination Of Granular Activated Carbon Adsorption And Deep-Bed Filtration As A Single Advanced Wastewater Treatment Step For Organic Micropollutant And Phosphorus Removal, Water Res. 92 (2016) 131–139. Doi:10.1016/J.Watres.2016.01.051.

[10] M. Al-Shannag, Z. Al-Qodah, K. Bani-Melhem, M.R. Qtaishat, M. Alkasrawi, Heavy Metal Ions Removal From Metal Plating Wastewater Using Electrocoagulation: Kinetic Study And Process Performance, Chem. Eng. J. 260 (2015) 749–756. Doi:10.1016/J.Cej.2014.09.035.

[11] T. Yamashita, T. Aketo, N. Minowa, K. Sugimoto, H. Yokoyama, A. Ogino, Y. Tanaka, Simultaneous Removal Of Colour, Phosphorus And Disinfection From Treated Wastewater Using An Agent Synthesized From Amorphous Silica And Hydrated Lime, Environ. Technol. (United Kingdom). 34 (2013) 1017–1025. Doi:10.1080/09593330.2012.733417.

[12] J. Altmann, A.S. Ruhl, F. Zietzschmann, M. Jekel, Direct Comparison Of Ozonation And Adsorption Onto Powdered Activated Carbon For Micropollutant Removal In Advanced Wastewater Treatment, Water Res. 55 (2014) 185–193. Doi:10.1016/J.Watres.2014.02.025.

[13] N.N. Nassar, L.A. Arar, N.N. Marei, M.M. Abu Ghanim, M.S. Dwekat, S.H. Sawalha,

Treatment Of Olive Mill Based Wastewater By Means Of Magnetic Nanoparticles: Decolourization, Dephenolization And Cod Removal, Environ. Nanotechnology, Monit. Manag. 1–2 (2014) 14–23. Doi:10.1016/J.Enmm.2014.09.001.

[14] S.C.R. Santos, R.A.R. Boaventura, Treatment Of A Simulated Textile Wastewater In A Sequencing Batch Reactor (Sbr) With Addition Of A Low-Cost Adsorbent, J. Hazard. Mater. 291 (2015) 74–82. Doi:10.1016/J.Jhazmat.2015.02.074.

[15] R. Lakshmanan, M. Sanchez-Dominguez, J.A. Matutes-Aquino, S. Wennmalm, G. Kuttuva Rajarao, Removal Of Total Organic Carbon From Sewage Wastewater Using Poly(Ethylenimine)-Functionalized Magnetic Nanoparticles, Langmuir. 30 (2014) 1036–1044. Doi:10.1021/La404076n.

[16] T.C. Nguyen, P. Loganathan, T.V. Nguyen, S. Vigneswaran, J. Kandasamy, R. Naidu, Simultaneous Adsorption Of Cd, Cr, Cu, Pb, And Zn By An Iron-Coated Australian Zeolite In Batch And Fixed-Bed Column Studies, Chem. Eng. J. 270 (2015) 393–404. Doi:10.1016/J.Cej.2015.02.047.

[17] J.L. Sotelo, G. Ovejero, A. Rodríguez, S. Álvarez, J. García, Analysis And Modeling Of Fixed-Bed Column Operations On Flumequine Removal Onto Activated Carbon: Ph Influence And Desorption Studies, Chem. Eng. J. 228 (2013) 102–113. Doi:10.1016/J.Cej.2013.04.088.

[18] A. Ahmad, A. Idris, B.H. Hameed, Modeling Of Disperse Dye Adsorption Onto Bamboo-Based Activated Carbon In Fixed-Bed Column, Desalin. Water Treat. 52 (2014) 248–256. Doi:10.1080/19443994.2013.794012.

[19] L.N. Nguyen, F.I. Hai, J. Kang, W.E. Price, L.D. Nghiem, Bioresource Technology Removal Of Trace Organic Contaminants By A Membrane Bioreactor – Granular Activated Carbon (Mbr – Gac) System, Bioresour. Technol. 113 (2012) 169–173. Doi:10.1016/J.Biortech.2011.10.051.

[20] I.P.P. Cansado, P.A.M. Mourão, A.I. Falcão, M.M.L.R. Carrott, P.J.M. Carrott, The Influence Of The Activated Carbon Post-Treatment On The Phenolic Compounds Removal, Fuel Process. Technol. 103 (2012) 64–70. Doi:10.1016/J.Fuproc.2011.10.015.

[21] K. Sarayu, S. Sandhya, Current Technologies For Biological Treatment Of Textile Wastewater-A Review, Appl. Biochem. Biotechnol. 167 (2012) 645–661. Doi:10.1007/S12010-012-9716-6.

[22] G. Skouteris, D. Saroj, P. Melidis, F.I. Hai, S. Ouki, The Effect Of Activated Carbon Addition On Membrane Bioreactor Processes For Wastewater Treatment And Reclamation - A Critical Review, Bioresour. Technol. 185 (2015) 399–410. Doi:10.1016/J.Biortech.2015.03.010.

[23] W. Li, T. Hua, Q. Zhou, S. Zhang, F. Li, Treatment Of Stabilized Landfill Leachate By The Combined Process Of Coagulation/Flocculation And Powder Activated Carbon Adsorption, Desalination. 264 (2010) 56–62. Doi:10.1016/J.Desal.2010.07.004.

[24] D. Mohan, C.U. Pittman, Activated Carbons And Low Cost Adsorbents For Remediation Of Tri- And Hexavalent Chromium From Water, J. Hazard. Mater. 137 (2006) 762–811.

Doi:10.1016/J.Jhazmat.2006.06.060.

[25] C. Stoquart, P. Servais, P.R. Bérubé, B. Barbeau, Hybrid Membrane Processes Using Activated Carbon Treatment For Drinking Water: A Review, J. Memb. Sci. 411–412 (2012) 1–12. Doi:10.1016/J.Memsci.2012.04.012.

[26] R. Toor, M. Mohseni, Uv-H2o2 Based Aop And Its Integration With Biological Activated Carbon Treatment For Dbp Reduction In Drinking Water, Chemosphere. 66 (2007) 2087–2095. Doi:10.1016/J.Chemosphere.2006.09.043.

[27] N.N. Nassar, Rapid Removal And Recovery Of Pb(Ii) From Wastewater By Magnetic Nanoadsorbents, J. Hazard. Mater. 184 (2010) 538–546. Doi:10.1016/J.Jhazmat.2010.08.069.

[28] A. El-Qanni, N.N. Nassar, G. Vitale, A. Hassan, Maghemite Nanosorbcats For Methylene Blue Adsorption And Subsequent Catalytic Thermo-Oxidative Decomposition: Computational Modeling And Thermodynamics Studies, J. Colloid Interface Sci. 461 (2016) 396–408. Http://Dx.Doi.Org/10.1016/J.Jcis.2015.09.041.

[29] N.N. Nassar, Chapter 3, (2012) 81–118.

[30] C.A. Franco, N.N. Nassar, F.B. Cortés, Removal Of Oil From Oil-In-Saltwater Emulsions By Adsorption Onto Nano-Alumina Functionalized With Petroleum Vacuum Residue, J. Colloid Interface Sci. 433 (2014) 58–67. Doi:10.1016/J.Jcis.2014.07.011.

[31] N.N. Nassar, Kinetics, Equilibrium And Thermodynamic Studies On The Adsorptive Removal Of Nickel, Cadmium And Cobalt From Wastewater By Superparamagnetic Iron Oxide Nanoadsorbents., Can. J. Chem. Eng. 90 (2011) 1231–1238. Doi:10.1002/Cjce.20613.

[32] P. Xu, G. Ming, D. Lian, C. Ling, S. Hu, M. Hua, Use Of Iron Oxide Nanomaterials In Wastewater Treatment : A Review, Sci. Total Environ. 424 (2012) 1–10. Doi:10.1016/J.Scitotenv.2012.02.023.

[33] N.N. Nassar, A. Ringsred, Rapid Adsorption Of Methylene Blue From Aqueous Solutions By Goethite Nanoadsorbents, Environ. Eng. Sci. 29 (2012) 790–797. Doi:10.1089/Ees.2011.0263.

[34] V.A. Online, Rsc Advances Modi Fi Ed Nano-Pyroxene On Adsorption Of, (2016) 64482–64493. Doi:10.1039/C6ra05838h.

[35] G. Lofrano, M. Carotenuto, G. Libralato, R.F. Domingos, A. Markus, L. Dini, R.K. Gautam, D. Baldantoni, M. Rossi, S.K. Sharma, M.C. Chattopadhyaya, M. Giugni, S. Meric, Polymer Functionalized Nanocomposites For Metals Removal From Water And Wastewater: An Overview, Water Res. 92 (2016) 22–37. Doi:10.1016/J.Watres.2016.01.033.

[36] C.A. Franco, F.B. Cortés, N.N. Nassar, Adsorptive Removal Of Oil Spill From Oil-In-Fresh Water Emulsions By Hydrophobic Alumina Nanoparticles Functionalized With Petroleum Vacuum Residue, J. Colloid Interface Sci. 425 (2014) 168–177. Doi:10.1016/J.Jcis.2014.03.051.

[37] Y. Zhao, J. Li, L. Zhao, S. Zhang, Y. Huang, X. Wu, X. Wang, Synthesis Of Amidoxime-Functionalized Fe3o4@Sio2 Core-Shell Magnetic Microspheres For Highly Efficient Sorption Of U(Vi), Chem. Eng. J. 235 (2014) 275–283. Doi:10.1016/J.Cej.2013.09.034.

[38] L. Giang, R. Islam, J. Tae, S. Seo, K. Taek, Encapsulation Of Fe3o4 Magnetic Nanoparticles With Poly (Methyl Methacrylate) Via Surface Functionalized Thiol-Lactam Initiated Radical Polymerization, Appl. Surf. Sci. 258 (2012) 2959–2966. Doi:10.1016/J.Apsusc.2011.11.016.

[39] B.R. Sedai, B.K. Khatiwada, H. Mortazavian, F.D. Blum, Development Of Superhydrophobicity In Fluorosilane-Treated Diatomaceous Earth Polymer Coatings, Appl. Surf. Sci. 386 (2016) 178–186. Doi:10.1016/J.Apsusc.2016.06.009.

[40] W.T. Tsai, C.W. Lai, K.J. Hsien, Characterization And Adsorption Properties Of Diatomaceous Earth Modified By Hydrofluoric Acid Etching, J. Colloid Interface Sci. 297 (2006) 749–754. Doi:10.1016/J.Jcis.2005.10.058.

[41] R.D.G. Franca, A. Vieira, A.M.T. Mata, G.S. Carvalho, H.M. Pinheiro, N.D. Lourenço, Effect Of An Azo Dye On The Performance Of An Aerobic Granular Sludge Sequencing Batch Reactor Treating A Simulated Textile Wastewater, Water Res. 85 (2015) 327–336. Doi:10.1016/J.Watres.2015.08.043.

[42] V.K. Gupta, R. Jain, A. Nayak, S. Agarwal, M. Shrivastava, Removal Of The Hazardous Dye-Tartrazine By Photodegradation On Titanium Dioxide Surface, Mater. Sci. Eng. C. 31 (2011) 1062–1067. Doi:10.1016/J.Msec.2011.03.006.

[43] P. Aravind, H. Selvaraj, S. Ferro, M. Sundaram, An Integrated (Electro- And Bio-Oxidation) Approach For Remediation Of Industrial Wastewater Containing Azo-Dyes: Understanding The Degradation Mechanism And Toxicity Assessment, J. Hazard. Mater. 318 (2016) 203–215. Doi:10.1016/J.Jhazmat.2016.07.028.

[44] R. Khan, P. Bhawana, M.H. Fulekar, Microbial Decolorization And Degradation Of Synthetic Dyes: A Review, Rev. Environ. Sci. Biotechnol. 12 (2013) 75–97. Doi:10.1007/S11157-012-9287-6.

[45] L. Labiadh, M.A. Oturan, M. Panizza, N. Ben, Complete Removal Of Ahps Synthetic Dye From Water Using New Electro-Fenton Oxidation Catalyzed By Natural Pyrite As Heterogeneous Catalyst, J. Hazard. Mater. 297 (2015) 34–41. Doi:10.1016/J.Jhazmat.2015.04.062.

[46] M. Tichonovas, E. Krugly, V. Racys, R. Hippler, V. Kauneliene, I. Stasiulaitiene, D. Martuzevicius, Degradation Of Various Textile Dyes As Wastewater Pollutants Under Dielectric Barrier Discharge Plasma Treatment, Chem. Eng. J. 229 (2013) 9–19. Http://Dx.Doi.Org/10.1016/J.Cej.2013.05.095.

[47] M. Punzi, F. Nilsson, A. Anbalagan, B. Svensson, K. Jönsson, B. Mattiasson, M. Jonstrup, Combined Anaerobic–Ozonation Process For Treatment Of Textile Wastewater : Removal Of Acute Toxicity And Mutagenicity, J. Hazard. Mater. 292 (2015) 52–60. Doi:10.1016/J.Jhazmat.2015.03.018.

[48] A. Asghar, A. Aziz, A. Raman, W. Mohd, A. Wan, Advanced Oxidation Processes For In-

Situ Production Of Hydrogen Peroxide/ Hydroxyl Radical For Textile Wastewater Treatment: A Review, J. Clean. Prod. 87 (2015) 826–838. Doi:10.1016/J.Jclepro.2014.09.010.

[49] V.K. Gupta, R. Jain, A. Mittal, T.A. Saleh, A. Nayak, S. Agarwal, S. Sikarwar, Photo-Catalytic Degradation Of Toxic Dye Amaranth On Tio2/Uv In Aqueous Suspensions, Mater. Sci. Eng. C. 32 (2012) 12–17. Doi:10.1016/J.Msec.2011.08.018.

[50] R. Saravanan, E. Sacari, F. Gracia, M.M. Khan, E. Mosquera, V.K. Gupta, Conducting Pani Stimulated Zno System For Visible Light Photocatalytic Degradation Of Coloured Dyes, J. Mol. Liq. 221 (2016) 1029–1033. Doi:10.1016/J.Molliq.2016.06.074.

[51] S. Rajendran, M.M. Khan, F. Gracia, J. Qin, V.K. Gupta, S. Arumainathan, Ce 3+ -Ion-Induced Visible-Light Photocatalytic Degradation And Electrochemical Activity Of Zno/Ceo 2 Nanocomposite, Nat. Publ. Gr. (2016) 1–11. Doi:10.1038/Srep31641.

[52] S. Karthikeyan, V.K. Gupta, R. Boopathy, A. Titus, G. Sekaran, A New Approach For The Degradation Of High Concentration Of Aromatic Amine By Heterocatalytic Fenton Oxidation: Kinetic And Spectroscopic Studies, J. Mol. Liq. 173 (2012) 153–163. Doi:10.1016/J.Molliq.2012.06.022.

[53] G. Han, C. Liang, T. Chung, M. Weber, C. Staudt, C. Maletzko, Combination Of Forward Osmosis (Fo) Process With Coagulation/Flocculation (Cf) For Potential Treatment Of Textile Wastewater, Water Res. 91 (2016) 361–370. Doi:10.1016/J.Watres.2016.01.031.

[54] A. Mittal, J. Mittal, A. Malviya, D. Kaur, V.K. Gupta, Decoloration Treatment Of A Hazardous Triarylmethane Dye, Light Green Sf (Yellowish) By Waste Material Adsorbents, J. Colloid Interface Sci. 342 (2010) 518–527. Doi:10.1016/J.Jcis.2009.10.046.

[55] A. Mittal, D. Kaur, A. Malviya, J. Mittal, V.K. Gupta, Adsorption Studies On The Removal Of Coloring Agent Phenol Red From Wastewater Using Waste Materials As Adsorbents, J. Colloid Interface Sci. 337 (2009) 345–354. Doi:10.1016/J.Jcis.2009.05.016.

[56] A. Mittal, J. Mittal, A. Malviya, V.K. Gupta, Adsorptive Removal Of Hazardous Anionic Dye “Congo Red” From Wastewater Using Waste Materials And Recovery By Desorption, J. Colloid Interface Sci. 340 (2009) 16–26. Doi:10.1016/J.Jcis.2009.08.019.

[57] A. Mittal, J. Mittal, A. Malviya, V.K. Gupta, Removal And Recovery Of Chrysoidine Y From Aqueous Solutions By Waste Materials, J. Colloid Interface Sci. 344 (2010) 497–507. Doi:10.1016/J.Jcis.2010.01.007.

[58] D. Balarak, J. Jaafari, G. Hassani, Y. Mahdavi, I. Tyagi, S. Agarwal, V.K. Gupta, The Use Of Low-Cost Adsorbent (Canola Residues) For The Adsorption Of Methylene Blue From Aqueous Solution: Isotherm, Kinetic And Thermodynamic Studies, Colloids Interface Sci. Commun. 7 (2015) 16–19. Doi:10.1016/J.Colcom.2015.11.004.

[59] V.. M.J.. V.H.. Mittal A.A Thakur, Process Development For The Removal Of Hazardous Anionic Azo Dye Congo Red From Wastewater By Using Hen Feather As Potential Adsorbent, Desalin. Water Treat. 52 (2014) 227–237. Doi:10.1080/19443994.2013.785030.

[60] V.K. Gupta, R. Kumar, A. Nayak, T.A. Saleh, M.A. Barakat, Adsorptive Removal Of Dyes From Aqueous Solution Onto Carbon Nanotubes: A Review, Adv. Colloid Interface Sci.

193–194 (2013) 24–34. Doi:10.1016/J.Cis.2013.03.003.

[61] R. Rushdy, M. Reza, G. Mckay, Combined Magnetic Field And Adsorption Process For Treatment Of Biologically Treated Palm Oil Mill Effluent (Pome), Chem. Eng. J. 243 (2014) 31–42. Doi:10.1016/J.Cej.2013.12.084.

[62] S. Chen, Q. Yue, B. Gao, Q. Li, X. Xu, K. Fu, Adsorption Of Hexavalent Chromium From Aqueous Solution By Modified Corn Stalk: A Fixed-Bed Column Study, Bioresour. Technol. 113 (2012) 114–120. Doi:10.1016/J.Biortech.2011.11.110.

[63] V.K. Gupta, S.K. Srivastava, D. Mohan, S. Sharma, Original Contribution Design Parameters For Fixed Bed Reactors Of Activated Carbon Developed From Fertilizer Waste For The Removal Of Some Heavy Metal Ions, Pergamon. 17 (1998) 517–522.

[64] F. Qian, X. Sun, Y. Liu, Removal Characteristics Of Organics In Bio-Treated Textile Wastewater Reclamation By A Stepwise Coagulation And Intermediate Gac/ O3 Oxidation Process, Chem. Eng. J. 214 (2013) 112–118. Http://Dx.Doi.Org/10.1016/J.Cej.2012.09.130.

[65] A. Bhatnagar, W. Hogland, M. Marques, M. Sillanpää, An Overview Of The Modification Methods Of Activated Carbon For Its Water Treatment Applications, Chem. Eng. J. 219 (2013) 499–511. Doi:10.1016/J.Cej.2012.12.038.

[66] R. Saravanan, F. Gracia, M.M. Khan, V. Poornima, V.K. Gupta, V. Narayanan, A. Stephen, Zno/Cdo Nanocomposites For Textile Effluent Degradation And Electrochemical Detection, J. Mol. Liq. 209 (2015) 374–380. Doi:10.1016/J.Molliq.2015.05.040.

[67] N. Bertrand, J. Wu, X. Xu, N. Kamaly, O.C. Farokhzad, Cancer Nanotechnology: The Impact Of Passive And Active Targeting In The Era Of Modern Cancer Biology, Adv. Drug Deliv. Rev. 66 (2014) 2–25. Doi:10.1016/J.Addr.2013.11.009.

[68] K.J. Mcdonald, B. Reynolds, K.J. Reddy, Intrinsic Properties Of Cupric Oxide Nanoparticles Enable Effective Filtration Of Arsenic From Water, Sci. Rep. 5 (2015) 11110. Doi:10.1038/Srep11110.

[69] V.K. Gupta, S. Agarwal, T.A. Saleh, Synthesis And Characterization Of Alumina-Coated Carbon Nanotubes And Their Application For Lead Removal, J. Hazard. Mater. 185 (2011) 17–23. Doi:10.1016/J.Jhazmat.2010.08.053.

[70] T.A. Saleh, V.K. Gupta, Photo-Catalyzed Degradation Of Hazardous Dye Methyl Orange By Use Of A Composite Catalyst Consisting Of Multi-Walled Carbon Nanotubes And Titanium Dioxide, J. Colloid Interface Sci. 371 (2012) 101–106. Doi:10.1016/J.Jcis.2011.12.038.

[71] H. Khani, M.K. Rofouei, P. Arab, V.K. Gupta, Z. Vafaei, Multi-Walled Carbon Nanotubes-Ionic Liquid-Carbon Paste Electrode As A Super Selectivity Sensor: Application To Potentiometric Monitoring Of Mercury Ion(Ii), J. Hazard. Mater. 183 (2010) 402–409. Doi:10.1016/J.Jhazmat.2010.07.039.

[72] N.N. Nassar, Kinetics, Mechanistic, Equilibrium, And Thermodynamic Studies On The Adsorption Of Acid Red Dye From Wastewater By Γ-Fe2o3 Nanoadsorbents, Sep. Sci. Technol. 45 (2010) 1092–1103. Http://Dx.Doi.Org/10.1080/01496391003696921.

[73] M.J.K. Ahmed, M. Ahmaruzzaman, M.H. Bordoloi, Novel Averrhoa Carambola Extract Stabilized Magnetite Nanoparticles: A Green Synthesis Route For The Removal Of Chlorazol Black E From Wastewater, Rsc Adv. 5 (2015) 74645–74655. Doi:10.1039/C5ra13970h.

[74] D. Zhu, J. Zhang, J. Song, H. Wang, Z. Yu, Y. Shen, A. Xie, Efficient One-Pot Synthesis Of Hierarchical Flower-Like ??-Fe 2o3 Hollow Spheres With Excellent Adsorption Performance For Water Treatment, Appl. Surf. Sci. 284 (2013) 855–861. Doi:10.1016/J.Apsusc.2013.08.022.

[75] V.K. Gupta, A. Nayak, Cadmium Removal And Recovery From Aqueous Solutions By Novel Adsorbents Prepared From Orange Peel And Fe 2o 3 Nanoparticles, Chem. Eng. J. 180 (2012) 81–90. Doi:10.1016/J.Cej.2011.11.006.

[76] R. Saravanan, M. Mansoob Khan, V.K. Gupta, E. Mosquera, F. Gracia, V. Narayanan, A. Stephen, Zno/Ag/Cdo Nanocomposite For Visible Light-Induced Photocatalytic Degradation Of Industrial Textile Effluents, J. Colloid Interface Sci. 452 (2015) 126–133. Doi:10.1016/J.Jcis.2015.04.035.

[77] L. Giang, R. Islam, J. Tae, S. Seo, K. Taek, Encapsulation Of Fe3o4 Magnetic Nanoparticles With Poly(Methyl Methacrylate) Via Surface Functionalized Thiol-Lactam Initiated Radical Polymerization, Appl. Surf. Sci. 258 (2012) 2959–2966. Doi:10.1016/J.Apsusc.2011.11.016.

[78] H. Basti, L. Ben Tahar, L.S. Smiri, F. Herbst, S. Nowak, C. Mangeney, S. Ammar, Surface Modification Of -Fe2o3 Nanoparticles By Grafting From Poly-(Hydroxyethylmethacrylate) And Poly-(Methacrylic Acid): Qualitative And Quantitative Analysis Of The Polymeric Coating, Colloids Surfaces A Physicochem. Eng. Asp. 490 (2016) 222–231. Http://Dx.Doi.Org/10.1016/J.Colsurfa.2015.11.013.

[79] A. Fornara, C. Okoli, A. Fornara, J. Qin, M.S. Toprak, G. Dalhammar, Characterization Of Supermagnetic Iron Oxide Nanoparticles And Its Application In Protein Purification, J. Nanosci. Nanotechnol. 11 (2011) 1–6. Doi:10.1166/Jnn.2011.5007.

[80] G. Vitale, Iron Silicate Nano-Crystals As Potential Catalysts Or Adsorbents For Heavy Hydrocarbons Upgrading (Phd Thesis), Univeristy Of Calgary, 2013. Http://Theses.Ucalgary.Ca/Bitstream/11023/557/2/Ucalgary_2013_Vitale_Gerardo.Pdf.

[81] M. Hmoudah, N.N. Nassar, G. Vitale, A. El-Qanni, Effect Of Nanosized And Surface-Structural-Modified Nano-Pyroxene On Adsorption Of Violanthrone-79, Rsc Adv. 6 (2016) 64482–64493. Doi:10.1039/C6ra05838h.

[82] A. Monshi, M.R. Foroughi, M.R. Monshi, Modified Scherrer Equation To Estimate More Accurately Nano-Crystallite Size Using Xrd, World J. Nano Sci. Eng. 2 (2012) 154. Doi:10.4236/Wjnse.2012.23020.

[83] Jade V 7.5.1 Xrd, Pattern Processing Identification & Quantification, Materials Data Inc Https://Www.Jadeworld.Com/Developer-Center/Download-Jade/., 2005; Available From:, (N.D.). Https://Www.Jadeworld.Com/Developer-Center/Download-Jade/.

[84] N.N. Nassar, A. Hassan, P. Pereira-Almao, Effect Of The Particle Size On Asphaltene

Adsorption And Catalytic Oxidation Onto Alumina Particles, Energy And Fuels. 25 (2011) 3961–3965. Doi:Dx.Doi.Org/10.1021/Ef2008387.

[85] N.N. Nassar, A. Hassan, P. Pereira-Almao, Metal Oxide Nanoparticles For Asphaltene Adsorption And Oxidation, Energy And Fuels. 25 (2011) 1017–1023. Doi:Dx.Doi.Org/10.1021/Ef101230g.

[86] Chemdraw V15.1 Structural Drawing Software, (2016). Http://Www.Cambridgesoft.Com/Support/Desktopsupport/Documentation/Chemdrawplugin/ (Accessed October 8, 2016).

[87] Biovia Materials Studio Modeling And Simulation Software Version 2017, Dassault Systemes, (N.D.). Http://Accelrys.Com/Products/Collaborative-Science/Biovia-Materials-Studio/ (Accessed October 8, 2016).

[88] M. Cameron, S. Sueno, C.T. Prewitt, J.J. Papike, High-Temperature Crystal Chemistry Of Acmite, Diopside, Hedenbergite, Jadeite, Spodumene, And Ureyite, Am. Mineral. 58 (1973) 594–618.

[89] A. Riedinger, P. Guardia, A. Curcio, M.A. Garcia, R. Cingolani, L. Manna, T. Pellegrino, Subnanometer Local Temperature Probing And Remotely Controlled Drug Release Based On Azo-Functionalized Iron Oxide Nanoparticles, Nano Lett. 13 (2013) 2399–2406. Doi:10.1021/Nl400188q.

[90] F. Rouquerol, J. Rouquerol, K.S.W. Sing, P.Llewllyn, And G. Maurin, Adsorption By Powders And Porous Solids: Principles, Methodology And Applications, Second, 2014. Https://Books.Google.Ca/Books?Hl=Ar&Lr=&Id=Uoe-Zsccyncc&Oi=Fnd&Pg=Pp1&Dq=Porosity+And++Bet+Surface+Area+Of+Non-Porous+Solids+&Ots=0r0vgxvlgc&Sig=Ydl1jnclmur5oisshgznnpkbjc&Redir_Esc=Y#V=Onepage&Q=Porosity And Bet Surface Area Of Non-Porous Solids&F=Fals.

[91] F. Franks, Freeze-Drying Of Bioproducts: Putting Principles Into Practice, Eur. J. Pharm. Biopharm. 45 (1998) 221–229. Doi:10.1016/S0939-6411(98)00004-6.

[92] W. Abdelwahed, G. Degobert, S. Stainmesse, H. Fessi, Freeze-Drying Of Nanoparticles: Formulation, Process And Storage Considerations, Adv. Drug Deliv. Rev. 58 (2006) 1688–1713. Doi:10.1016/J.Addr.2006.09.017.

[93] Z. Xu, C. Shen, Y. Hou, H. Gao, S. Sun, Oleylamine As Both Reducing Agent And Stabilizer In A Facile Synthesis Of Magnetite Nanoparticles, Chem. Mater. 21 (2009) 1778–1780. Doi:10.1021/Cm802978z.

[94] N.N. Marei, N.N. Nassar, G. Vitale, The Effect Of The Nanosize On Surface Properties Of Nio Nanoparticles For The Adsorption Of Quinolin-65., Phys. Chem. Chem. Phys. 18 (2016) 6839–49. Doi:10.1039/C6cp00001k.

[95] L. Wang, H. Lei, Q. Bu, S. Ren, Y. Wei, L. Zhu, X. Zhang, Y. Liu, G. Yadavalli, J. Lee, S. Chen, J. Tang, Aromatic Hydrocarbons Production From Exsitu Catalysis Of Pyrolysis Vapor Over Zinc Modified Zsm-5 In A Packed-Bed Catalysis Coupled With Microwave Pyrolysis Reactor, Fuel. 129 (2014) 78–85. Doi:10.1016/J.Fuel.2014.03.052.

[96] S. Skidkidmore, Temperature And Ph Responsive Polyethylenimine Systems As Potentail

Nonviral Gene Vectors (Master Thesis), Case Western Reserve University, 2010. Http://Corescholar.Libraries.Wright.Edu/Cgi/Viewcontent.Cgi?Article=2150&Context=Etd_All.

[97] M. Fleischer, C. Schmuck, Ph-Switchable Hydrogel By Additional, Chem. Commun. 50 (2014) 10464–10467. Doi:10.1039/C4cc03281k.

[98] N.N. Nassar, N.N. Marei, G. Vitale, L.A. Arar, Adsorptive Removal Of Dyes From Synthetic And Real Textile Wastewater Using Magnetic Iron Oxide Nanoparticles: Thermodynamic And Mechanistic Insights, Can. J. Chem. Eng. 93 (2015) 1965–1974. Doi:10.1002/Cjce.22315.

[99] G.C.R. D.C. Montgomery, Applied Statistics And Srobability For Engineers, 4th Ed., New York, 2006. Https://Books.Google.Ca/Books?Hl=Ar&Lr=&Id=_F4krecnafec&Oi=Fnd&Pg=Pa1&Dq=+Applied+Statistics+And+Srobability+For+Engineers&Ots=Zxwz2pn5_D&Sig=G75kd0npif53j6ecqrdqjfmr8ge&Redir_Esc=Y#V=Onepage&Q=Applied Statistics And Srobability For Engineers&F=False.

[100] J.C. Carmona, N.N. Nassar, C.A. Franco, F.B. Corte, Role Of Particle Size And Surface Acidity Of Silica Gel Nanoparticles In Inhibition Of Formation Damage By Asphaltene In Oil Reservoirs, Ind. Eng. Chem. Res. 55 (2016) 6122–6132. Doi:10.1021/Acs.Iecr.6b01187.

[101] R. Li, L. Zhang, P. Wang, Rational Design Of Nanomaterials For Water Treatment, Nanoscale. 7 (2015) 17167–17194. Doi:10.1039/C5nr04870b.

[102] J. Blanco, F. Torrades, M. De La Varga, J. García-Montaño, Fenton And Biological-Fenton Coupled Processes For Textile Wastewater Treatment And Reuse, Desalination. 286 (2012) 394–399. Doi:10.1016/J.Desal.2011.11.055.

[103] J. Lin, C.Y. Tang, W. Ye, S.P. Sun, S.H. Hamdan, A. Volodin, C. Van Haesendonck, A. Sotto, P. Luis, B. Van Der Bruggen, Unraveling Flux Behavior Of Superhydrophilic Loose Nanofiltration Membranes During Textile Wastewater Treatment, J. Memb. Sci. 493 (2015) 690–702. Doi:10.1016/J.Memsci.2015.07.018.

[104] L. Ma, R. Zhuo, H. Liu, D. Yu, M. Jiang, X. Zhang, Y. Yang, Efficient Decolorization And Detoxification Of The Sulfonated Azo Dye Reactive Orange 16 And Simulated Textile Wastewater Containing Reactive Orange 16 By The White-Rot Fungus Ganoderma Sp . En3 Isolated From The Forest Of Tzu-Chin Mountain In China, Biochem. Eng. J. 82 (2014) 1–9. Doi:10.1016/J.Bej.2013.10.015.

[105] M. Punzi, F. Nilsson, A. Anbalagan, B. Svensson, K. Jönsson, B. Mattiasson, M. Jonstrup, Combined Anaerobic–Ozonation Process For Treatment Of Textile Wastewater: Removal Of Acute Toxicity And Mutagenicity, J. Hazard. Mater. 292 (2015) 52–60.

[106] A.K. Verma, R.R. Dash, P. Bhunia, A Review On Chemical Coagulation/Flocculation Technologies For Removal Of Colour From Textile Wastewaters, J. Environ. Manage. 93 (2012) 154–168. Doi:10.1016/J.Jenvman.2011.09.012.

[107] M.T. Yagub, T.K. Sen, S. Afroze, H.M. Ang, Dye And Its Removal From Aqueous Solution

By Adsorption: A Review, Adv. Colloid Interface Sci. 209 (2014) 172–184. Doi:10.1016/J.Cis.2014.04.002.

[108] A. Dalvand, R. Nabizadeh, M. Reza Ganjali, M. Khoobi, S. Nazmara, A. Hossein Mahvi, Modeling Of Reactive Blue 19 Azo Dye Removal From Colored Textile Wastewater Using Larginine-Functionalized Fe3o4 Nanoparticles: Optimization, Reusability, Kinetic And Equilibrium Studies, J. Magn. Magn. Mater. 404 (2016) 179–189. Doi:10.1016/J.Jmmm.2015.12.040.

[109] R. Elmoubarki, F.Z. Mahjoubi, H. Tounsadi, J. Moustadraf, M. Abdennouri, A. Zouhri, A. El Albani, N. Barka, Adsorption Of Textile Dyes On Raw And Decanted Moroccan Clays: Kinetics, Equilibrium And Thermodynamics, Water Resour. Ind. 9 (2015) 16–29. Doi:10.1016/J.Wri.2014.11.001.

[110] M. Auta, B.H. Hameed, Coalesced Chitosan Activated Carbon Composite For Batch And Fixed-Bed Adsorption Of Cationic And Anionic Dyes, Colloids Surfaces B Biointerfaces. 105 (2013) 199–206. Doi:10.1016/J.Colsurfb.2012.12.021.

[111] A. Afkhami, R. Moosavi, Adsorptive Removal Of Congo Red, A Carcinogenic Textile Dye, From Aqueous Solutions By Maghemite Nanoparticles, J. Hazard. Mater. 174 (2010) 398–403. Doi:10.1016/J.Jhazmat.2009.09.066.

[112] A.A. Rajabi, Y. Yamini, M. Faraji, F. Nourmohammadian, Modified Magnetite Nanoparticles With Cetyltrimethylammonium Bromide As Superior Adsorbent For Rapid Removal Of The Disperse Dyes From Wastewater Of Textile Companies, Nanochemistry Res. 1 (2016) 49–56. Doi:10.7508/Ncr.2016.01.006.

[113] M. Jain, V.K. Garg, K. Kadirvelu, Cadmium(Ii) Sorption And Desorption In A Fixed Bed Column Using Sunflower Waste Carbon Calcium-Alginate Beads, Bioresour. Technol. 129 (2013) 242–248. Doi:10.1016/J.Biortech.2012.11.036.

[114] S. Kango, S. Kalia, A. Celli, J. Njuguna, Y. Habibi, R. Kumar, Surface Modification Of Inorganic Nanoparticles For Development Of Organic-Inorganic Nanocomposites - A Review, Prog. Polym. Sci. 38 (2013) 1232–1261. Doi:10.1016/J.Progpolymsci.2013.02.003.

[115] N.N. Nassar, Kinetics, Equilibrium And Thermodynamic Studies On The Adsorptive Removal Of Nickel, Cadmium And Cobalt From Wastewater By Superparamagnetic Iron Oxide Nanoadsorbents, Can. J. Chem. Eng. 90 (2012) 1231–1238. Doi:10.1002/Cjce.20613.

[116] N.N. Nassar, Kinetics, Mechanistic, Equilibrium, And Thermodynamic Studies On The Adsorption Of Acid Red Dye From Wastewater By Γ-Fe 2 O 3 Nanoadsorbents, Sep. Sci. Technol. 45 (2010) 1092–1103. Doi:10.1080/01496391003696921.

[117] N.N. Nassar, Iron Oxide Nanoadsorbents For Removal Of Various Pollutants From Wastewater: An Overview ., Appl. Adsorbents Water Pollut. Control. (2012) 81–118. Doi:10.1073/Pnas.0703993104.

[118] L. Zhou, B. He, J. Huang, One-Step Synthesis Of Versatile Amine- And Vinyl-Capped Magnetic Iron Oxide Nanoparticles For Polymer Grafting, Dye Adsorption And Catalysis,

Acs Appl. Mater. Interfaces. (2013). Doi:10.1021/Am402334f.

[119] K. Gul, S. Sohni, M. Waqar, F. Ahmad, N.A.N. Norulaini, M.O. A. K., Functionalization Of Magnetic Chitosan With Graphene Oxide For Removal Of Cationic And Anionic Dyes From Aqueous Solution, Carbohydr. Polym. 152 (2016) 520–531. Doi:10.1016/J.Carbpol.2016.06.045.

[120] K.J. Reddy, K.J. Mcdonald, H. King, A Novel Arsenic Removal Process For Water Using Cupric Oxide Nanoparticles, J. Colloid Interface Sci. 397 (2013) 96–102. Doi:10.1016/J.Jcis.2013.01.041.

[121] A. Hethnawi, N.N. Nassar, G. Vitale, Poly(Ethyleneminine)-Functionalized Pyroxene Nanoparticles For Removal Of Dyes From Textile Wastewaters, Rsc Adv. (2017) (Submitted).

[122] M. Brdar, M. Šćiban, A. Takači, T. Došenović, Comparison Of Two And Three Parameters Adsorption Isotherm For Cr(Vi) Onto Kraft Lignin, Chem. Eng. J. 183 (2012) 108–111. Doi:10.1016/J.Cej.2011.12.036.

[123] F.C.C. Assis, S. Albeniz, A. Gil, S.A. Korili, R. Trujillano, M.A. Vicente, L. Marcal, M. Saltarelli, K.J. Ciuffi, Removal Of Organic Pollutants From Industrial Wastewater: Performance Evaluation Of Inorganic Adsorbents Based On Pillared Clays, Desalin. Water Treat. 39 (2012) 316–322. Doi:10.5004/Dwt.2012.3354.

[124] R. Han, Y. Wang, X. Zhao, Y. Wang, F. Xie, J. Cheng, M. Tang, Adsorption Of Methylene Blue By Phoenix Tree Leaf Powder In A Fixed-Bed Column: Experiments And Prediction Of Breakthrough Curves, Desalination. 245 (2009) 284–297. Doi:10.1016/J.Desal.2008.07.013.

[125] M. Bhaumik, K. Setshedi, A. Maity, M.S. Onyango, Separation And Purification Techn Ology Chromium (Vi) Removal From Water Using Fixed Bed Column Of Polypyrrole / Fe 3 O 4 Nanocomposite, Sep. Purif. Technol. 110 (2013) 11–19. Doi:10.1016/J.Seppur.2013.02.037.

[126] S. Afroze, T.K. Sen, H.M. Ang, Adsorption Performance Of Continuous Fixed Bed Column For The Removal Of Methylene Blue (Mb) Dye Using Eucalyptus Sheathiana Bark Biomass, Res. Chem. Intermed. 42 (2016) 2343–2364. Doi:10.1007/S11164-015-2153-8.

[127] I. Ali, Water Treatment By Adsorption Columns: Evaluation At Ground Level, Sep. Purif. Rev. 43 (2014) 175–205. Doi:10.1080/15422119.2012.748671.

[128] P. Das Saha, S. Chakraborty, S. Chowdhury, Batch And Continuous (Fixed-Bed Column) Biosorption Of Crystal Violet By Artocarpus Heterophyllus (Jackfruit) Leaf Powder, Colloids Surfaces B Biointerfaces. 92 (2012) 262–270. Doi:10.1016/J.Colsurfb.2011.11.057.

[129] A.P. Lim, A.Z. Aris, Continuous Fixed-Bed Column Study And Adsorption Modeling: Removal Of Cadmium (Ii) And Lead (Ii) Ions In Aqueous Solution By Dead Calcareous Skeletons, Biochem. Eng. J. 87 (2014) 50–61. Doi:10.1016/J.Bej.2014.03.019.

[130] E. Oguz, M. Ersoy, Biosorption Of Cobalt(Ii) With Sunflower Biomass From Aqueous Solutions In A Fixed Bed Column And Neural Networks Modelling, Ecotoxicol. Environ.

Saf. 99 (2014) 54–60. Doi:10.1016/J.Ecoenv.2013.10.004.

[131] L. Markovska, V. Meshko, V. Noveski, M. Marinkovski, Solid Diffusion Control Of The Adsorption Of Basic Dyes Onto Granular Activated Carbon And Natural Zeolite In Fixed Bed Columns, J. Serbian Chem. Soc. 66 (2001) 463–475.

[132] A.D. Da Luz, S.M.D.A. Guelli Ulson De Souza, C. Da Luz, J.M.M. De Mello, A.A. Ulson De Souza, Analysis Of Competition Between Multicomponent Btx Compounds For The Active Site Of Adsorption In A Fixed-Bed Column, Ind. Eng. Chem. Res. 52 (2013) 16911–16921. Doi:10.1021/Ie402452h.

[133] S. Pilani, Modeling And Simulation For Dynamics Of Packed Bed Adsorption, Proc. Int. Symp. 57th Annu. Sess. Iiche Assoc. With Aiche. (2004). Doi:Https://Www.Researchgate.Net/Profile/Dr_B_V_Babu/Publication/242425077_Modeling_And_Simulation_For_Dynamics_Of_Packed_Bed_Adsorption/Links/0c96053877f982d7a0000000.Pdf.

[134] S. Saraji, L. Goual, M. Piri, Adsorption Of Asphaltenes In Porous Media Under Flow Conditions, Energy And Fuels. 24 (2010) 6009–6017. Doi:10.1021/Ef100881k.

[135] J.R. Evans, W.G. Davids, J.D. Macrae, A. Amirbahman, Kinetics Of Cadmium Uptake By Chitosan-Based Crab Shells, Water Res. 36 (2002) 3219–3226. Doi:10.1016/S0043-1354(02)00044-1.

[136] H. Moon, W. Kook Lee, Intraparticle Diffusion In Liquid-Phase Adsorption Of Phenols With Activated Carbon In Finite Batch Adsorber, J. Colloid Interface Sci. 96 (1983) 162–171. Doi:10.1016/0021-9797(83)90018-8.

[137] D.M. Ruthven, Principles Of Adsorption And Adsorption Processes, 1984. Https://Books.Google.Ca/Books?Id=U7wq21njr3uc&Printsec=Frontcover&Dq=Principles+Of+Adsorption+And+Adsorption+Processes&Hl=Ar&Sa=X&Ved=0ahukewieq9a8npdrahvi0gmkhepjao0q6aeiizaa#V=Onepage&Q=Principles Of Adsorption And Adsorption Processes&F=False.

[138] B.V. Babu, S. Gupta, Modeling And Simulation For Dynamics Of Packed Bed Adsorption, Environ. Eng. (2004). Doi:Https://Www.Researchgate.Net/Profile/Dr_B_V_Babu/Publication/242425077_Modeling_And_Simulation_For_Dynamics_Of_Packed_Bed_Adsorption/Links/0c96053877f982d7a0000000.Pdf.

[139] L.M. Cotoruelo, M.D. Marqués, F.J. Díaz, J. Rodríguez-Mirasol, J.J. Rodríguez, T. Cordero, Equilibrium And Kinetic Study Of Congo Red Adsorption Onto Lignin-Based Activated Carbons, Transp. Porous Media. 83 (2010) 573–590. Doi:10.1007/S11242-009-9460-8.

[140] L. Huijun, G. Hua, K. Qingqing, C. Zhongxiu, Adsorption Of Tetrahydrofuran + Water Solution Mixtures By Zeolite 4a In A Fixed Bed, J. Chem. Eng. Data. 52 (2007) 695–698. Doi:10.1021/Je060239g.

[141] J. Kumar, I.A. Ganaie, V.K. Kukreja, Application Of Mathematica Software To Solve Pulp Washing Model, Isrn Chem. Eng. 2013. 2013 (2013). Doi:Org/10.1155/2013/765896.

[142] N.S. Raghavan, D.M. Ruthven, Numerical Simulation Of A Fixed-Bed Adsorption Column By The Method Of Orthogonal Collocation., Aiche J. 29 (1983) 922–925. Doi:10.1002/Aic.690290608.

[143] S.M.A.G.U. De Souza, H. De L. Brandão, A.A. Ulson De Souza, Modeling Of Liquid Pollutant Biodegradation Process In A Fluidized Bed Reactor With Biofilm, Sep. Purif. Technol. 60 (2008) 162–173. Doi:10.1016/J.Seppur.2007.08.002.

[144] K.N. Gupta, A. Shrivastava, Orthogonal Collocation Solution Of Non- Linear Coupled-Partial Differential Equations In Fixed Bed Adsorption Column, South African J. Chem. 20 (2015) 61–80.

[145] W.E. Schiesser, The Numerical Method Of Lines: Integration Of Partial Differential Equations., Elsevier, 2012. Https://Books.Google.Ca/Books?Hl=Ar&Lr=&Id=2ydncgaaqbaj&Oi=Fnd&Pg=Pp1&Dq=Schiesser,+William+E.+The+Numerical+Method+Of+Lines:+Integration+Of+Partial+Differential+Equations.+Elsevier,+2012&Ots=Punfdvs_S4&Sig=Uokqol7rxcexux1z0-0sw4ljan8&Redir_Esc=Y#V=Onepag.

[146] H. Binous, A.A. Shaikh, Introduction Of The Arc-Length Continuation Technique In The Chemical Engineering Graduate Program At Kfupm, Comput. Appl. Eng. Educ. 23 (2015) 344–351. Doi:10.1002/Cae.21604.

[147] W. Plazinski, W. Rudzinski, Kinetics Of Adsorption At Solid/Solution Interfaces Controlled By Intraparticle Diffusion: A Theoretical Analysis, J. Phys. Chem. C. 113 (2009) 12495–12501. Doi:10.1021/Jp902914z.

[148] J.J. Moré, The Levenberg-Marquardt Algorithm: Implementation And Theory." Numerical Analysis. Springer, 1978.

[149] D.M. Ruthven, Principles Of Adsorption And Adsorption Processes, 1984. Https://Books.Google.Ca/Books?Hl=Ar&Lr=&Id=U7wq21njr3uc&Oi=Fnd&Pg=Pr18&Dq=Ruthven,+Douglas+M.+Principles+Of+Adsorption+And+Adsorption+Processes.+John+Wiley+&+Sons,+1984&Ots=Wa_Pkpdgpu&Sig=Rtwdcrxvn6vg0zvudmaizkiudse&Redir_Esc=Y#V=Onepage&Q=Ruthven, Dougla.

[150] M.A. Al-Ghouti, M.A.M. Khraisheh, S.J. Allen, M.N. Ahmad, The Removal Of Dyes From Textile Wastewater: A Study Of The Physical Characteristics And Adsorption Mechanisms Of Diatomaceous Earth, J. Environ. Manage. 69 (2003) 229–238. Doi:10.1016/J.Jenvman.2003.09.005.

[151] J.M. Zalc, S.C. Reyes, E. Iglesia, The Effects Of Diffusion Mechanism And Void Structure On Transport Rates And Tortuosity Factors In Complex Porous Structures, Chem. Eng. Sci. 59 (2004) 2947–2960. Doi:10.1016/J.Ces.2004.04.028.

[152] M. Gholami, M.R. Talaie, S.F. Aghamiri, The Development Of A New Ldf Mass Transfer Correlation For Adsorption In Fixed Beds, Adsorption. 22 (2016) 195–203. Doi:10.1007/S10450-015-9730-4.

[153] D. Mu, Z.S. Liu, C. Huang, N. Djilali, Determination Of The Effective Diffusion Coefficient In Porous Media Including Knudsen Effects, Microfluid. Nanofluidics. 4 (2008)

257–260. Doi:10.1007/S10404-007-0182-3.

[154] Y. Shi, Y.T. Lee, A.S. Kim, Knudsen Diffusion Through Cylindrical Tubes Of Varying Radii: Theory And Monte Carlo Simulations, Transp. Porous Media. 93 (2012) 517–541. Doi:10.1007/S11242-012-9966-3.

[155] J. Cruz-Olivares, C. Pérez-Alonso, C. Barrera-Díaz, F. Ureña-Nuñez, M.C. Chaparro-Mercado, B. Bilyeu, Modeling Of Lead (Ii) Biosorption By Residue Of Allspice In A Fixed-Bed Column, Chem. Eng. J. 228 (2013) 21–27. Doi:10.1016/J.Cej.2013.04.101.

[156] S. Ghorai, K.K. Pant, Investigations On The Column Performance Of Fluoride Adsorption By Activated Alumina In A Fixed-Bed, Chem. Eng. J. 98 (2004) 165–173. Doi:10.1016/J.Cej.2003.07.003.

[157] M.J. Daisy, J.N. Patra, Fixed-Bed Column Studies For The Removal Of Hazardous Malachite Green Dye From Aqueous Solution Using Novel Nano Zerovalent Iron Algal Biocomposite, Nanotechnol. Environ. Eng. 1 (2016) 1–10. Doi:10.1007/S41204-016-0007-2.

[158] M. Khitous, S. Moussous, A. Selatnia, M. Kherat, Biosorption Of Cd(Ii) By Pleurotus Mutilus Biomass In Fixed-Bed Column: Experimental And Breakthrough Curves Analysis, Desalin. Water Treat. 57 (2016) 16559–16570. Doi:10.1080/19443994.2015.1081625.

[159] J.M.P.Q. Delgado, A Critical Review Of Dispersion In Packed Beds, Heat Mass Transf. Und Stoffuebertragung. 42 (2006) 279–310. Doi:10.1007/S00231-005-0019-0.

[160] E.J. Wilson, C.J. Geankoplis, Liquid Mass Transfer At Very Low Reynolds Numbers In Packed Beds, Ind. Eng. Chem. Fundam. 5 (1966) 9–14. Doi:10.1021/I160017a002.

[161] A. Olgun, N. Atar, S. Wang, Batch And Column Studies Of Phosphate And Nitrate Adsorption On Waste Solids Containing Boron Impurity, Chem. Eng. J. 222 (2013) 108–119. Doi:10.1016/J.Cej.2013.02.029.

[162] T.A.H. Nguyen, H.H. Ngo, W.S. Guo, T.Q. Pham, F.M. Li, T. V. Nguyen, X.T. Bui, Adsorption Of Phosphate From Aqueous Solutions And Sewage Using Zirconium Loaded Okara (Zlo): Fixed-Bed Column Study, Sci. Total Environ. 523 (2015) 40–49. Doi:10.1016/J.Scitotenv.2015.03.126.

[163] F.J. García-Mateos, R. Ruiz-Rosas, M.D. Marqués, L.M. Cotoruelo, J. Rodríguez-Mirasol, T. Cordero, Removal Of Paracetamol On Biomass-Derived Activated Carbon: Modeling The Fixed Bed Breakthrough Curves Using Batch Adsorption Experiments, Chem. Eng. J. 279 (2015) 18–30. Doi:10.1016/J.Cej.2015.04.144.

[164] P. Liao, Z. Zhan, J. Dai, X. Wu, W. Zhang, K. Wang, S. Yuan, Adsorption Of Tetracycline And Chloramphenicol In Aqueous Solutions By Bamboo Charcoal: A Batch And Fixed-Bed Column Study, Chem. Eng. J. 228 (2013) 496–505. Doi:10.1016/J.Cej.2013.04.118.

[165] G. Vázquez, R. Alonso, S. Freire, J. González-Álvarez, G. Antorrena, Uptake Of Phenol From Aqueous Solutions By Adsorption In A Pinus Pinaster Bark Packed Bed, J. Hazard. Mater. 133 (2006) 61–67. Doi:10.1016/J.Jhazmat.2004.12.041.

[166] N. ???W Han, J. Bhakta, R.G. Carbonell, Longitudinal And Lateral Dispersion In Packed

Beds: Effect Of Column Length And Particle Size Distribution, Aiche J. 31 (1985) 277–288. Doi:10.1002/Aic.690310215.

[167] M. Amanullah, S. Farooq, S. Viswanathan, Modeling And Simulation Of A Biofilter, Ind. Eng. Chem. Res. 38 (1999) 2765–2774. Doi:10.1021/Ie9807708.

[168] Y. Segura, F. Martínez, J.A. Melero, J.L.G. Fierro, Zero Valent Iron (Zvi) Mediated Fenton Degradation Of Industrial Wastewater: Treatment Performance And Characterization Of Final Composites, Chem. Eng. J. 269 (2015) 298–305. Doi:10.1016/J.Cej.2015.01.102.

[169] C.Y. Teh, T.Y. Wu, J.C. Juan, Optimization Of Agro-Industrial Wastewater Treatment Using Unmodified Rice Starch As A Natural Coagulant, Ind. Crops Prod. 56 (2014) 17–26. Doi:10.1016/J.Indcrop.2014.02.018.

[170] A. Daverey, S.H. Su, Y.T. Huang, S.S. Chen, S. Sung, J.G. Lin, Partial Nitrification And Anammox Process: A Method For High Strength Optoelectronic Industrial Wastewater Treatment, Water Res. 47 (2013) 2929–2937. Doi:10.1016/J.Watres.2013.01.028.

[171] A. Asghar, A. Aziz, A. Raman, W. Mohd, A. Wan, Advanced Oxidation Processes For In-Situ Production Of Hydrogen Peroxide / Hydroxyl Radical For Textile Wastewater Treatment : A Review, 87 (2015).

[172] R. Mailler, J. Gasperi, Y. Coquet, A. Bulet??, E. Vulliet, S. Deshayes, S. Zedek, C. Mirande-Bret, V. Eudes, A. Bressy, E. Caupos, R. Moilleron, G. Chebbo, V. Rocher, Removal Of A Wide Range Of Emerging Pollutants From Wastewater Treatment Plant Discharges By Micro-Grain Activated Carbon In Fluidized Bed As Tertiary Treatment At Large Pilot Scale, Sci. Total Environ. 542 (2016) 983–996. Doi:10.1016/J.Scitotenv.2015.10.153.

[173] L. Chu, C. Liu, G. Zhou, R. Xu, Y. Tang, Z. Zeng, S. Luo, A Double Network Gel As Low Cost And Easy Recycle Adsorbent: Highly Efficient Removal Of Cd(Ii) And Pb(Ii) Pollutants From Wastewater, J. Hazard. Mater. 300 (2015) 153–160. Doi:10.1016/J.Jhazmat.2015.06.070.

[174] A. Asadi, A.A. Zinatizadeh, M. Van Loosdrecht, A Novel Continuous Feed And Intermittent Discharge Airlift Bioreactor (Cfidab) For Enhanced Simultaneous Removal Of Carbon And Nutrients From Soft Drink Industrial Wastewater, Chem. Eng. J. 292 (2016) 13–27. Doi:10.1016/J.Cej.2016.01.110.

[175] C.Z. Liang, S.P. Sun, F.Y. Li, Y.K. Ong, T.S. Chung, Treatment Of Highly Concentrated Wastewater Containing Multiple Synthetic Dyes By A Combined Process Of Coagulation/Flocculation And Nanofiltration, J. Memb. Sci. 469 (2014) 306–315. Doi:10.1016/J.Memsci.2014.06.057.

[176] E. Ellouze, N. Tahri, R. Ben Amar, Enhancement Of Textile Wastewater Treatment Process Using Nanofiltration, Desalination. 286 (2012) 16–23. Doi:10.1016/J.Desal.2011.09.025.

[177] Y.I. L And R.S. A. Imaii*@, K. Onuma 2, Biodegradation And Adsorption In Refractory Leachate Treatment By The Biological Activated Carbon Fluidized Bed Process, Water Res. 29 (1995). Http://Ac.Els-Cdn.Com/004313549400147y/1-S2.0-004313549400147y-Main.Pdf?_Tid=E9aa7ece-E8e3-11e6-8b16-00000aacb361&Acdnat=1485997805_1449cd47152c930ca7ada90f2115054a.

[178] R. Lakshmanan, M. Sanchez-Dominguez, J.A. Matutes-Aquino, S. Wennmalm, G.K. Rajarao, Removal Of Total Organic Carbon From Sewage Wastewater Using Poly (Ethylenimine) -Functionalized Magnetic Nanoparticles, Langmuir. 30 (2014).

[179] P. Xu, G. Ming, D. Lian, C. Ling, S. Hu, M. Hua, Use Of Iron Oxide Nanomaterials In Wastewater Treatment : A Review, Sci. Total Environ. 424 (2012) 1–10. Doi:10.1016/J.Scitotenv.2012.02.023.

[180] T. Poursaberi, M. Hassanisadi, K. Torkestani, M. Zare, Development Of Zirconium (Iv)-Metalloporphyrin Grafted Fe 3o 4 Nanoparticles For Efficient Fluoride Removal, Chem. Eng. J. 189–190 (2012) 117–125. Doi:10.1016/J.Cej.2012.02.039.

[181] A. Hethnawi, N.. Nassar, G. Vitale, A. Manasarah, Poly(Ethylenimine)-Functionalized Pyroxene Nanoparticles Embedded On Diatomite For Adsorptive Removal Of Dye From Textile Wastewater: Batch And Fixed-Bed Studies, Chem. Eng. J. (2017).

[182] J. Lyklema, Points Of Zero Charge In The Presence Of Specific Adsorption, J. Colloid Interface Sci. 99 (1984) 109–117. Doi:10.1016/0021-9797(84)90090-0.

[183] F. Loosli, P. Le Coustumer, S. Stoll, Effect Of Electrolyte Valency, Alginate Concentration And Ph On Engineered Tio2 Nanoparticle Stability In Aqueous Solution, Sci. Total Environ. 535 (2015) 28–34. Doi:10.1016/J.Scitotenv.2015.02.037.

[184] J.H. Bruus, P.H. Nielsen, K. Keiding, On The Stability Of Activated Sludge Flocs With Implications To Dewatering, Water Res. 26 (1992) 1597–1604. Doi:10.1016/0043-1354(92)90159-2.

[185] J. Davis, R. James, J. Leckie, Surface Ionization And Complexation At The Oxide / Water Interface, J. Colloid Interface Sci. 63 (1978) 480–499. Doi:10.1016/S0021-9797(78)80009-5.

[186] R. Tovar-Gómez, M.R. Moreno-Virgen, J.A. Dena-Aguilar, V. Hernández-Montoya, A. Bonilla-Petriciolet, M.A. Montes-Morán, Modeling Of Fixed-Bed Adsorption Of Fluoride On Bone Char Using A Hybrid Neural Network Approach, Chem. Eng. J. 228 (2013) 1098–1109. Doi:10.1016/J.Cej.2013.05.080.

[187] B. Zhao, Y. Shang, W. Xiao, C. Dou, R. Han, Adsorption Of Congo Red From Solution Using Cationic Surfactant Modified Wheat Straw In Column Model, J. Environ. Chem. Eng. 2 (2014) 40–45. Doi:10.1016/J.Jece.2013.11.025.

[188] K.H. Chu, Fixed Bed Sorption: Setting The Record Straight On The Bohart-Adams And Thomas Models, J. Hazard. Mater. 177 (2010) 1006–1012. Doi:10.1016/J.Jhazmat.2010.01.019.

[189] R. Han, Y. Wang, W. Zou, Y. Wang, J. Shi, Comparison Of Linear And Nonlinear Analysis In Estimating The Thomas Model Parameters For Methylene Blue Adsorption Onto Natural Zeolite In Fixed-Bed Column, J. Hazard. Mater. 145 (2007) 331–335. Doi:10.1016/J.Jhazmat.2006.12.027.

[190] Z. Zulfadhly, M.D. Mashitah, S. Bhatia, Heavy Metals Removal In Fixed-Bed Column By The Macro Fungus Pycnoporus Sanguineus, Environ. Pollut. 112 (2001) 463–470. Doi:10.1016/S0269-7491(00)00136-6.

[191] W. Weber, R.K. Chakravorti, Pore And Solid Diffusion Models For Fixed Bed Adsorbers, Am. Inst. Chem. Eng. J. 20 (1974) 229–238.

[192] K.H. Chu, Improved Fixed Bed Models For Metal Biosorption, Chem. Eng. J. 97 (2004) 233–239. Doi:10.1016/S1385-8947(03)00214-6.

[193] L. Cavas, Z. Karabay, H. Alyuruk, H. Doĝan, G.K. Demir, Thomas And Artificial Neural Network Models For The Fixed-Bed Adsorption Of Methylene Blue By A Beach Waste Posidonia Oceanica (L.) Dead Leaves, Chem. Eng. J. 171 (2011) 557–562. Doi:10.1016/J.Cej.2011.04.030.

[194] B. Balci, O. Keskinkan, M. Avci, Use Of Bdst And An Ann Model For Prediction Of Dye Adsorption Efficiency Of Eucalyptus Camaldulensis Barks In Fixed-Bed System, Expert Syst. Appl. 38 (2011) 949–956. Doi:10.1016/J.Eswa.2010.07.084.

[195] M. Sadeghi-Kiakhani, M. Arami, K. Gharanjig, Dye Removal From Colored-Textile Wastewater Using Chitosan-Ppi Dendrimer Hybrid As A Biopolymer: Optimization, Kinetic, And Isotherm Studies, J. Appl. Polym. Sci. 127 (2013) 2607–2619. Doi:10.1002/App.37615.

[196] P. Sharma, L. Singh, J. Mehta, Cod Reduction And Colour Removal Of Simulated Textile Mill Wastewater By Mixed Bacterial Consortium, Rasayan J. Chem. 3 (2010) 731–735.

[197] K. Miyabe, M. Ando, N. Ando, G. Guiochon, External Mass Transfer In High Performance Liquid Chromatography Systems, J. Chromatogr. A. 1210 (2008) 60–67. Doi:10.1016/J.Chroma.2008.09.035.

[198] A.H. Sulaymon, B.A. Abid, J.A. Al-Najar, Removal Of Lead Copper Chromium And Cobalt Ions Onto Granular Activated Carbon In Batch And Fixed-Bed Adsorbers, Chem. Eng. J. 155 (2009) 647–653. Doi:10.1016/J.Cej.2009.08.021.

[199] N. Abdel-Jabbar, S. Al-Asheh, B. Hader, Modeling, Parametric Estimation, And Sensitivity Analysis For Copper Adsorption With Moss Packed-Bed, Sep. Sci. Technol. 36 (2001) 2811–2833. Doi:10.1081/Ss-100107631.

[200] Z. Saadi, R. Saadi, R. Fazaeli, Fixed-Bed Adsorption Dynamics Of Pb (Ii) Adsorption From Aqueous Solution Using Nanostructured Γ-Alumina, J. Nanostructure Chem. 48 (2013) 2–8. Doi:10.1186/2193-8865-3-48.

[201] N.E. Davila-Guzman, F.J. Cerino-Córdova, E. Soto-Regalado, M. Loredo-Cancino, J.A. Loredo-Medrano, R.B. García-Reyes, A Mass Transfer Model For The Fixed-Bed Adsorption Of Ferulic Acid Onto A Polymeric Resin: Axial Dispersion And Intraparticle Diffusion., Environ. Technol. 3330 (2016) 1–9. Doi:10.1080/09593330.2015.1135993.

[202] M. Bhaumik, K. Setshedi, A. Maity, M.S. Onyango, Removal From Water Using Fixed Bed Column Of Polypyrrole/Fe 3o4 Nanocomposite, Sep. Purif. Technol. 110 (2013) 11–19. Doi:10.1016/J.Seppur.2013.02.037.

[203] H. Bessbousse, T. Rhlalou, J.F. Verchère, L. Lebrun, Removal Of Heavy Metal Ions From Aqueous Solutions By Filtration With A Novel Complexing Membrane Containing Poly(Ethyleneimine) In A Poly(Vinyl Alcohol) Matrix, J. Memb. Sci. 307 (2008) 249–259. Doi:10.1016/J.Memsci.2007.09.027.

APPENDIX A 1

S.1 X-ray diffraction (XRD)

Both the original dye sample and the extracted one were analyzed at the same time under the same conditions using X-ray diffraction (XRD). The obtained patterns were compared with a NaCl reference sample. As shown in Figure. S1 the crystalline patterns confirm the structural peaks of halite (NaCl). In the region of 31.71(2Ɵ value) for the plane of 200 (Miller indices), the peak areas were 56445, 46762, and 13542 for the halite (NaCl), the commercial red dye, and the extracted red dye samples, respectively. Therefore, the weight percentages of the samples were quantified based on NaCl for both the commercial dye and the extracted dye, giving 82.8, and 24.0 wt%, respectively.

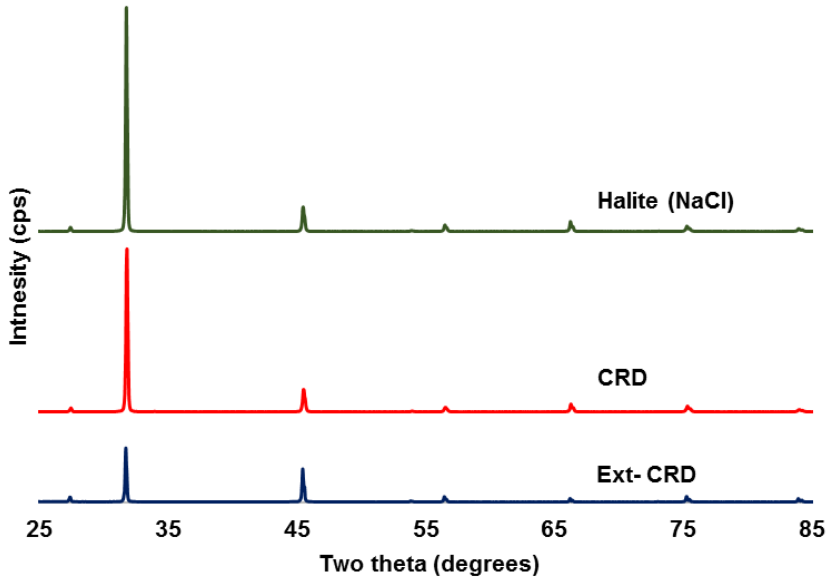

Figure S1. X-ray diffraction in the region 25-85^{o} of the halite (NaCl) compared with the commercial dye (CRD) and the extracted by (Ext-CRD) samples.